

---

# Site U1369<sup>1</sup>

---

Expedition 329 Scientists<sup>2</sup>

## Chapter contents

Background and objectives . . . . .	1
Operations . . . . .	2
Lithostratigraphy . . . . .	3
Igneous lithostratigraphy, petrology, alteration, and structural geology . . . . .	5
Physical properties . . . . .	6
Paleomagnetism . . . . .	7
Biogeochemistry . . . . .	8
Microbiology . . . . .	10
References . . . . .	12
Figures . . . . .	14
Tables . . . . .	48

## Background and objectives

Integrated Ocean Drilling Program (IODP) Site U1369 (proposed Site SPG-10A) was selected as a drilling target because

- Its microbial activities and cell counts were expected to be characteristic of midway between gyre center and the southern gyre edge and
- Its basement age renders it a reasonable location for testing the extent of sediment-basement interaction in a thinly sedimented region of ~58 Ma basaltic basement.

The principal objectives at Site U1369 were

- To document the habitats, metabolic activities, genetic composition, and biomass of microbial communities in subsurface sediment with very low total activity;
- To test how oceanographic factors (such as surface ocean productivity, sedimentation rate, and distance from shore) control variation in sedimentary habitats, activities, and communities from gyre center to gyre margin;
- To quantify the extent to which these sedimentary microbial communities may be supplied with electron donors by water radiolysis; and
- To determine how sediment-basement exchange and potential activities in the basaltic basement vary with basement age and hydrologic regime (from ridge crest to abyssal plain).

Site U1369 (5277 meters below sea level) is in the South Pacific Gyre within a region of abyssal hill topography trending northwest-southeast (335°) with relief ranging from 300 to 500 m (Fig. F1). Abyssal hill spacing is ~4–10 km with a very pronounced topography. No obvious seamounts are present. The closest previous drilling site is Deep Sea Drilling Project Leg 92 Site 597, 1350 nmi away.

Because of insufficient coverage of magnetic data, the age of the crust is estimated from extrapolated magnetic models and changes in spreading rate recorded by neighboring magnetic profiles. Our best estimate of the crustal age is ~58 Ma, which corresponds to magnetic polarity Chron 25r (57.2–58.4 Ma; Gradstein et al., 2004). Based on the age of the crust and regional tectonic history, the crust was accreted along the Pacific-Farallon spreading center at ~58 Ma. The calculated spreading rate from our magnetic survey suggests an intermediate- to fast-spreading ridge system with spreading half-rates of ~25–30 km/m.y. These slower

<sup>1</sup>Expedition 329 Scientists, 2011. Site U1369. In D'Hondt, S., Inagaki, F., Alvarez Zarikian, C.A., and the Expedition 329 Scientists, *Proc. IODP, 329*: Tokyo (Integrated Ocean Drilling Program Management International, Inc.).  
doi:10.2204/iodp.proc.329.107.2011

<sup>2</sup>Expedition 329 Scientists' addresses.



spreading rates are consistent with the relatively rough abyssal hill topography.

Many geological and geophysical characteristics of the target site were characterized by the 2006/2007 KNOX-02RR survey expedition (D'Hondt et al., 2011) (Figs. F1, F2, F3, F4, F5, F6). The shallow sediment (0–5.6 meters below seafloor [mbsf]) consists of homogeneous brown clay with yellowish brown circular mottles (D'Hondt et al., 2009). Smear slides are barren of microfossils and contain micronodules. Manganese nodules were found on the top of all 12 cores taken by the survey and in the uppermost meter of sediment. The nodules are uniformly ~8–10 cm in diameter.

D'Hondt et al. (2009) documented the presence of microbial cells and oxic respiration throughout the uppermost 5.6 m of sediment at Site U1369. Cell concentrations were approximately three orders of magnitude lower than at similar depths in previously drilled marine sediment of other regions. Net respiration was similarly much lower than at previously drilled sites. From extrapolation of dissolved oxygen content in the uppermost 5.6 m of sediment, Fischer et al. (2009) predicted that dissolved oxygen penetrates the entire sediment column, from seafloor to basement.

## Operations

### Transit to Site U1369

After a 98.1 h transit from Site U1368, covering 1073 nmi and averaging 10.9 kt, speed was reduced and thrusters were lowered. Dynamic positioning was initiated over Site U1369 at 1454 h on 22 November 2010. The position reference was a combination of GPS signals. No acoustic beacon was deployed, but a beacon remained on standby in the event of a loss of GPS satellite coverage. Whereas automatic input into the dynamic positioning system was not possible because of a system malfunction, it was possible to manually hold the vessel in position to clear the seafloor with the bottom-hole assembly if necessary.

All times in this section are given in local ship time unless otherwise noted. For most of the expedition, local time was Universal Time Coordinated – 10 h.

### Site U1369

Five holes were drilled or cored at Site U1369 (Table T1). The first hole was a washdown hole drilled with the center bit in order to establish the sediment depth of 12.2 mbsf. The next four holes were cored with the advanced piston corer (APC) system. The advanced piston corer temperature tool was not deployed because of the shallow sediment depth. Per-

fluorocarbon tracer (PFT) was pumped for the entire drilling/coring interval until the last core was on deck. APC system recovery for Site U1369 was 108%. A total of 10 cores were attempted while coring 46.1 m. The total length of core recovered at this site was 49.81 m (108.0% recovery).

### Hole U1369A

Rig floor operations commenced at 1445 h on 22 November 2010. The trip to the seafloor was uneventful. The top drive was picked up and the drill string was spaced out and spudded at 0040 h on 23 November. The PFT pump was turned on to displace the drill string with the contamination testing fluid. The washdown hole was drilled to determine depth of basement. Mudline was established at 5290.5 meters below rig floor (mbrf) by tagging with the bit. After drilling down, basement was established at 12.2 mbsf. The bit was pulled back above the seafloor, clearing the seafloor at 0125 h and ending Hole U1369A.

### Hole U1369B

After clearing the seafloor, the center bit was pulled by wireline, the vessel was offset 20 m west, and the drill string was spaced out to spud Hole U1369B. After making up the first APC core barrel, the core barrel was run to bottom on the wireline and Hole U1369B was spudded at 0350 h on 23 November. Seafloor depth was established at 5286.3 mbrf with a mudline core. APC coring continued to 15.9 mbsf. An extended core barrel was dropped after an initial analysis from the science party based on concern that the deepest material recovered might not have been igneous in origin. Subsequent analysis verified the rock samples to be igneous in origin and the core barrel was pulled without advancing. Three cores were taken with a total recovery of 18.14 m (114.1%). After Core 329-U1369B-3H, the bit was tripped back to just above the seafloor, ending Hole U1369B at 1030 h. PFT was mixed with the drilling fluid (seawater) and pumped on all cores for contamination testing.

### Hole U1369C

Hole U1369C began at 1030 h when the APC assembly cleared the seafloor after completing Hole U1369B. After offsetting the vessel 20 m north, Hole U1369C was spudded at 1135 h and advanced with the APC system to 14.6 mbsf before encountering basement. Seafloor was established at 5288.0 mbrf. PFT was mixed with the drilling fluid (seawater) and pumped on all cores for contamination testing. Three cores were taken with a total recovery of 16.1 m (110.3%). The drill string was tripped to just above

the mudline, clearing the seafloor at 1530 h on 23 November and ending Hole U1369C.

### Hole U1369D

Hole U1369D began at 1530 h when the APC assembly cleared the seafloor after completing Hole U1369C. After offsetting the vessel 20 m east, Hole U1369D was spudded at 1615 h on 23 November. The core liner was shattered and even though the core barrel extended 9.5 m, manganese nodules in the core catcher comprised the only material recovered. Hole U1369D was abandoned. Seafloor was established at 5288.0 mbrf using an offset from the previous hole. Recovery was limited to a 0.08 m core length, and the advance was recorded as 0.1 m. Percentage of recovery is recorded as 80%. PFT was mixed with the drilling fluid (seawater) and pumped on all cores for contamination testing. The hole ended at 1615 h with the mudline shot.

### Hole U1369E

Hole U1369E began at 1615 h on 23 November after the failed mudline core on Hole U1369D. The vessel was offset 20 m east of Hole U1369D. After making up the first APC core barrel, the core barrel was run to bottom on the wireline and Hole U1369E was spudded at 1745 h. Seafloor depth was established with a mudline core at 5288.8 mbrf. The APC system was used to take three cores to 15.5 mbsf with a 15.49 m recovery (99.9%). PFT was mixed with the drilling fluid (seawater) and pumped on all cores for contamination testing. The drill string was tripped to the surface, clearing the rotary table at 0645 h on 24 November. The rig floor and secured for the 625 nmi transit to the next site, ending Hole U1369F and Site U1369 at 0730 h on 24 November.

## Lithostratigraphy

Sediment at Site U1369 consists of ~16 m of zeolitic metalliferous clay. The principal components of the clay are phillipsite, red-brown to yellow-brown semi-opaque oxide (RSO), and clay (see Site U1369 smear slides in “[Core descriptions](#)”; Fig. F7). The strata of the three holes at Site U1369 are divided into two lithologic units based on RSO abundance and size of phillipsite crystals (Fig. F8). The average RSO content of Unit I is 33%, and most of its phillipsite crystals are <10 µm in length. In the underlying Unit II, RSO concentration is ~42% and phillipsite crystals are frequently >50 µm long. Three manganese nodules were recovered from the mudline of Holes U1369B–U1369D. One additional nodule was found near the bottom of Unit II in Hole U1369B (Fig. F9A). A thin (~10 cm) layer of vitric sand/breccia was recovered

from the base of Hole U1369E. Micro- and nannofossils are almost completely absent; only rare fish teeth were observed in the sediment.

The overall texture of the sediment at Site U1369 is massive and appears to be the result of thorough bioturbation. *Planolites* burrows, increasing with depth, are outlined clearly in sediment that contains elevated abundances of phillipsite. Lithostratigraphic correlation among Site U1369 holes shows that sediment thickness and composition remain fairly uniform (Fig. F8).

The pelagic sediment rests on vitric and altered basalt, which was sampled in small fragments in Holes U1369B, U1369C, and U1369E. See “[Igneous lithostratigraphy, petrology, alteration, and structural geology](#)” for more details regarding the basaltic rock recovered at Site U1369.

## Description of units

### Unit I

Intervals: 329-U1369B-1H-1, 0 cm, to 1H-4, 80 cm; 329-U1369C-1H-1, 0 cm, to 1H-CC, 21 cm, through 2H-1, 0 cm; 329-U1369E-1H-1, 0 cm, to 1H-4, 70 cm through 110 cm

Depths: Hole U1368B = 0–5.3 mbsf, Hole U1368C = 0–6.0 mbsf, Hole U1368E = 0–5.2 through 5.6 mbsf

Lithology: metalliferous zeolitic pelagic clay

The overall color of the clay is brown (7.5YR 5/3) (Fig. F9B). Circular and elliptical rings, 1–2 mm thick with diameters between 1 and 3 cm, are very pale brown (10YR 8/4) with occasional black (2.5Y 2.5/1) grains located along the inner and outer rims of the rings. The manganese nodules recovered in Holes U1369B and U1369D are also black (2.5Y 2.5/1). A claystone recovered from interval 329-U1369E-1H-2, 115–117 cm, is very pale brown.

Smear slide analyses identify phillipsite, RSO, and clay as the dominant sedimentary components of Unit I (Fig. F7). Phillipsite abundance varies between 38% and 63%. The higher modal abundances are associated with pale brown (10YR 8/4) and brown (7.5YR 5/4) ellipses as thick as 4 mm (Fig. F9B). Phillipsite crystals are very small (<10 µm) but euhedral (Fig. F10A). RSO grains are rounded to irregularly shaped, range in size from several micrometers to 50 µm, and constitute 24%–38% of the sediment. Clay abundance is generally low (~13%). Minerals identified by X-ray diffraction (XRD) analyses of the upper portion of clay in Unit I are smectite, illite, and chlorite (Fig. F11A). The characteristic XRD pattern of chlorite was not present in a second sample drawn from the gradational transition zone between Units I and II. Both samples, however, produced XRD pat-

terns consistent with quartz and opal CT. Pebble- and cobble-sized manganese nodules are present at the top of Unit I in Cores 1H from Holes U1369B–U1369E. Approximately 17 g (dry mass) of Sample 329-U1369-1H-CC, 8–10 cm (the “PAL” biostratigraphy sample), was washed over 38 and 63  $\mu\text{m}$  sieves to identify microfossil type and abundance. Only several fish teeth were observed in the remaining debris, and no calcareous or siliceous microfossils were found.

Unit I sediment changes gradually from very poorly consolidated near the mudline to poorly consolidated at the base of the subunit. A very small number of highly indurated grains resisted grinding during preparation of the XRD samples. The individual grains were easily separated from the clay matrix, crushed, and remixed thoroughly with the remaining sample prior to XRD analysis.

The structure in Unit I is massive with occasional burrows and rare very pale brown laminations. The burrows are *Planolites* associated with horizontal traces formed in the seafloor transition layer (5–8 cm) (Ekdale et al., 1984). A thoroughly bored hard-ground of very pale brown sediment was recovered from interval 329-U1369E-1H-2, 115–117 cm (Fig. F9C). The lower contact with Unit II is gradational, occurring through a 20–80 cm vertical length.

## Unit II

Intervals: 329-U1369B-1H-4, 80 cm, to 2H-7, 40 cm; 329-U1369C-1H-CC, 21 cm through 2H-1, 0 cm, to 3H-CC, 1 cm; 329-U1369E-1H-4, 70 cm through 110 cm, to 2H-CC, 2 cm

Depths: Hole U1368B = 5.3–15.6 mbsf, Hole U1368C = 6.0–16.06 mbsf, Hole U1368E = 5.2 through 5.6–15.41 mbsf

Lithology: zeolitic metalliferous pelagic clay

Clay in this unit is dark brown to very dark brown (7.5YR 3/4, 3/3, 2.5/3) (Fig. F9D). Circular and elliptical rings, 1–2 mm thick with diameters between 1 and 3 cm, are very pale brown (10YR 8/4) with occasional black (2.5Y 2.5/1) grains associated with the edges of the rings. A manganese nodule recovered from the lower part of Hole U1369B is black (2.5Y 2.5/1). The lowermost 13 cm of Hole U1369E contains a distinctive sand/breccia of olive-yellow (5Y 6/8) angular grains with lesser amounts of white and red (2.5YR 4/8) interspersed clay.

Smear slide analyses identify clay, RSO, and phillipsite as the dominant sedimentary components of Unit II (Fig. F7). RSO grains are rounded to irregularly shaped, range in size from <10 to 50  $\mu\text{m}$ , and constitute an average of 42% of the sediment. Phillipsite abundance varies between 35% and 70%, with

an approximate modal average of 40%. Many euhedral phillipsite crystals are large (>50  $\mu\text{m}$ ) (Fig. F10B). Clay abundance varies between 9% and 15%. The XRD peaks resulting from analysis of Sample 329-U1369B-2H-4, 80–82 cm, are representative of phillipsite, smectite, illite, chlorite, quartz, and opal CT (Fig. F11B). The olive-yellow sand/breccia in the lowermost 13 cm of Hole U1369E consists of angular grains of altered glass and clay. We refer to the coarse sand layer as a sand/breccia because its particles are particularly angular, but the grain size is considerably finer than typical breccias. Granules in the sand/breccia are translucent and possess concentric color bands similar to those associated with agates. However, XRD analyses of the sand/breccia indicates the granules are glass (i.e., incapable of producing an XRD peak characteristic of crystalline substances; see Fig. F11B). The XRD pattern of the sand/breccia's clay fraction appears to be a mixture of phillipsite and illite/smectite.

Consolidation of Unit II is uniformly firm. Sediment in Sections 329-U1369B-2H-7, 3H-1, 3H-2, and 3H-CC are flow-in. The sand/breccia at the base of Hole U1369E contains loose grains and clay that are easily disaggregated.

Unit II structure is massive with increasingly common burrows in the 0.5–1 m of clay overlying its lower contact. The majority of burrows identified in Holes U1369B, U1369C, and U1369E are *Planolites*. Section 329-U1369E-2H-5 also contains wide (1 cm), highly vertical traces indicative of *Thalassinoidies*. The transition from clay to sand/breccia in the lowermost part of Hole U1369E is extremely abrupt and steeply (~75°) dipping (Fig. F9E). This contact is described more fully in the following section.

## Sediment/Basalt contact

We attempted to sample the sediment/basalt interface in each hole. Three small pieces of vitric basalt were recovered in Section 329-U1369B-3H-CC. See “[Igneous lithostratigraphy, petrology, alteration, and structural geology](#)” for a description of the basalt. Sediment surrounding the basaltic fragments was thoroughly disturbed. The soupy, very dark brown clayey sediment continued for a full 2 m above the interval containing the basaltic fragments. The first consolidated sediment overlying the interval of fragmented basaltic rock (interval 329-U1369B-3H-1, 15–19 cm) contains a manganese nodule. The sediment immediately overlying the nodule is dark brown zeolitic metalliferous pelagic clay.

Fragments of altered basalt were recovered in Section 329-U1369C-2H-CC. The sediment in the core catcher was flow-in. The first sediment overlying the

interval containing the basaltic fragments and not removed by whole-round sampling is interval 329-U1369C-2H-7, 51–53 cm. The sediment is massive dark brown zeolitic metalliferous pelagic clay.

The lowermost interval of Hole U1369E contained two indicators of the sediment/basalt interface: (1) a chip of altered basalt was extracted from the lowermost part of the olive-yellow sand/breccia found in Sections 329-U1369E-2H-6 and 2H-CC (see [“Igneous lithostratigraphy, petrology, alteration, and structural geology”](#) for a description of the basaltic fragment) and (2) the sand/breccia overlying the basaltic fragment consists of vitric grains that were probably derived from volcanism that preceded sediment accumulation. The contact between the sand/breccia and overlying clay is unaltered, very sharp, and the clay and vitric materials do not intermingle. Within several centimeters above the sand/breccia-to-clay contact, the clay assumes the character typical of the remaining parts of Unit II, very dark brown, zeolitic, metalliferous, and extensively burrowed.

### Interhole correlation

Lithologic units are correlated among holes at Site U1369 to facilitate the integration of physical properties, geochemical, and microbiological data. The stratigraphic correlation panel for Site U1369 is presented in Figure F8. Correlations shown in this figure are based on principal characteristics of the sediment: (1) variable RSO concentration and phillipsite crystal size occurs abruptly between 5.5 and 6.5 mbsf (Fig. F7) and (2) magnetic susceptibility, gamma ray attenuation (GRA), and natural gamma ray (NGR) physical properties logs exhibit sharp increases through the interval that corresponds to the lithologic Unit I/II boundary. Correlations show that strata at Site U1369 have uniform unit thickness and composition.

## Igneous lithostratigraphy, petrology, alteration, and structural geology

At Site U1369, basaltic fragments were found at the bottom of Holes U1369B and U1369C. The fragments consist of a number of altered cryptocrystalline to glassy pieces in dark pelagic sediment (see [“Lithostratigraphy”](#)) in Hole U1369C and one large (3 cm) fragment of altered cryptocrystalline phyric basalt with a large glassy margin in Hole U1369B (Fig. F12). Basaltic fragments recovered from both holes are moderately to highly altered.

## Basaltic fragments

### Hole U1369B

The basaltic fragments recovered in Section 329-U1369B-3H-CC range from 5 to 35 mm in size and consist of cryptocrystalline to glassy phyric basalt with a large glassy rind. The basalt has a spinifex texture composed of plagioclase with interstitial, partially formed clinopyroxene, Fe-Ti oxide crystals, and glass. Phenocrysts include lath to prismatic plagioclase that range in size from 0.2 to 1.3 mm and minor clinopyroxene (0.2–0.4 mm). Plagioclase phenocrysts make up ~4% of the groundmass, whereas clinopyroxene makes up ~1% of the groundmass. Phenocrysts are partially to nearly completely corroded with a ring of fibrous clay mineral (saponite) propagating perpendicular to the phenocrysts. Vesicles make up 1% of the rock and are filled with saponite and iron oxyhydroxides. The glassy portion of the fragments is 90% fresh with a vitreous, jet-black surface that exhibits conchoidal fracturing.

The basaltic groundmass is moderately altered to highly altered to saponite and iron oxyhydroxides. Alteration is most common around phenocrysts, within the glass, and in interstitial zones between the plagioclase groundmass. It is manifested as several hairline fractures of saponite, iron oxyhydroxide, and quartz that impart curved subhorizontal banding of alteration between the glassy margin and the basalt. The presence of a fresh, curved glassy margin suggests that the fragment at the base of Hole U1369C is the uppermost extrusive lava of the basement.

### Holes U1369C and U1369E

The basaltic fragments in interval 329-U1369C-2H-CC, 0–5 cm, and Section 329-U1369E-2H-CC range in size from 10 to 25 mm. They were found intermixed with dark brown pelagic sediment (see [“Lithostratigraphy”](#) for detailed description of the sediment) in Section 329-U1369C-2H-CC and with disturbed pebbly sand in Section 329-U1369E-2H-6. Section 329-U1369E-2H-CC contained basaltic fragments within a completely disturbed clay sediment. The basaltic fragments are moderately to highly altered to saponite and iron oxyhydroxides. A number of the fragments in Hole U1369C are flanked by glassy margins that are variably altered to a yellow to pale brown clay mineral, possibly saponite and iron oxyhydroxides.

The original basaltic groundmass appears to have been cryptocrystalline to glassy and aphyric. Primary mineralogy is spinifex plagioclase with amorphous clinopyroxene and glassy textures. Alteration in the

groundmass is patchy but pervasive, with an orange-brown clay mineral (saponite?) partially corroding the plagioclase groundmass and replacing interstitial zones. Detailed petrographic studies will be required to further determine the primary mineralogy at this site. The presence of altered glassy margins and cryptocrystalline to glassy textures within the groundmass suggests that the basaltic chips represent the top of an eruptive basaltic unit (e.g., a pillow lava or sheet flow). However, because they were recovered as flow-in during retrieval of the piston core, their geological relationship to the sediment remains unknown. The surrounding sediment in Hole U1369C does not show any signs of being an alteration product. Sediment in contact with basalt fragments in Hole U1369E is sandy with olive-green patches (clay minerals), which indicates that the olive-green portions may represent completely altered basalt.

## Physical properties

At Site U1369, physical properties measurements were made to provide basic information characterizing lithologic units. After sediment cores reached thermal equilibrium with ambient temperature at  $\sim 20^{\circ}\text{C}$ , GRA density, magnetic susceptibility, and  $P$ -wave velocity were measured with the Whole-Round Multisensor Logger (WRMSL). After WRMSL scanning, the whole-round sections were logged for NGR. Thermal conductivity was measured using the full-space method on sediment cores. Discrete  $P$ -wave measurements were made on split sediment cores using the Section Half Measurement Gantry. Moisture and density (MAD) were measured on discrete subsamples collected from the working halves of the split sediment cores. Additional discrete measurements of electrical resistivity were made on the split sediment sections to calculate formation factor. The Section Half Imaging Logger was used to collect images of the split surfaces of the archive-half cores, and a color spectrophotometer was used to measure color reflectance on the Section Half Multisensor Logger (SHMSL). Holes U1369B–U1369E targeted the sedimentary cover. Hole U1369D was impeded by manganese nodules and did not proceed. The most complete hole for logging physical properties was Hole U1369B. Holes through the sediments have not been correlated and offsets exist.

### Density and porosity

Bulk density values at Site U1369 were determined from both GRA measurements on whole cores and mass/volume measurements on discrete samples from the working halves of split cores in Hole U1369B (see “[Physical properties](#)” in the “Methods”

chapter [Expedition 329 Scientists, 2011a]). A total of 10 discrete samples were analyzed for MAD.

Bulk density values in all holes are shown in Figure [F13](#). The mean value of bulk density in Hole U1369B is  $1.3\text{ g/cm}^3$ , and the density is slightly greater in lithologic Unit II than in Unit I. The scattered values in Hole U1369B deeper than 15.5 mbsf likely reflect core disturbance. Gaps and scatter in bulk density values for Holes U1369C and U1369E are caused by whole rounds being taken for geochemical and microbiological sampling prior to WRMSL measurements.

Bulk density, grain density, and porosity values were calculated from Hole U1369B (Fig. [F14](#)). Bulk density values are systematically offset relative to values derived from WRMSL measurements. The reason for this offset is unclear. The mean grain density is  $2.5\text{ g/cm}^3$  and increases slightly with depth. Porosity values vary between 86% and 76% and decrease slightly with depth. A step toward lower porosity values occurs between lithologic Units I and II.

### Magnetic susceptibility

Volumetric magnetic susceptibilities were measured using the WRMSL, and point measurements were made on the SHMSL in all recovered cores from Site U1369. Uncorrected values of magnetic susceptibility are presented for Holes U1369B, U1369C, and U1369E (Fig. [F15](#)). Point measurements from archive halves are much more scattered than whole-core measurements. The spatial resolution of the WRMSL magnetic susceptibility loop is  $\sim 5\text{ cm}$ , and the observed ringing in Holes U1369C and U1369E is due to edge effects.

Magnetic susceptibility varies between  $\sim 0$  and  $100 \times 10^{-5}\text{ SI}$  in Hole U1369B. Magnetic susceptibility values are somewhat higher in lithologic Unit II than in Unit I, likely because of the higher RSO content in Unit II (see “[Lithostratigraphy](#)”).

### Natural gamma radiation

NGR results are reported in counts per second (Fig. [F16](#)). NGR counting intervals were  $\sim 30\text{ min}$  per whole-core interval for Hole U1369B and decreased to 15 min per whole-core interval for Holes U1369C and U1369E. NGR counts are considered reliable. NGR at the tops of Holes U1369B and U1369E are high, indicating that the sediment/water interface was sampled. A whole round was removed from the top of Hole U1369C before that section was measured.

In general, NGR counts are higher in lithologic Unit II than in Unit I. Ringing is more prevalent in cores from Holes U1369C and U1369E because only short

core pieces remained after whole-round sampling prior to NGR measurements.

### P-wave velocity

P-wave velocity at Site U1369 was determined from measurements on whole-round sediment cores (Fig. F17) and on discrete samples from the working halves of sediment split cores (see “Physical properties” in the “Methods” chapter [Expedition 329 Scientists, 2011a]). Only two discrete measurements of P-wave velocity were measured. The mean value of all whole-core measurements is ~1530 m/s (Fig. F17B). In Hole U1369B, compressional wave velocities are relatively uniform except between 6 and 11 mbsf, where velocities show modest variation. The lowermost portion of Hole U1369B appears noisy.

### Formation factor

Electrical conductivity was measured on working halves of the split sediment cores from Hole U1369B. Measurements in Hole U1369B were made at a nominal interval of 10 cm. For each measurement, the temperature of the section was also noted. Surface seawater was used as a standard and measured at least twice per section (Table T2), normally prior to making measurements for that section and then around the 75 cm offset of each section. These measurements were used to compute the drift, which is small for this set of measurements (Fig. F18). The temperature dependence of electrical conductivity was corrected and all reported measurements correspond to a temperature of 20°C. Electrical conductivity measurements were transformed to a dimensionless formation factor by dividing the measurements for the drift (Table T3).

Within lithologic Unit I, the formation factor generally increases with depth (Fig. F19). Formation factor values in Unit II are >2 and also increase with depth. This pattern is generally inversely correlated with the porosity (Fig. F14).

### Thermal conductivity

Thermal conductivity measurements were conducted on sediment whole-round cores using the needle-probe method. The mean and standard deviation of thermal conductivity values are 0.7 and 0.07 W/(m·K), respectively (Fig. F20). These values compare favorably with needle-probe measurements from the KNOX-02RR site survey cruise (R. Harris, unpubl. data). A best fitting trend to these measurements shows a slight increase with depth, which is supposed to be related to the decrease in porosity with depth.

### Color spectrometry

Spectral reflectance was measured on split archive-half sections from Holes U1368B–U1369D. Measurements from Hole U1368B are shown in Figure F21.  $L^*$  varies between ~20 and 40 with a minimum at ~9 mbsf,  $a^*$  varies between 0 and 10, and  $b^*$  varies between 0 and 20. Spectral reflectance values tend to show more scatter in lithologic Unit I than in Unit II. Values of  $L^*$  and  $a^*$  appear inversely correlated to a modest extent, whereas values of  $b^*$  decrease with depth.

### Paleomagnetism

At Site U1369, we measured natural remanent magnetization of all archive-half sections for Holes U1369B, U1369C, and U1369E using the three-axis cryogenic magnetometer at 2.5 cm intervals before demagnetization. The archive-half sections were demagnetized at alternating fields (AF) of 10 and 20 mT. The present-day normal field in this region, as expected from the geocentric axial dipole model at Site U1369, has a negative inclination (approximately  $-58.6^\circ$ ), so positive remanence inclinations indicate reversed polarity. Data from Holes U1369C and U1369E provide only a partial record because whole-round core samples were taken from these holes for geochemical and microbiological analyses. From Hole U1369B, 11 discrete sediment samples (7 cm<sup>3</sup> cubes) were taken and compatibility of magnetization between archive half and working half was analyzed. The primary objective of the shipboard measurements for Site U1369 was to provide chronostratigraphic constraint by determining magnetic polarity stratigraphy. During the coring operation at Site U1369, neither nonmagnetic core barrels nor the Flexit core orientation tool were used because of the shallow drilling depth of the sediment column (see “Operations”).

### Results

Paleomagnetic data for Holes U1369B, U1369C, and U1369E are presented in Figures F22, F23, and F24, together with the whole-core susceptibility data measured on the WRMSL (see “Physical properties”). The lithology at Site U1369 changes from metalliferous zeolitic pelagic clay (lithologic Unit I) at the top to zeolitic metalliferous pelagic clay (Unit II) at the bottom (see “Lithostratigraphy”). The metalliferous zeolitic pelagic clay unit extends from 0 to ~6 mbsf in Hole U1369B. Using magnetic susceptibility data, it was possible to correlate between Holes U1369B and U1369C (Fig. F25). This correla-

tion was applied to the magnetic intensity data and to the inclination and declination data (Fig. F26).

Magnetic directions at Site U1369 show both reversed and normal polarity. The records show steep normal polarity for most of the site, possibly because of a magnetic overprint acquired during coring (high negative inclination), viscous remanent magnetization, or diagenetic changes in the sediment.

Given the difficulty in determining the age of the sediment section by shipboard paleomagnetic studies, chronostratigraphy for Site U1369 must be determined by postexpedition studies, including use of other chronostratigraphic tools and further magnetic cleaning by increased magnetic field AF demagnetization.

## Biogeochemistry

Site U1369 is located approximately midway between the center of the South Pacific Gyre and its southern edge. Together with the previous Site U1368, it possesses one of the two thinnest sedimentary sequences (~16–20 m thick) cored during Expedition 329. The sediment sequence is dominated by zeolitic metalliferous clay (see “Lithostratigraphy”).

The biogeochemistry group performed extensive sampling and analytical activities to address questions regarding how biogeochemical parameters in the sediment and pore water vary from gyre center (Site U1368) to midway to the southern gyre edge (Site U1369) with oceanographic factors such as ocean productivity and sedimentation rate.

Sediment samples for biogeochemical study were taken mostly from Hole U1369C. Dissolved oxygen concentrations were measured on all cores from Holes U1369B and U1369E using both electrode and optode techniques (177 total measurements) (Tables T4, T5). Thirty-three samples were collected for hydrogen analyses (Table T6), and six samples were collected for methane quantification. Twenty-three interstitial water samples were collected by whole-round squeezing (including 12 samples on the catwalk) (Table T7), and 21 samples were collected by Rhizon sampling (for nitrate and onshore analyses of nitrogen stable isotope) (Table T8). Sixteen samples were taken for solid-phase carbon and nitrogen analyses (Table T9).

### Dissolved oxygen

Dissolved oxygen (O<sub>2</sub>) was measured by optodes and electrodes in intact 1.5 m core sections from Cores 329-U1369B-1H and 2H. Further measurements using electrodes were performed on the 20–110 cm long whole-round section pieces remaining after bio-

geochemistry and microbiology sampling (Cores 329-U1369C-1H and 2H and 329-U1369E-1H and 2H). Measurements on Hole U1369B samples were performed in 10 (electrode) and 10–20 cm (optode) depth intervals in the uppermost 3 m and in 20 (electrode) and 50 cm (optode) intervals below this depth. Electrode measurements in Holes U1369C and U1369E were performed at 15–50 cm intervals in the remaining whole rounds (Table T4).

Dissolved oxygen penetrates from the seafloor to the sediment/basalt interface at Site U1369. Very good agreement exists between optode and electrode measurements in the uppermost 3 m in Hole U1369B (Fig. F27). However, the near-seafloor oxygen concentrations measured by electrode are higher in the uppermost 3 m of Hole U1369C (170–204 μM) than in Hole U1369B (158 μM) (Fig. F27). This larger value measured at the surface in Hole U1369C approximates the regional bottom water oxygen concentration (Talley, 2007). Otherwise, the oxygen profiles from Holes U1369C and U1369E are similar to those from Hole U1369B.

Oxygen concentrations (both electrode and optode) generally decline very gradually with sediment depth (Tables T4, T5; Fig. F27). This linear decrease with depth is consistent with a very slight flux of oxygen toward the basalt/sediment interface.

### Dissolved hydrogen and methane

Dissolved hydrogen (H<sub>2</sub>) concentration was quantified in 33 samples collected from Hole U1369C (Fig. F28; Table T6). Seven samples were taken on the catwalk and 26 samples were taken in the core refrigerator on the Hold Deck. The depths analyzed ranged from 0.2 to 15.7 mbsf. Based on the average of 13 blanks, the detection limit at this site is 1.3 nM. Concentration of H<sub>2</sub> is consistently low, ranging from 1.3 to 6.3 nM in the sediment column. Ten of the 33 samples were below the detection limit.

Methane concentrations are below the detection limit (<0.98 μM) in all six samples from Hole U1369B (both the IODP standard safety protocol and the refined protocol). The detection limit is defined here as three times the standard deviation of the blank (ambient air).

### Interstitial water samples

Twenty-one Rhizon samples for dissolved nitrate analyses were obtained from the whole-round samples of Hole U1369C. Two samples per section (approximate intervals from 0.5 to 1 m) were obtained. The standard deviation of duplicate analyses is 0.4%. Nitrate concentration is 38 μM in the shallowest sample (0.35 mbsf; Sample 329-U1369C-1H-1, 30–40

cm) (Fig. F29A; Table T8). This value is  $\sim 5 \mu\text{M}$  higher than inferred local bottom water (Talley, 2007). At greater depth, concentrations increase slightly but continuously to  $40.5 \mu\text{M}$  at 14.35 mbsf (Sample 329-U1369C-2H-6, 80–90 cm). The offset from bottom water and the continued increase are most likely due to mineralization of organic matter. However, the nitrate value at 15.30 mbsf (Sample 329-U1369C-2H-7, 25–35 cm) is above the general profile trend; contamination of this sample is suspected.

Phosphate was measured on 23 interstitial water samples obtained through squeezing and on an additional 20 interstitial water samples obtained with Rhizon samplers. The concentration of phosphate exhibits a clear peak in the uppermost 2 m of sediment, increasing from  $1.78 \mu\text{M}$  (Sample 329-U1369C-1H-1, 5–15 cm) to a peak of  $2.27 \mu\text{M}$  at 2.95 mbsf (Sample 1H-2, 140–150 cm) (Fig. F29B; Table T7). Below 3 mbsf, the concentration of phosphate decreases with a concave-upward profile to 10 mbsf, at which point mean phosphate concentration becomes constant with depth ( $0.95 \mu\text{M}$ ). The pooled standard deviation ( $1\sigma$ ) based on three replicate measurements of each interstitial water sample is  $0.05 \mu\text{M}$  (see “Biogeochemistry” in the “Methods” chapter [Expedition 329 Scientists, 2011a]). No significant difference was noted between samples taken on the catwalk and samples taken later in the core refrigerator on the Hold Deck. Phosphate concentrations obtained with the Rhizon sampling method (Table T8) deviate from the smooth profile obtained with the squeezed samples. Whereas the Rhizon phosphate values follow the same broad trend in concentration with depth as the squeezed samples, they deviate from the phosphate profile obtained from the squeezed interstitial water samples towards greater concentrations of  $0.9 \mu\text{M}$  at 9.45 mbsf (Sample 329-U1369C-2H-3, 90–100 cm) and  $0.8 \mu\text{M}$  at 13.85 mbsf (Sample 2H-6, 30–70 cm). The reason for this difference between the Rhizon samples and the squeezed samples is not clear, but blank tests showed that contamination by the Rhizon samplers is not the cause. The variable nature and sharp peaks in the Rhizon sampling-derived profile suggest that Rhizon sampling itself may induce artifacts. Rhizon sampling times can be up to 6 h in duration (see Fig. F11 in the “Methods” chapter [Expedition 329 Scientists, 2011a]).

Dissolved silicate concentrations exhibit a slight increase with increasing depth, from  $\sim 245 \mu\text{M}$  near the surface to nearly  $300 \mu\text{M}$  at depth (Fig. F29C). These concentrations are similar to those obtained at Sites U1367 and U1368. Pooled standard deviation for duplicate measurements is  $5 \mu\text{M}$ .

Alkalinity is  $\sim 2.5 \text{ mM}$  (Fig. F29D) in surface seafloor sediment and gradually increases to  $2.9 \text{ mM}$  at 16 mbsf (the base of the sediment column). This slight increase may be attributed to consumption of organic matter. No obvious offset was observed between alkalinity of interstitial water samples and immediately squeezed “catwalk” samples. Standard deviation and error of alkalinity measurements on standard seawater CRM94 are  $0.034$  and  $0.010 \text{ mM}$  ( $N = 11$ ), respectively.

Dissolved inorganic carbon (DIC) increases from  $2.43 \text{ mM}$  at the sediment surface to  $2.87 \text{ mM}$  at 15.4 mbsf (Fig. F29E). Two minima are observed at 3.95 mbsf ( $2.39 \text{ mM}$ ) and 12.95 mbsf ( $2.66 \text{ mM}$ ). The range in DIC values is  $0.48 \text{ mM}$ . Average standard deviation of triplicate injection of the samples is  $0.019 \text{ mM}$ . Catwalk samples do not show as large a deviation from samples stored longer as was observed at previous sites (e.g. Site U1368).

Sulfate was determined for the squeezed interstitial water samples and the Rhizon samples. The trends from the two data sets are consistent with each other (Tables T7, T8). Sulfate concentrations are  $<28.6 \text{ mM}$  throughout the entire section ( $28.6 \text{ mM}$  is inferred to be the concentration in local bottom water) (Fig. F29F). The range in the sulfate anomaly (see “Biogeochemistry” in the “Methods” chapter [Expedition 329 Scientists, 2011a]) is from  $-1.5\%$  to  $-5.7\%$  (Table T7), with the value generally decreasing with depth (Fig. F29G). The variation in the sulfate anomaly may be due to adsorption onto sediment during sample recovery and extraction, as well as uptake into the underlying basalt.

Chloride was determined in the squeezed interstitial water and Rhizon samples (Tables T7, T8). The Rhizon samples showed a general offset of  $0.2\%$  from the squeezed samples but with the same trend as the squeezed samples. Three Rhizon samples appear to be compromised and fall off the trend toward higher values. The general offset is likely caused by evaporation, as the Rhizon aliquots were smaller and stored in vials with relatively more headspace. The chloride concentration near the seafloor is indistinguishable from the inferred local bottom water (Fig. F29H). Below this depth, concentration monotonically increases by  $\sim 2 \text{ mM}$  to 10 mbsf. Below this depth, there is no significant gradient. This increase may be due to relict higher salinity seawater from the Last Glacial Maximum or to hydration of the underlying igneous crust.

As at previous sites, cations were measured at Site U1369 by both inductively coupled plasma-atomic emission spectroscopy (ICP-AES) and ion chromatog-

raphy. For the ICP-AES analyses, samples were measured in duplicate (same solution twice in two separate analytical batches) with the exception of Sr, which was measured once. The precision of cation measurements by ICP-AES was, as quantified by multiple triplicate and quadruplicate analyses of International Association for the Physical Sciences of the Oceans (IAPSO) standard seawater and internal matrix matched standards,

Ca = 0.7% of the measured value,  
 Mg = 0.7% of the measured value,  
 Na = 0.6% of the measured value,  
 K = 0.7% of the measured value,  
 Fe = 3% of the measured value,  
 Mn = 2% of the measured value,  
 B = 0.9% of the measured value, and  
 Sr = 0.9% of the measured value.

Analyzing the samples in duplicate did not appreciably change the precision of the measurements for Ca or Mg but significantly improved the precision of the measurement of Na and K and the trace elements. Accuracy of the ICP-AES results, as quantified by comparison to multiple replicate analyses of IAPSO seawater not included in the calibration, was within precision of the measurement. For the ion chromatography analyses, precision (pooled standard deviation,  $1\sigma$ ) was

Ca = 0.7%,  
 Mg = 0.3%,  
 Na = 0.2%, and  
 K = 0.3%.

The shape of the concentration profiles determined by ICP-AES and ion chromatography agree well. The absolute values of the concentrations differ by a very slight amount that is minimally greater than the respective analytical precision, as was the case at Site U1368. Again, the ion chromatography data at Site U1369 are slightly higher than the ICP-AES data. This contrast is most pronounced for Ca and less so for Na, Mg, and K. Although the ICP-AES and ion chromatography protocols were both rigorously calibrated against multiple replicate analyses of IAPSO standard, with identical items analyzed by both instruments and with detailed determinations of analytical precision, the cause of this discrepancy remains unclear. Postcruise shore-based analyses will aim to resolve this slight ambiguity.

The profile of dissolved Ca shows a slight decrease with depth, although it is difficult to resolve because of the variability with depth (Fig. F29I). Ca concentrations are lower than that of typical seawater (10.5 mM). Mg decreases by ~1–2 mM through the 16 m of the profile (Fig. F29J). This probably reflects clay alteration rather than uptake by basalt alteration,

given the near constancy (or decrease) of the Ca profile. The Na profile shows no significant change with depth, whereas that of K shows structure that is confirmed by both the ICP-AES and ion chromatography analyses (Figs. F29K, F29L). Boron concentrations are higher than typical seawater (Fig. F29M) and are constant to ~6 mbsf, after which they steadily increase to values near 530  $\mu\text{M}$ . This increase broadly follows the increase in chloride, and the concentrations are well correlated ( $r = 0.86$ ,  $p < 0.001$ ).

Concentrations of dissolved Fe and Mn are above detection limits (both ~1  $\mu\text{M}$ ), are reproducible, and co-vary (Figs. F29N, F29O). Because it is difficult to explain the presence of appreciable amounts of dissolved Fe and Mn in these oxygenated pore waters, the Fe and Mn data may record a very fine particulate or colloidal phase that is an artifact of the squeezing process. Sr appears constant with depth (Fig. F29P).

Comparison of the catwalk samples (squeezed immediately upon core recovery) to those samples stored in the core refrigerator on the Hold Deck (see “**Bio-geochemistry**” in the “Methods” chapter [Expedition 329 Scientists, 2011a]) shows no offset between the data sets for any cation.

### Solid-phase carbon and nitrogen

Contents of total carbon, total organic carbon (TOC), total inorganic carbon (TIC), and total nitrogen were determined for 16 samples from Hole U1369B (Fig. F30; Table T9). Total nitrogen rapidly decreases from 0.070 wt% at the seafloor to 0.026 wt% at 2.86 mbsf, followed by a smaller decrease toward the basement, reaching 0.010 wt% at 15.45 mbsf. TOC also rapidly decreases from 0.19 wt% at 0.11 mbsf to 0.07 wt% at 2.86 mbsf, gently decreasing thereafter to 0.03 wt% at 15.45 mbsf. Total carbon decreases from 0.24 wt% at 0.11 mbsf to 0.08 wt% at 4.36 mbsf and then is 0.06 wt% to basement (15.45 mbsf).

The TIC values obtained by coulometry follow a pattern very different from the total carbon content obtained from the CHNS elemental analyzer. Calculated  $\text{CaCO}_3$  content increases from 0.07 wt% at 0.11 mbsf to 0.35 wt% at 15.45 mbsf. TIC content increases from 0.01 wt% at 0.11 mbsf to 0.04 wt% at 15.45 mbsf.

## Microbiology

Sediment samples for microbiological studies were obtained by APC coring, primarily in Holes U1369C and U1369E. Sample contamination was monitored

by PFT injection into the drilling fluid. Samples for cell counting and virus-like particle (VLP) abundance were taken from the cut cores facing interstitial water whole-round samples. After core recovery on the catwalk, core sections were immediately transferred to the core refrigerator on the Hold Deck, where microbiological whole-round cores were sampled. The temperature of the core refrigerator was 7°–10°C. Microbiological whole-round cores were generally taken at a high depth resolution from the first core (1H), as well as the core above the sediment/basalt interface (Core 2H).

### Cell abundance

Microbial cells were enumerated by direct counting using epifluorescence microscopy (see “**Microbiology**” in the “Methods” chapter [Expedition 329 Scientists, 2011a]). Sediment subcores (2 cm<sup>3</sup>) were taken using tip-cut syringes from Hole U1369C for shipboard analysis. For shore-based analysis, 10 cm whole-round cores were taken from Hole U1369E and frozen at –80°C. Thirty-two 2 cm<sup>3</sup> syringe samples (Table **T10**) and six whole-round cores (Sections 329-U1369E-1H-1, 1H-2, 1H-4, 2H-2, 2H-4, and 2H-5) were taken from Site U1369.

Six blanks were prepared and counted during processing of the samples from Site U1369. Instead of Tris-EDTA (TE) buffer, a slurry of heat-sterilized sediment (4 h at 450°C) was used as a blank. The mean values of the heat sterilized blanks was  $6.1 \times 10^2$  cells/cm<sup>3</sup> with a standard deviation of  $2.9 \times 10^2$  cells/cm<sup>3</sup>, resulting in a minimum detection limit (MDL; blank plus three times standard deviation) of  $1.5 \times 10^3$  cells/cm<sup>3</sup>. As the blanks did not vary much between sites, they were pooled from all sites. At the end of the expedition, a single MDL for all sites ( $1.4 \times 10^3$  cells/cm<sup>3</sup>) was calculated based on the extended database.

Cell abundance in the uppermost sample (329-U1369C-1H-1, 15–20 cm) is  $\sim 8 \times 10^4$  cells/cm<sup>3</sup>. Numbers decreased sharply to  $\sim 10^3$  cells/cm<sup>3</sup> at 2 mbsf (Sample 1H-2, 50–60 cm) and remained below the MDL downhole to the basement (Fig. **F31**). Because of the limited transit time from Site U1369 to U1370, only two samples (329-U1369C-1H-1, 15–20 cm, and 135–140 cm) were recounted by another shipboard microbiologist for cross-comparison. These counts were in good agreement with each other, suggesting that differences in cell recognition among microscope observers is small (Table **T10**). Cell counts on samples without cell extraction were made on the three uppermost samples (329-U1369C-1H-1, 15–20 cm, 50–60 cm, and 100–110 cm). Cells were only detected in the topmost nonextracted sample, where

abundance was  $\sim 4 \times 10^5$  cells/cm<sup>3</sup> (slightly higher than in the extracted samples). Both deeper samples were below the blank.

### Virus abundance

Samples for counting VLPs at a high depth resolution were taken from Holes U1369C and U1369E (Table **T11**). A subset of these samples was used for shipboard counting of VLPs, and other syringe samples were preserved at –80°C for shore-based analyses. Enumeration of VLPs followed the protocol described in “**Microbiology**” in the “Methods” chapter (Expedition 329 Scientists, 2011a).

For the uppermost sample (329-U1369C-1H-1, 15–20 cm),  $1.7 \times 10^6$  VLP/cm<sup>3</sup> were observed. VLP abundance decreased rapidly within the uppermost 2 m of the sediment column, and the numbers of VLPs are generally higher than cell numbers estimated by direct microscopic count (Fig. **F31**). The number of VLPs is  $\sim 10^5$  VLP/cm<sup>3</sup> (Sample 329-U1369C-1H-2, 135–140 cm) at 2 mbsf and decreases slightly with depth. Samples from deeper horizons (Sections 329-U1369C-2H-3 and 2H-6 and 329-U1369E-2H-5 and 2H-6) were not counted onboard due to ship movement during transit.

### Cultivation

#### Sediment samples

Sediment whole-round cores were subsampled aseptically with sterilized tip-cut syringes to make slurries for inoculation of a variety of media (Table **T12**). Additional samples (referred to as SLURRY in Table **T12**) were stored in N<sub>2</sub>-flushed serum bottles or in syringes packed in sterile foil packs and stored at 4°C for shore-based cultivation experiments.

#### Seawater control sample

A surface seawater sample was collected from Site U1369 with a sterile 500 mL glass bottle immediately after the R/V *JOIDES Resolution* arrived at the site. Cultivation of aerobic heterotrophic bacteria in the seawater sample was performed on marine agar and marine R2A plates (see Table **T8** in Expedition 329 Scientists, 2011a) at 25°C. The abundance of cultivable aerobic heterotrophic bacteria on marine R2A plates was  $\sim 1$  colony-forming unit (cfu)/mL. No visible colonies were observed on marine agar after three days of incubation.

Bottom seawater was collected from the mudline of the upper core (1H) of Holes U1369A–U1369D, placed in a sterile plastic bag, and stored at 4°C. The water was filtered through 0.2 μm pore sized polycarbonate filters into sterile 50 mL serum bottles and

flushed with N<sub>2</sub> for 5 min. The bottles were capped with rubber stoppers and aluminum crimp caps and stored at 4°C for future preparation of liquid media on shore. Aerobic heterotrophic bacteria were cultured from the unfiltered sample at 25°C for 3 days. The abundance of cultivable aerobic heterotrophic bacteria on marine agar and R2A plates were  $\sim 5.7 \times 10^3$  and  $\sim 5.2 \times 10^3$  cfu/mL, respectively, which is in marked contrast to numbers obtained from surface seawater as described above. The estimated abundance of *Vibrio*-like species, based on selective enrichment for this genus on thiosulfate citrate bile salts sucrose agar, was  $\sim 15$  cfu/mL.

## Molecular analyses

### Sediment samples

Three whole-core samples were taken from Hole U1369E (Sections 329-U1369E-1H-3, 2H-2, and 2H-4) as routine microbiology samples (curatorial code MBIO) and transferred to  $-80^\circ\text{C}$  freezers for storage. These samples will be available for shore-based molecular studies (See “[Microbiology](#)” in the “Methods” chapter [Expedition 329 Scientists, 2011a]).

### Deep seawater control samples

As a control sample for shore-based molecular analyses,  $\sim 300$  mL of bottom seawater was collected from the mudline of the uppermost cores (1H) of Holes U1369A–U1369D. The water was collected in a sterile plastic bag and stored at 4°C in the Microbiology Laboratory until further processing. The sample was filtered through 0.2  $\mu\text{m}$  polycarbonate membrane filters under aseptic conditions and stored at  $-80^\circ\text{C}$  for shore-based microbiological analyses.

## Fluorescence in situ hybridization analysis

Duplicate 10 cm<sup>3</sup> subcores of sediment from Sections 329-U1369E-1H-1, 1H-2, 2H-1, 2H-3, and 2H-6 were fixed as described in “[Microbiology](#)” in the “Methods” chapter (Expedition 329 Scientists, 2011a) for shore-based fluorescence in situ hybridization analyses.

## Radioactive and stable isotope tracer incubation experiments

Stable isotope (<sup>13</sup>C and <sup>15</sup>N) experiments to measure carbon and nitrogen uptake activities were initiated on board in the Isotope Isolation Van. Sediment subcores (15 cm<sup>3</sup>) were taken from the inner part of 20 cm whole-round cores, placed in a sterile glass vials, flushed with N<sub>2</sub>, sealed with a rubber stopper, and stored until processing in the core refrigerator on the Hold Deck (see “[Microbiology](#)” in the “Methods” chapter [Expedition 329 Scientists, 2011a]). From

Site U1369, four whole-round cores (Sections 329-U1369E-1H-2, 2H-2, 2H-5, and 2H-6) were processed for the stable isotope tracer incubation experiments, as described in the U1365 site report (see “[Microbiology](#)” in the “Site U1365” chapter [Expedition 329 Scientists, 2011b]).

Four whole-round intervals from Site U1369 were collected for slurry experiments on potential metabolic activities (i.e., assimilation and dissimilative respiration) using radio- and stable isotopes (intervals 329-U1369C-1H-2, 110–130 cm; 1H-4, 100–123 cm; 2H-3, 120–140 cm; and 2H-6, 110–130 cm) (see “[Microbiology](#)” in the “Methods” chapter [Expedition 329 Scientists, 2011a]) and stored in the core refrigerator of the Hold Deck prior to the isotopic sample processing.

For stable isotope probing and nuclear magnetic resonance biomass experiments, two sediment whole-round cores were collected from Hole U1369C (Samples 329-U1369C-1H-1, 120–130 cm, and 2H-5, 120–130 cm). Subsamples were taken with 5 cm<sup>3</sup> tip-cut syringes and amended with stable isotope tracers dissolved in low-nutrient growth media (<sup>13</sup>C-labeled acetate, benzoate, methanol, and methane sulfonic acid) and incubated at 4°C (see “[Microbiology](#)” in the “Methods” chapter [Expedition 329 Scientists, 2011a]) in the Isotope Isolation Van.

For sulfate reduction rate measurements, four whole-round cores were collected from Hole U1369C (Samples 329-U1369C-1H-2, 60–65 cm; 2H-1, 60–65 cm; 2H-4, 60–65 cm; and 2H-7, 54–59 cm). Five to seven subsamples ( $\sim 2.5$  cm<sup>3</sup>) were collected from each whole-round core for the shore-based distillation analysis of <sup>35</sup>S-labeled reduced sulfur (see “[Microbiology](#)” in the “Methods” chapter [Expedition 329 Scientists, 2011a]).

## Contamination assessment

### Perfluorocarbon tracer

We used perfluoromethylcyclohexane as PFT to monitor the level of drilling fluid contamination in sediment cores. PFT was continuously injected into drilling fluids during APC coring in Holes U1369C and U1369E. Sediment subcores (3 cm<sup>3</sup>) were taken from whole-round cores on the catwalk and in the core refrigerator and stored in vials with 2 mL of water for postexpedition gas chromatography measurement (see “[Microbiology](#)” in the “Methods” chapter [Expedition 329 Scientists, 2011a]).

## References

- D’Hondt, S., Abrams, L.J., Anderson, R., Dorrance, J., Durbin, A., Ellett, L., Ferdelman, T., Fischer, J.,

- Forschner, S., Fuldauer, R., Goldstein, H., Graham, D., Griffith, W., Halm, H., Harris, R., Harrison, B., Hasiuk, F., Horn, G., Kallmeyer, J., Lever, M., Meyer, J., Morse, L., Moser, C., Murphy, B., Nordhausen, A., Parry, L., Pockalny, R., Puschell, A., Rogers, J., Schrum, H., Smith, D.C., Soffientino, B., Spivack, A.J., Stancin, A., Steinman, M., and Walczak, P., 2011. KNOX-02RR: drilling site survey—life in subseafloor sediments of the South Pacific Gyre. *In* D'Hondt, S., Inagaki, F., Alvarez Zarikian, C.A., and the Expedition 329 Scientists, *Proc. IODP, 329*: Tokyo (Integrated Ocean Drilling Program Management International, Inc.). [doi:10.2204/iodp.proc.329.112.2011](https://doi.org/10.2204/iodp.proc.329.112.2011)
- D'Hondt, S., Spivack, A.J., Pockalny, R., Ferdelman, T.G., Fischer, J.P., Kallmeyer, J., Abrams, L.J., Smith, D.C., Graham, D., Hasiuk, F., Schrum, H., and Stancine, A.M., 2009. Subseafloor sedimentary life in the South Pacific Gyre. *Proc. Natl. Acad. Sci. U. S. A.*, 106(28):11651–11656. [doi:10.1073/pnas.0811793106](https://doi.org/10.1073/pnas.0811793106)
- Ekdale, A.A., Bromley, R.G., and Pemberton, S.G. (Eds.), 1984. *Ichnology: The Use of Trace Fossils in Sedimentology and Stratigraphy*. SEPM Short Course, 15.
- Expedition 329 Scientists, 2011a. Methods. *In* D'Hondt, S., Inagaki, F., Alvarez Zarikian, C.A., and the Expedition 329 Scientists, *Proc. IODP, 329*: Tokyo (Integrated Ocean Drilling Program Management International, Inc.). [doi:10.2204/iodp.proc.329.102.2011](https://doi.org/10.2204/iodp.proc.329.102.2011)
- Expedition 329 Scientists, 2011b. Site U1365. *In* D'Hondt, S., Inagaki, F., Alvarez Zarikian, C.A., and the Expedition 329 Scientists, *Proc. IODP, 329*: Tokyo (Integrated Ocean Drilling Program Management International, Inc.). [doi:10.2204/iodp.proc.329.103.2011](https://doi.org/10.2204/iodp.proc.329.103.2011)
- Fischer, J.P., Ferdelman, T.G., D'Hondt, S., Røy, H., and Wenzhöfer, F., 2009. Oxygen penetration deep into the sediment of the South Pacific Gyre. *Biogeosciences*, 6:1467–1478. <http://www.biogeosciences.net/6/1467/2009/bg-6-1467-2009.pdf>
- Gradstein, F.M., Ogg, J.G., and Smith, A.G. (Eds.), 2004. *A Geologic Time Scale 2004*: Cambridge (Cambridge Univ. Press). <http://cambridge.org/uk/catalogue/catalogue.asp?isbn=9780521781428>
- Talley, L.D., 2007. *Hydrographic Atlas of the World Ocean Circulation Experiment (WOCE) (Vol. 2): Pacific Ocean*. Sparrow, M., Chapman, P., and Gould, J. (Eds.): Southampton, U.K. (International WOCE Project Office). [http://www-pord.ucsd.edu/whp\\_atlas/pacific\\_index.html](http://www-pord.ucsd.edu/whp_atlas/pacific_index.html)

**Publication:** 13 December 2011

**MS 329-107**

**Figure F1.** Multibeam bathymetry of the Site U1369 survey area with the KNOX-02RR survey track overlain. sol = start of seismic line, eol = end of seismic line, z = time (Greenwich Mean Time), sp = shotpoint.

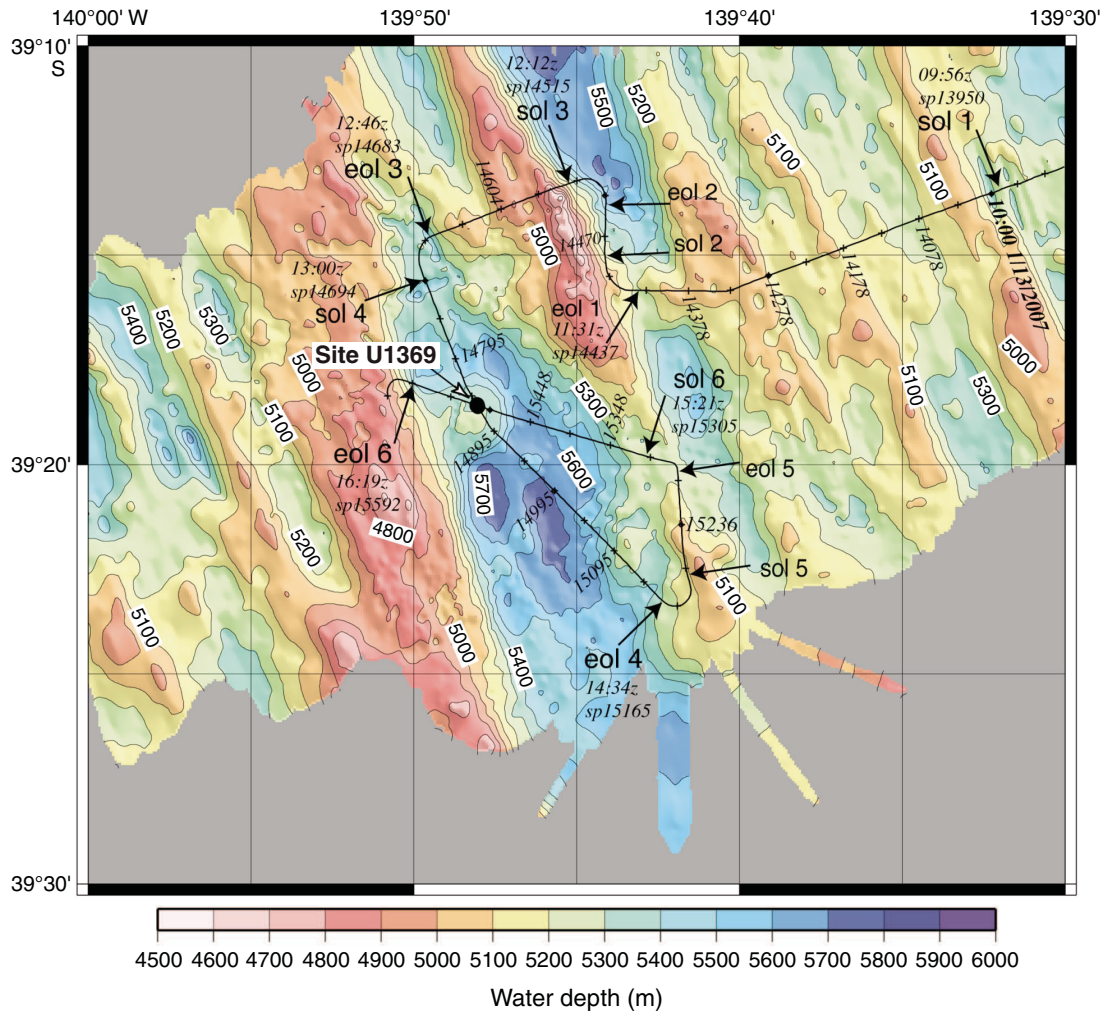


**Figure F2.** KNOX-02RR seismic survey track, Site U1369. sol = start of seismic line, eol = end of seismic line, z = time (Greenwich Mean Time), sp = shotpoint.

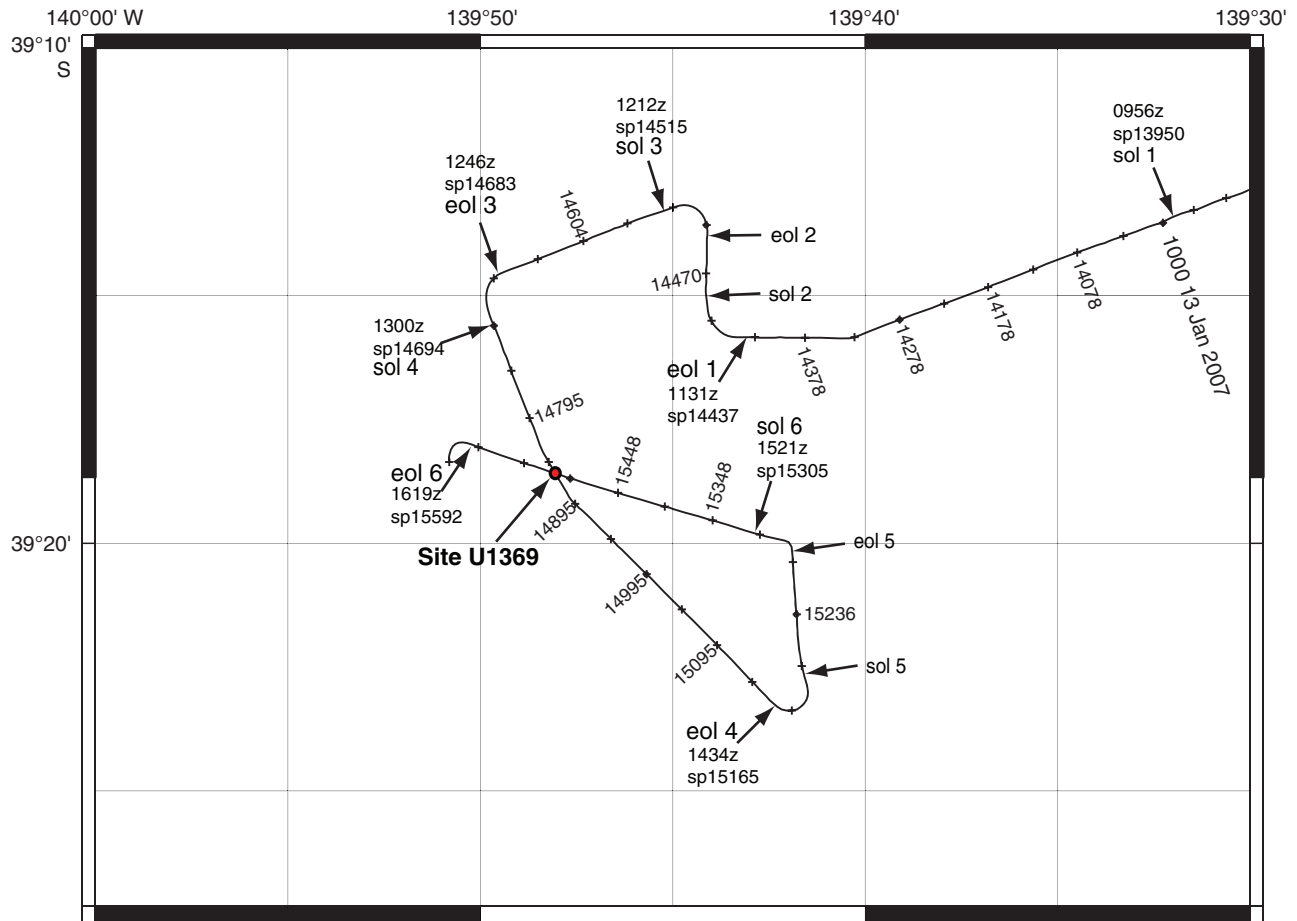




**Figure F3.** Portion of KNOX-02RR Channel 48 of MCS Line 4 across Site U1369. z = time (Greenwich Mean Time), SP = shotpoint, MORB = mid-ocean-ridge basalt, WD = water depth, SCS = single-channel seismic, BP = band-pass, AGC = automatic gain control, VE = vertical exaggeration.

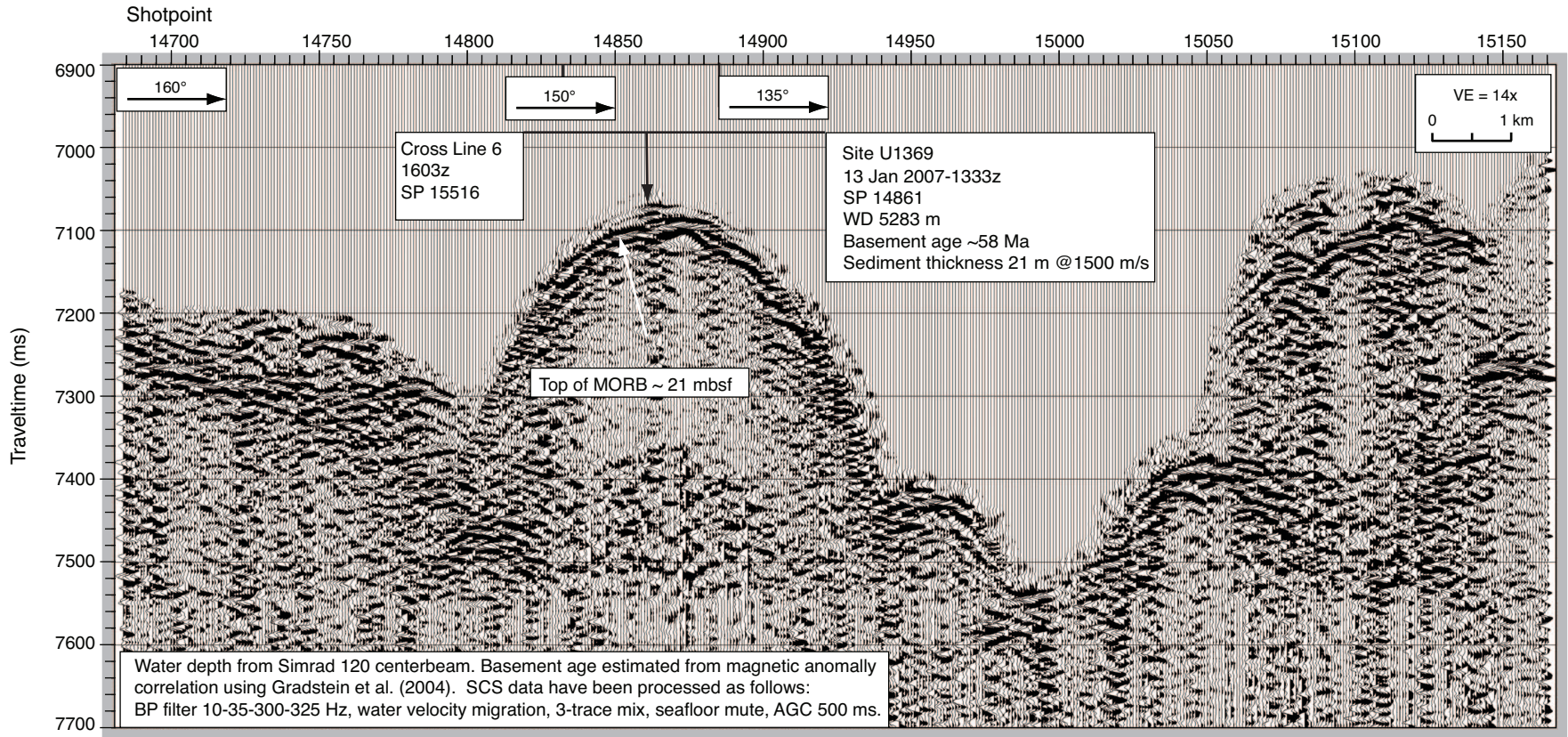




**Figure F4.** Portion of KNOX-02RR Channel 48 of MCS Line 6 crossing MCS Line 4, northeast of Site U1369.  $z$  = time (Greenwich Mean Time), SP = shotpoint, MORB = mid-ocean-ridge basalt, WD = water depth, SCS = single-channel seismic, BP = band-pass, AGC = automatic gain control, VE = vertical exaggeration.

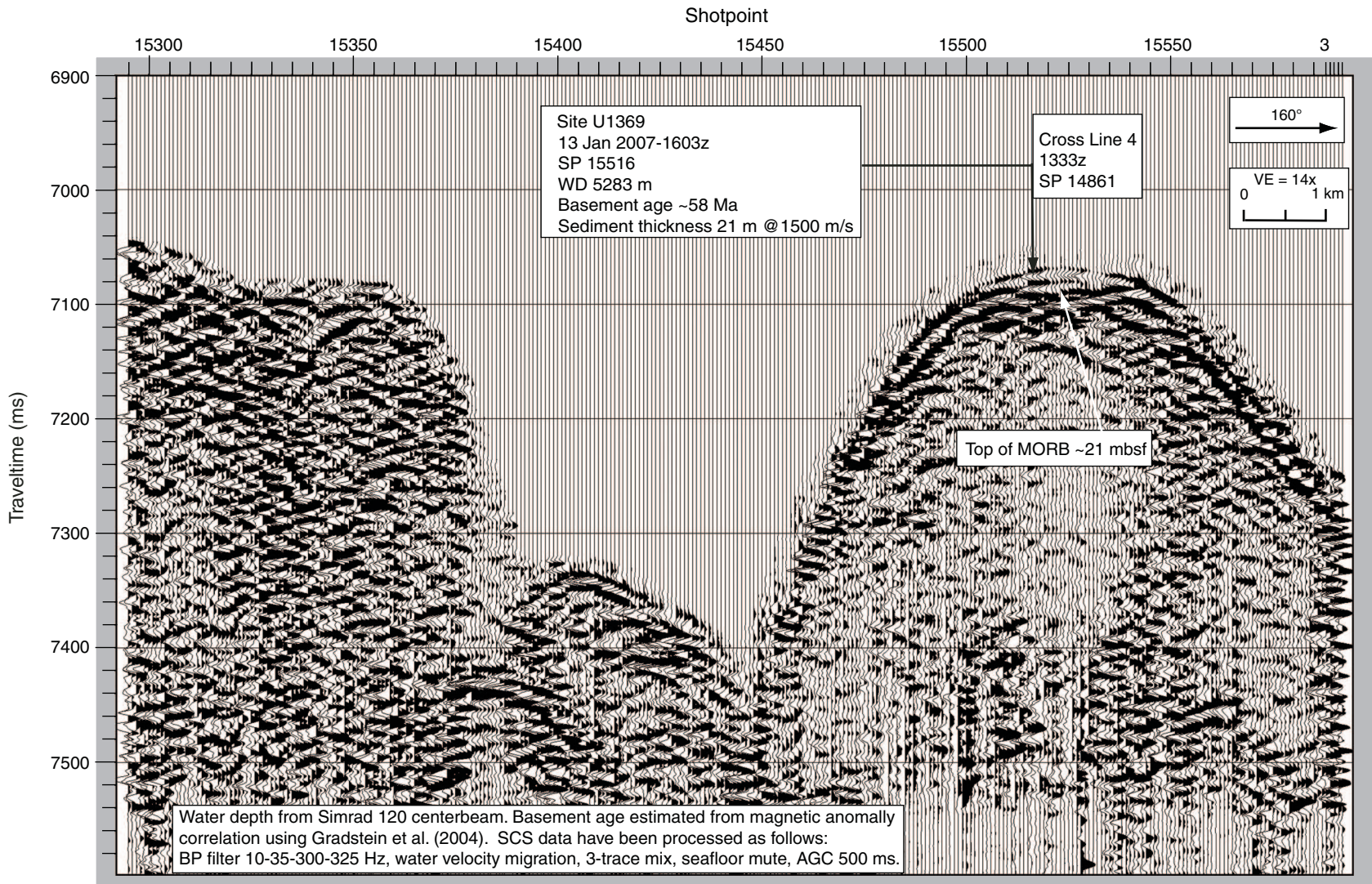




Figure F5. Portion of KNOX-02RR, 3.5 kHz Line 4 across Site U1369. MORB = mid-ocean-ridge basalt.

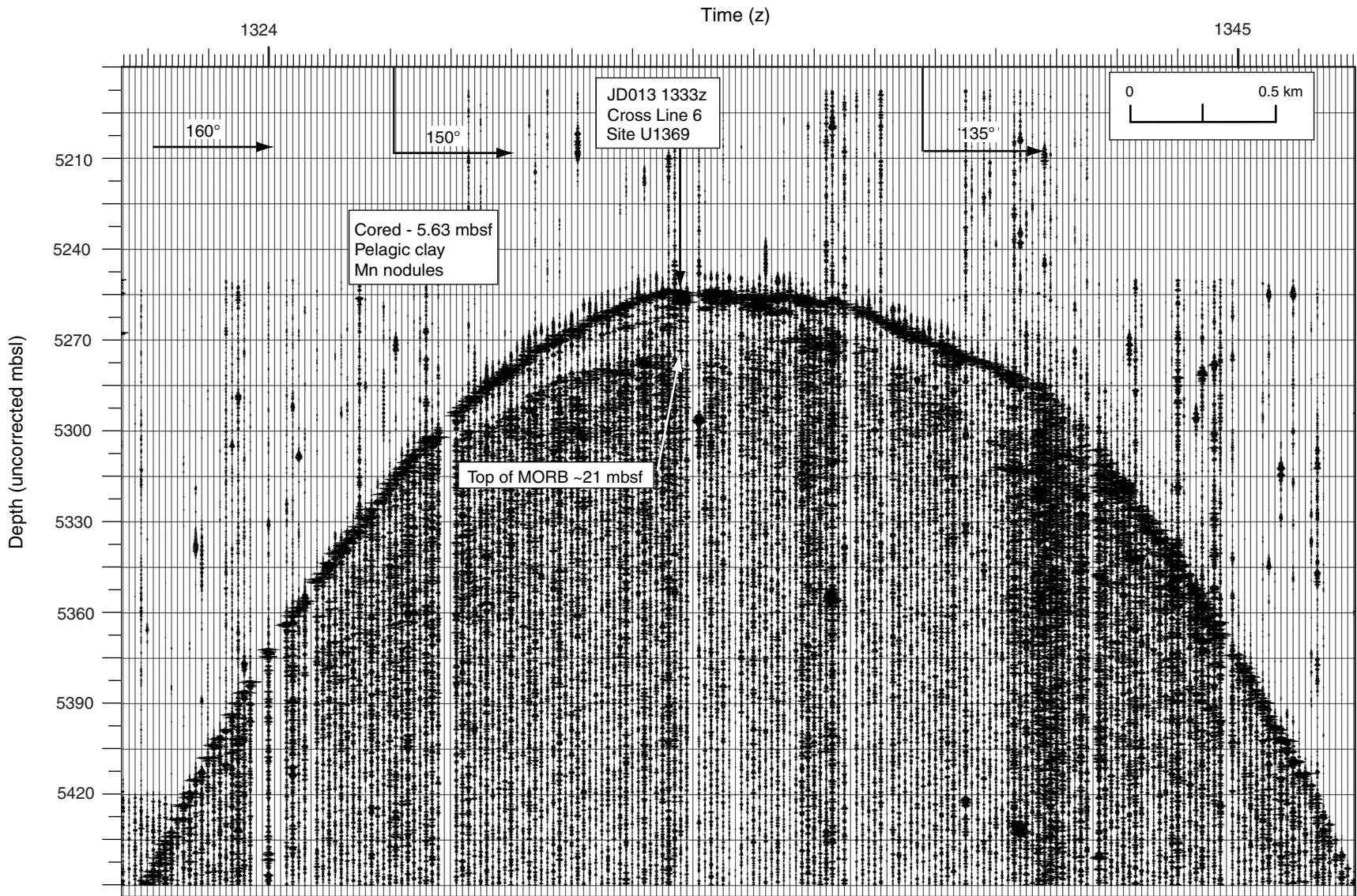
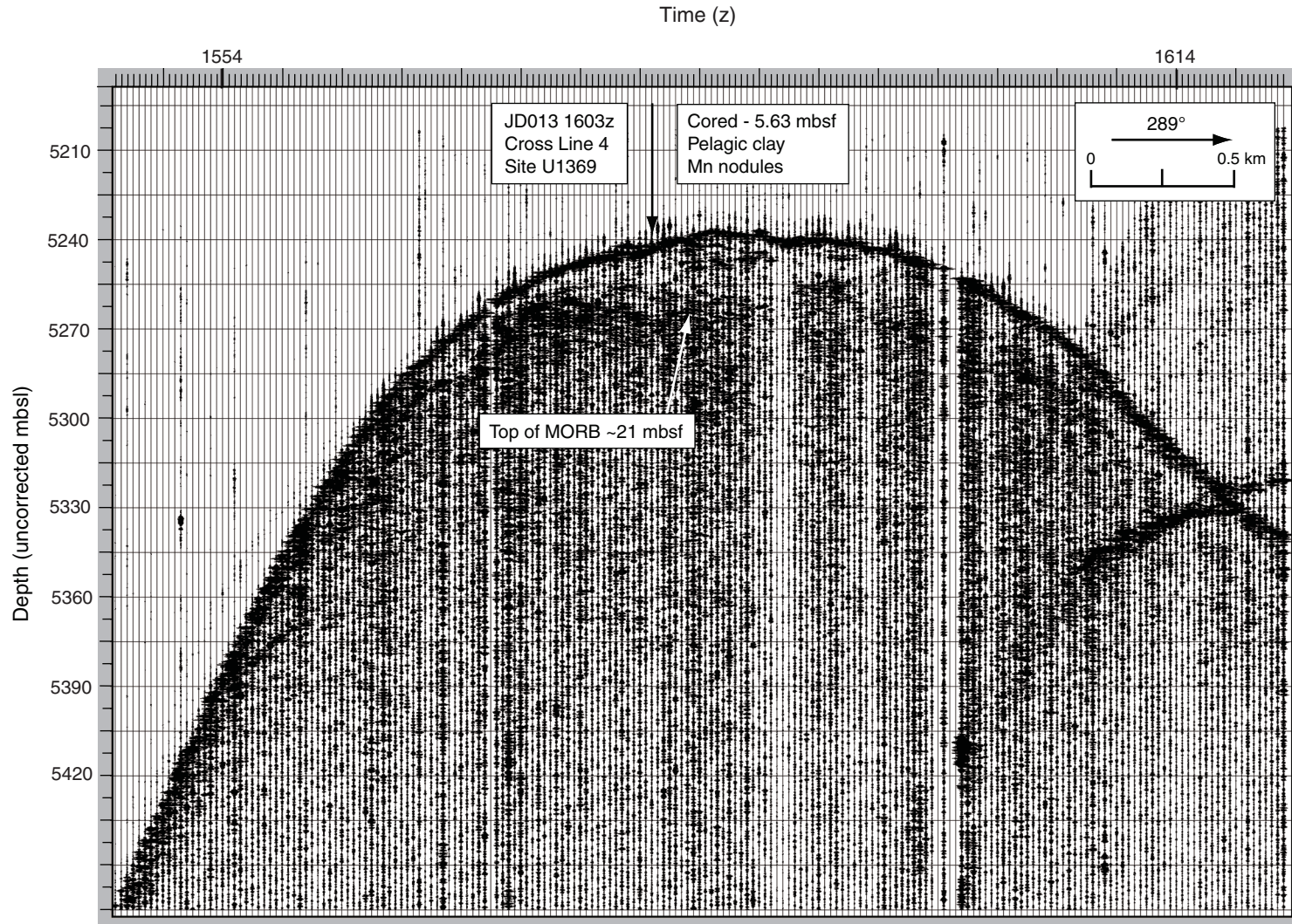




Figure F6. A portion of KNOX-02RR, 3.5 kHz Line 6 across Site U1369. MORB = mid-ocean-ridge basalt.



**Figure F7.** Lithology summary and physical property data, Hole U1369B. MS = magnetic susceptibility, GRA = gamma ray attenuation, K = absolute potassium concentration, based on analysis of spectral gamma ray responses, NGR = natural gamma radiation, RSO = red-brown to yellow-brown semiopaque oxide.

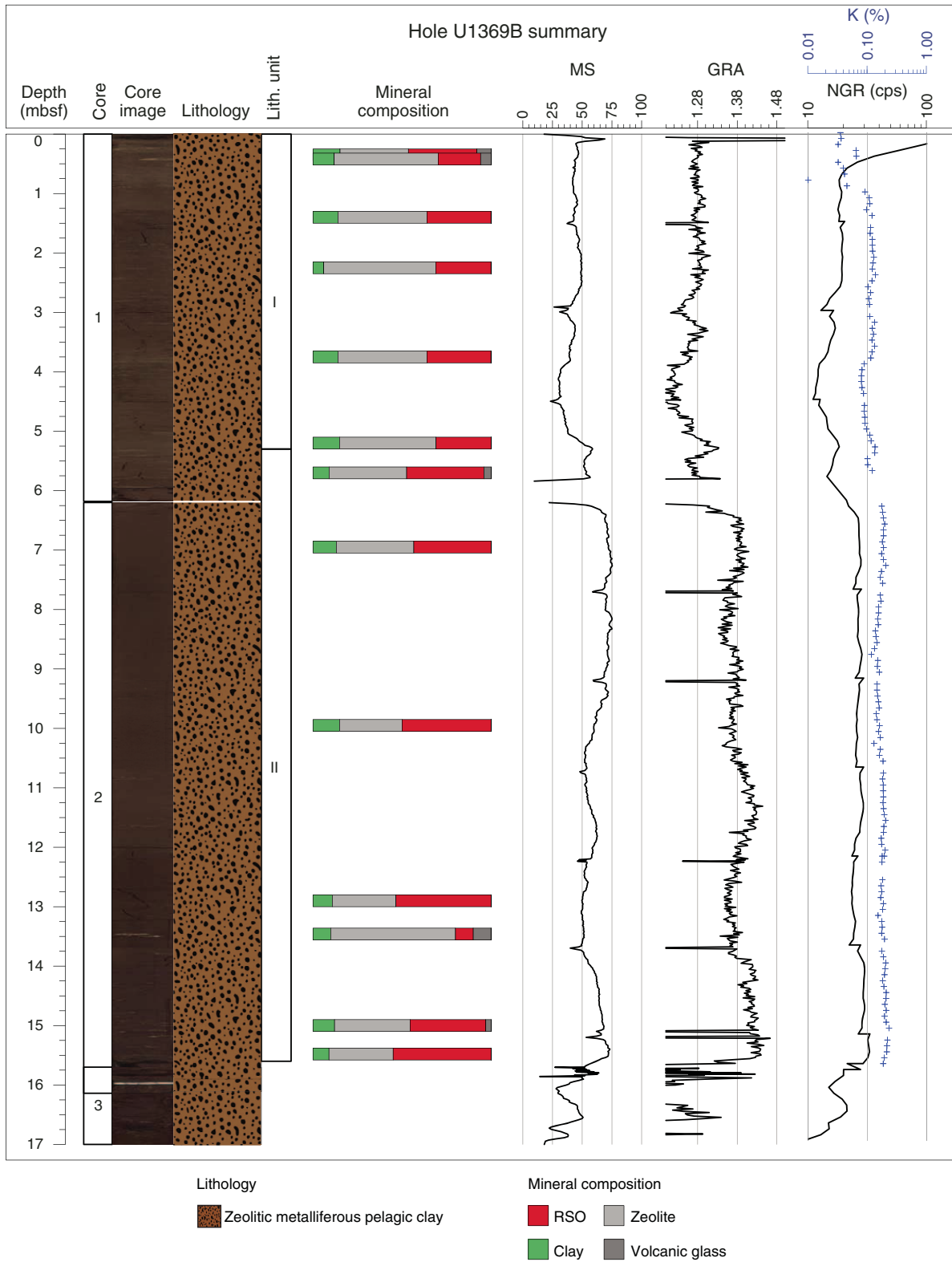
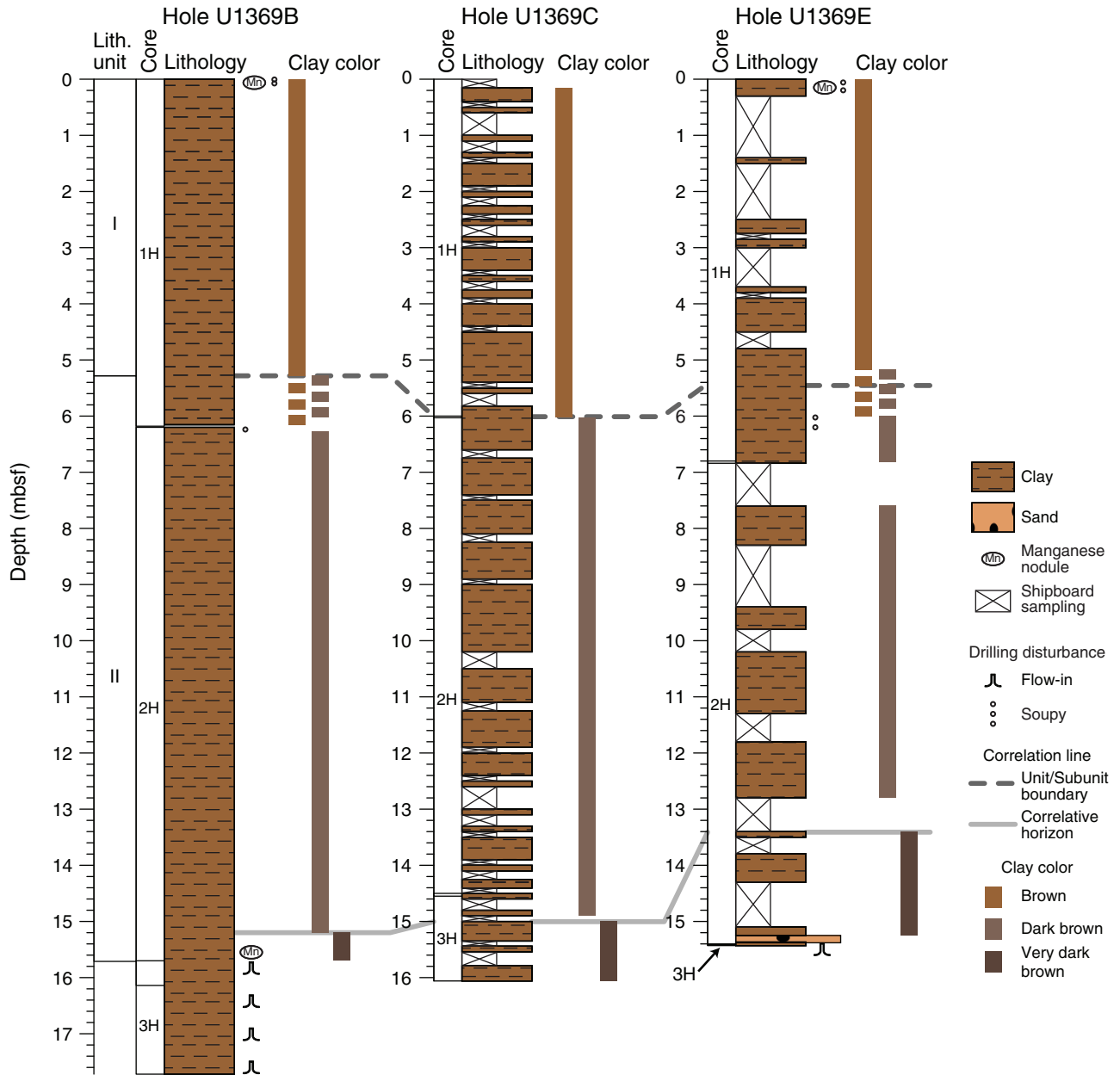
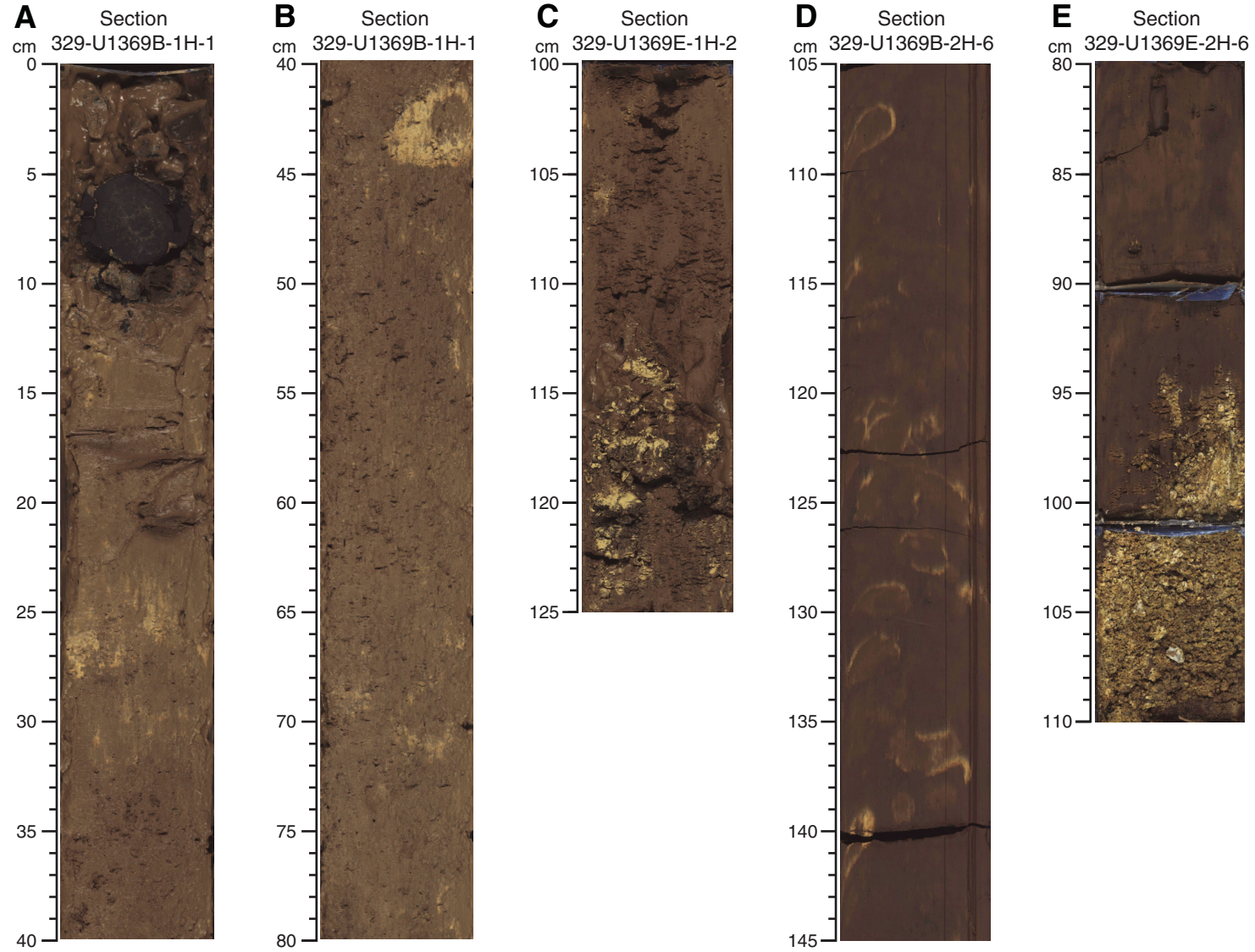


Figure F8. Lithostratigraphic correlations of holes at Site U1369.

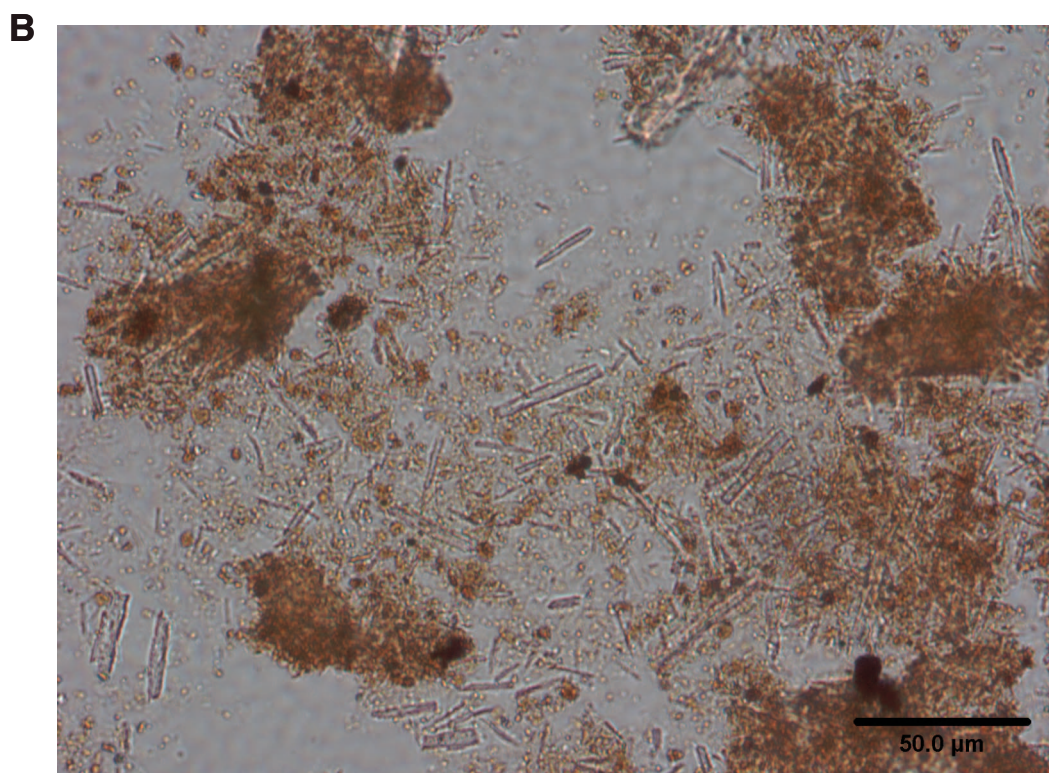
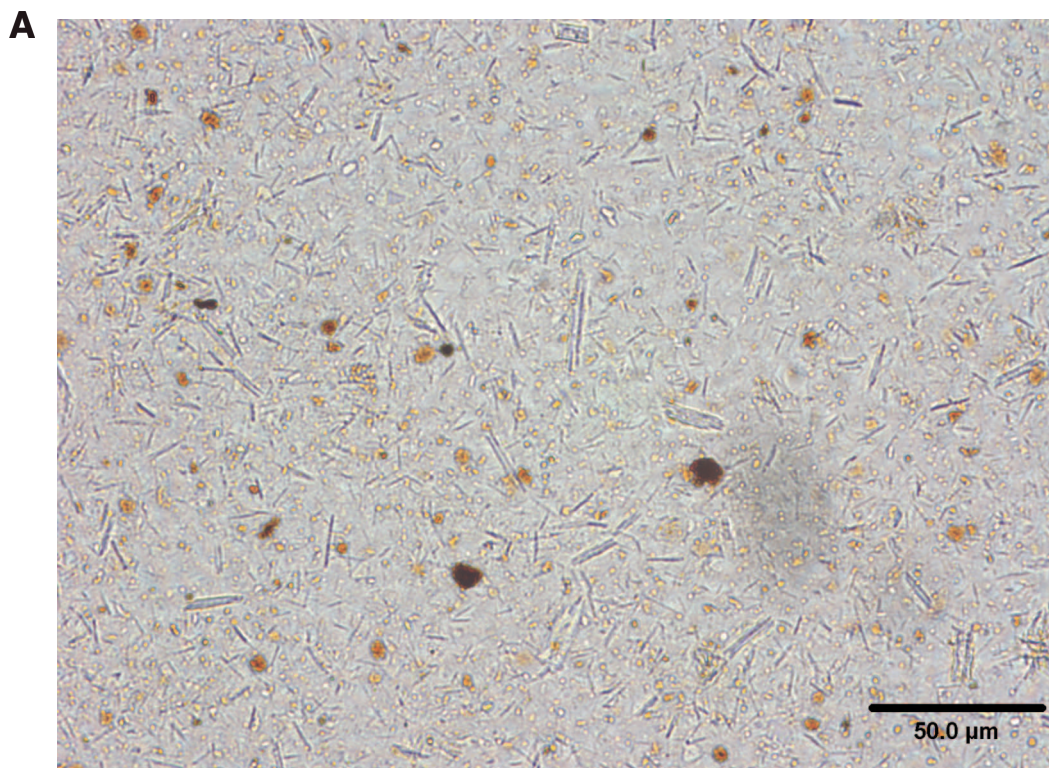




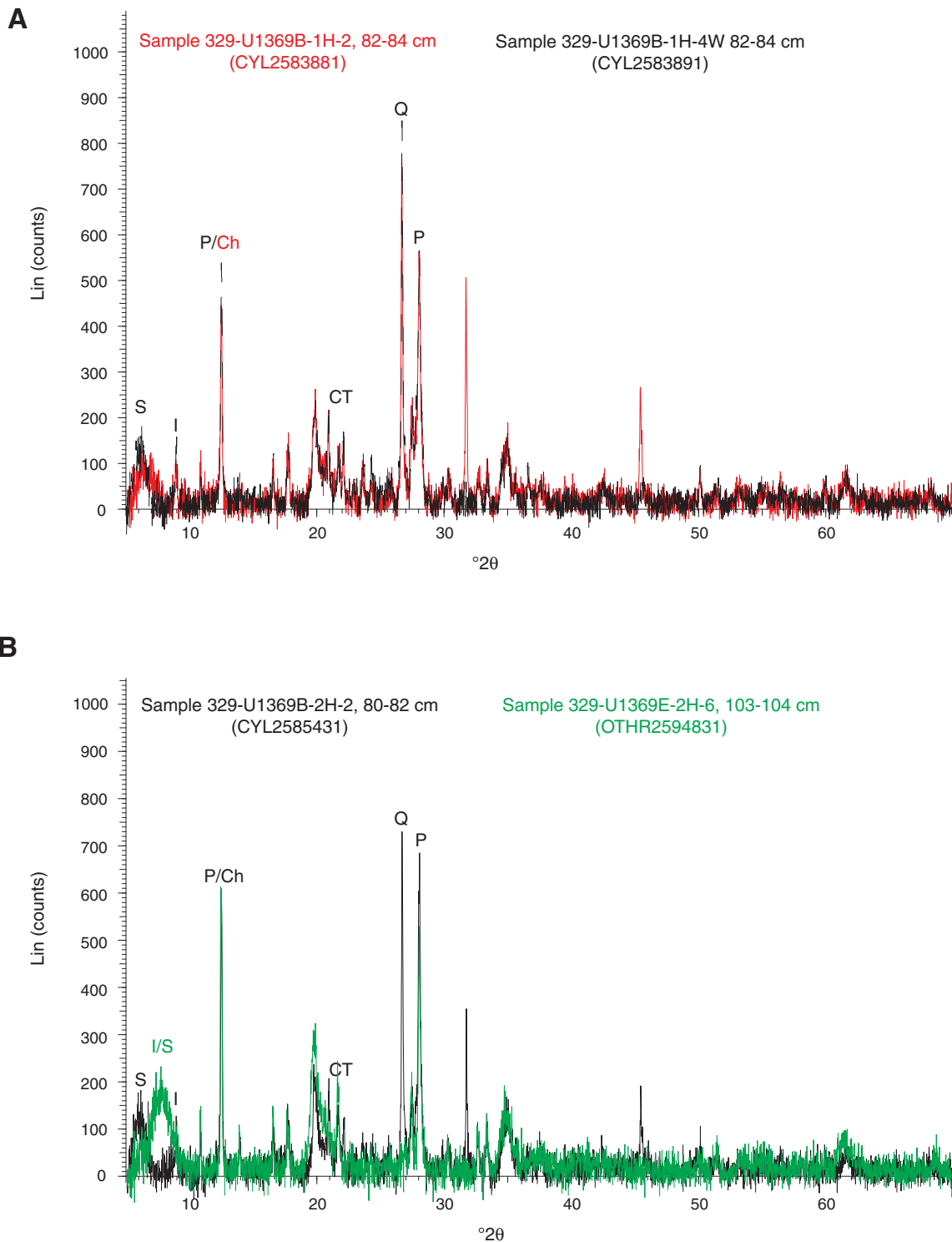
**Figure F9.** Representative core photographs, Site U1369. **A.** Manganese nodule at the top of Unit I (interval 329-U1369B-1H-1, 0–40 cm). **B.** Brown zeolitic metalliferous pelagic clay containing burrows in Unit I (interval 329-U1369B-1H-1, 40–80 cm). **C.** Brown zeolitic metalliferous pelagic clay containing hardground in Unit I (interval 329-U1369E-1H-2, 100–125 cm). **D.** Very dark brown zeolitic metalliferous clay containing burrows in Unit II (interval 329-U1369B-2H-6, 105–145 cm). **E.** Contact with altered basalt, lowermost part of Unit II (interval 329-U1369E-2H-6, 80–110 cm).



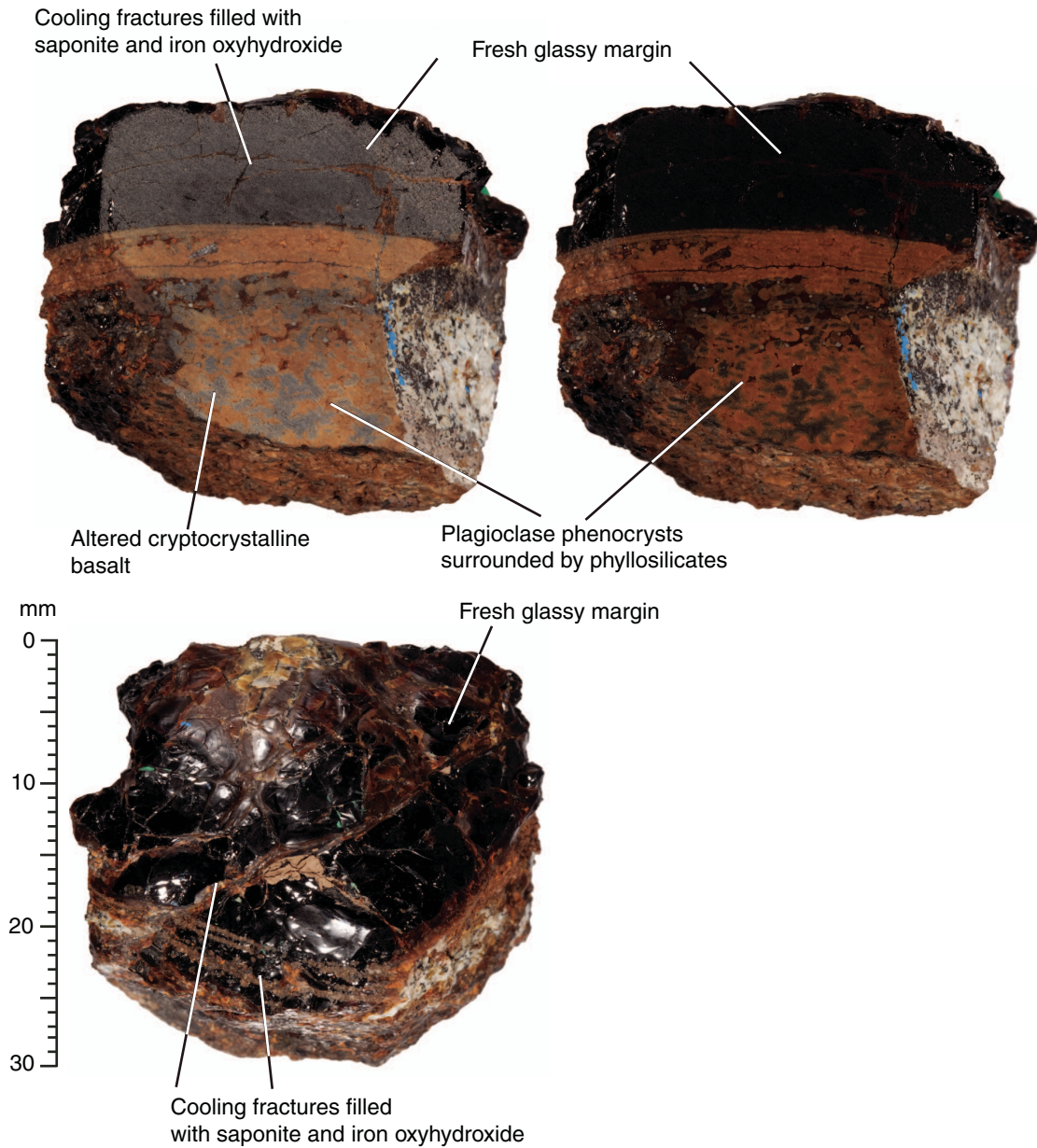
**Figure F10.** Selected smear slide photomicrographs of clay-rich sediment, Site U1369. **A.** Middle of Unit I showing the abundance of phillipsite that is typical of this interval. **B.** Enlarged crystal size of phillipsite and increased concentration of RSO.

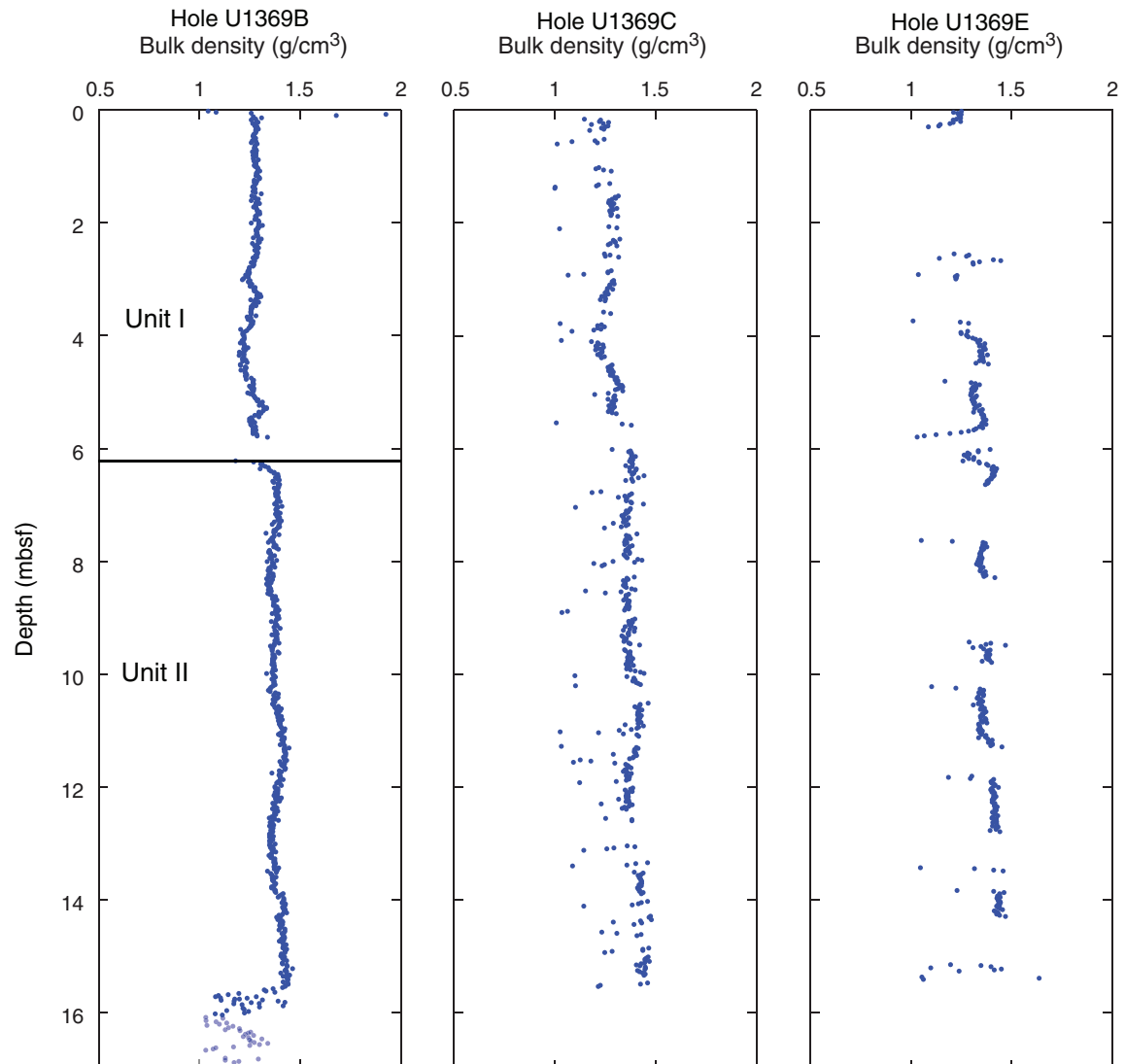


**Figure F11.** X-ray diffractograms of selected sediment, Site U1369. **A.** Unit I. Red = upper part of Unit I, black = clay from Unit I–II transition. Phillipsite (P), smectite (S), illite (I), cristobalite-tridymite (CT), and quartz (Q) peaks are present in both samples. Only principal peaks are annotated. Chlorite (Ch) is only present in the upper sample. **B.** Unit II. Upper sample (black) is representative of the majority of Unit II lithology. Lower sample (green) is from the olive-yellow sand/breccia underlying Unit II pelagic clay. Phillipsite peaks are expressed in both diffractograms. Illite/smectite (I/S) is an XRD pattern distinct from the smectite and illite peaks found in other clay at Site U1369.

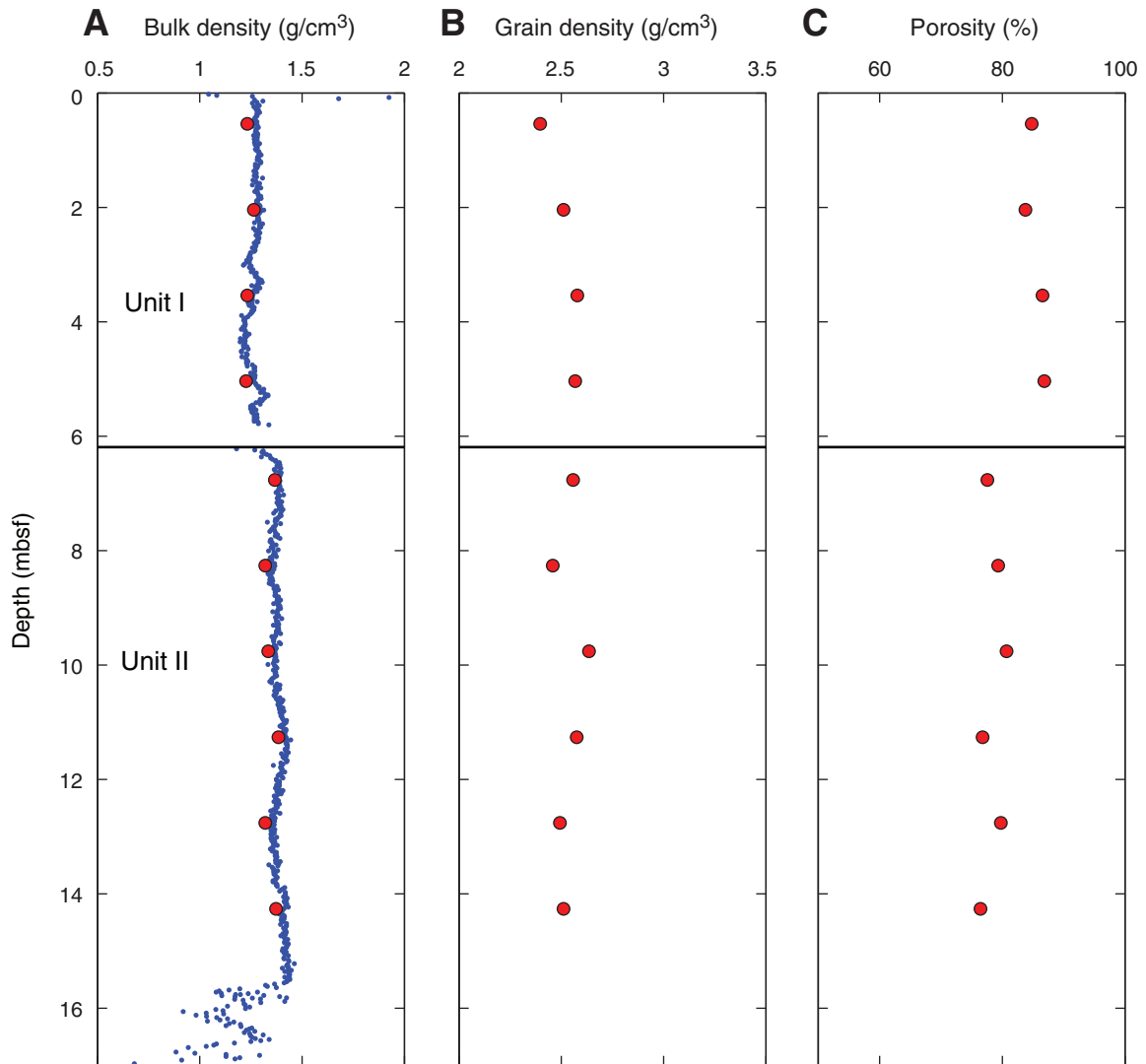


**Figure F12.** Core images and photomicrograph of basaltic fragment (interval 329-U1369B-3H-CC, 0–5 cm; plane-polarized light at 5× magnification).

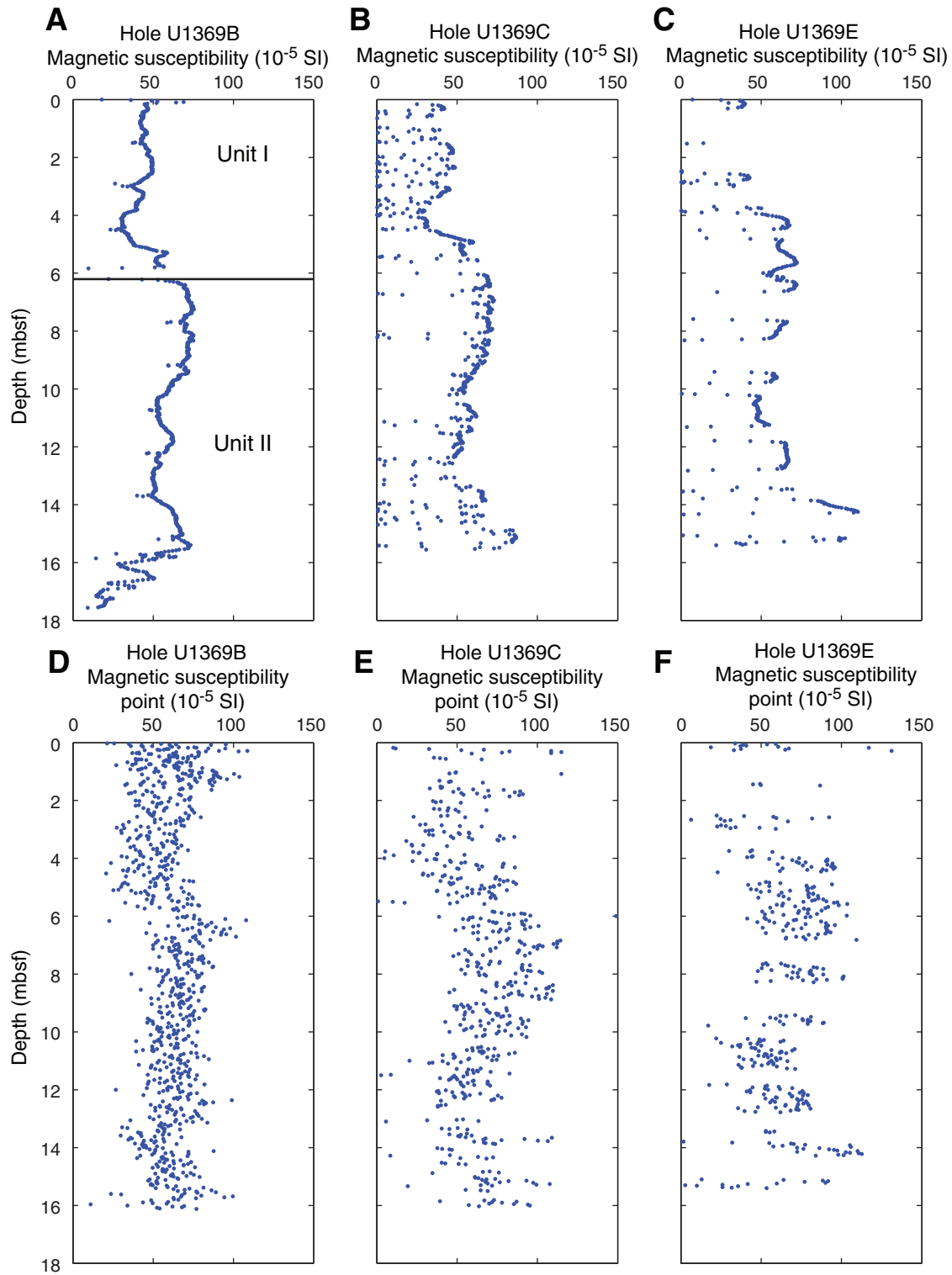


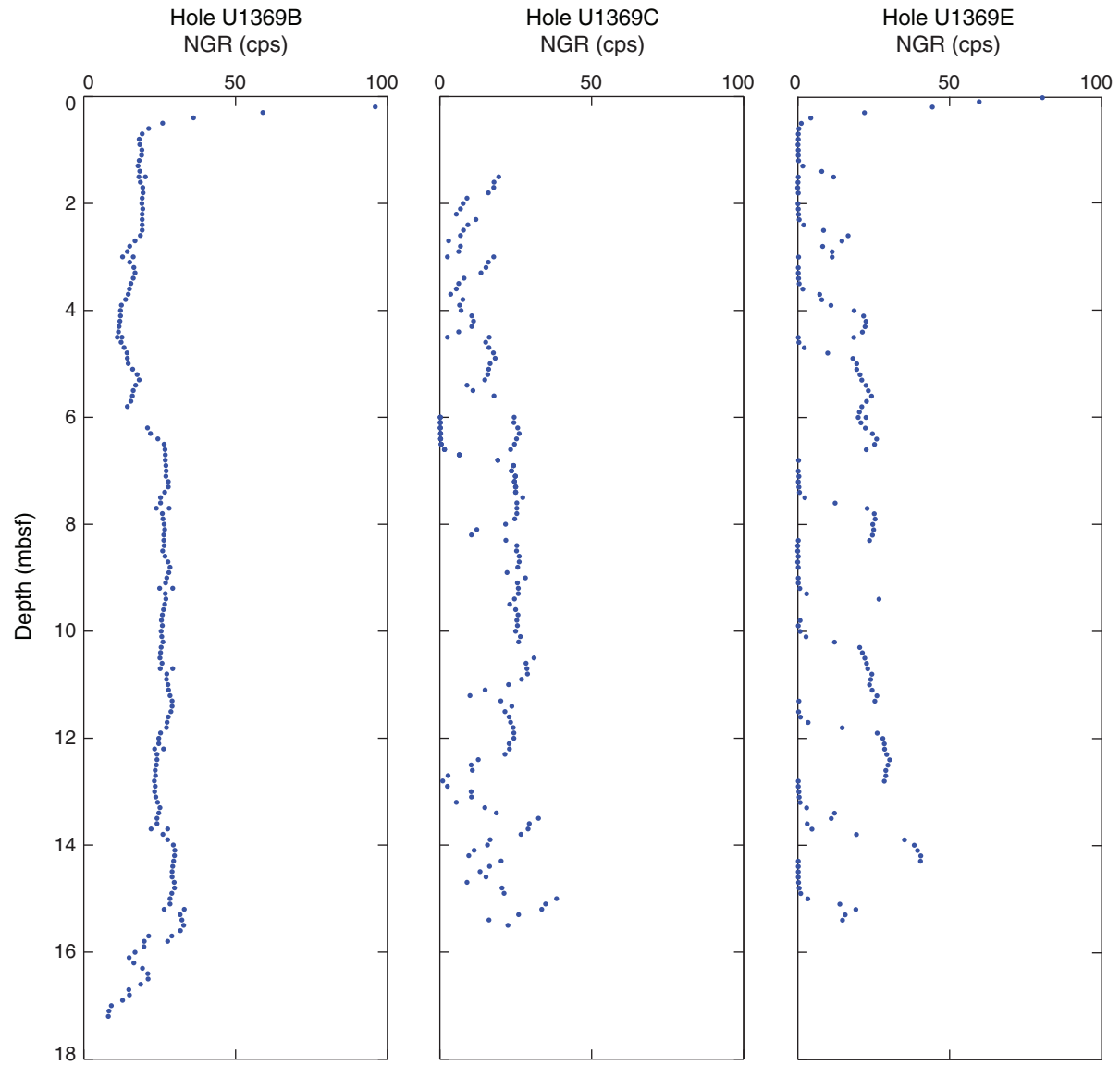
**Figure F13.** Plots of bulk density values determined by gamma ray attenuation, Site U1369.

**Figure F14.** Plots of moisture and density (MAD) measurements, Hole U1369B. A. Bulk density. Red = bulk density derived from MAD Method C, blue = bulk density derived from gamma ray attenuation. B. Grain density. C. Porosity.



**Figure F15.** Plots of (A–C) magnetic susceptibility measurements made on the Whole-Core Multisensor Logger and (D–F) point magnetic susceptibility measurements made on the Section Half Multisensor Logger, Site U1369.



**Figure F16.** Plots of natural gamma radiation (NGR) as a function of depth, Site U1369.

**Figure F17. A.** Plots of compressional wave velocity measured on the Whole-Round Multisensor Logger (WRMSL), Site U1369. Red circles = discrete measurements of compressional wave velocity. **B.** Histogram of WRMSL *P*-wave velocity from all holes.

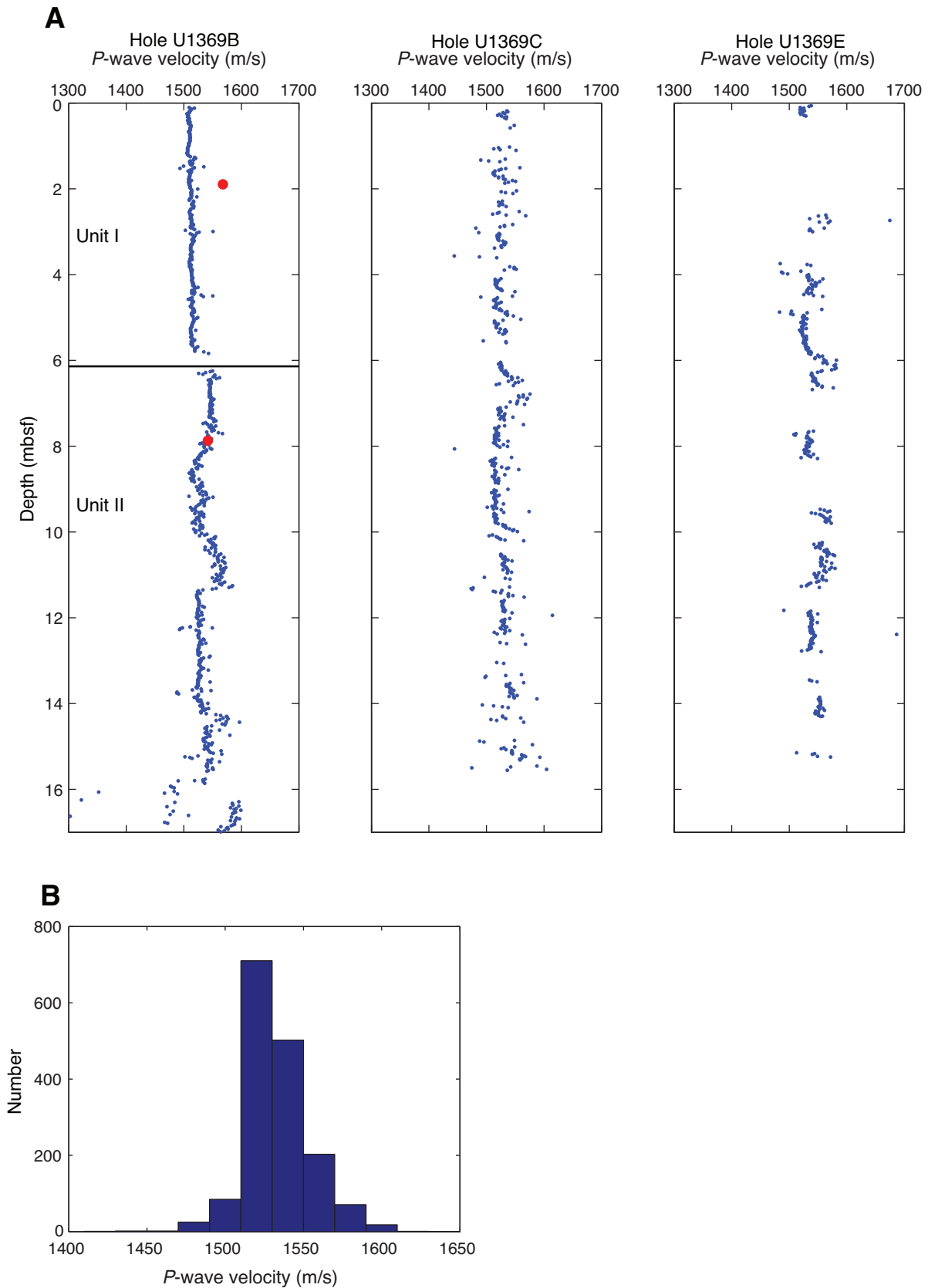


**Figure F18.** Plot of electrical conductivity measured on surface seawater standard, Site U1369. Line shows best linear fit to the data. The best fitting slope and  $\gamma$ -intercept are  $-1.5 \times 10^{-3}$  mS/m/measurement number and 49.66 mS/m, respectively.

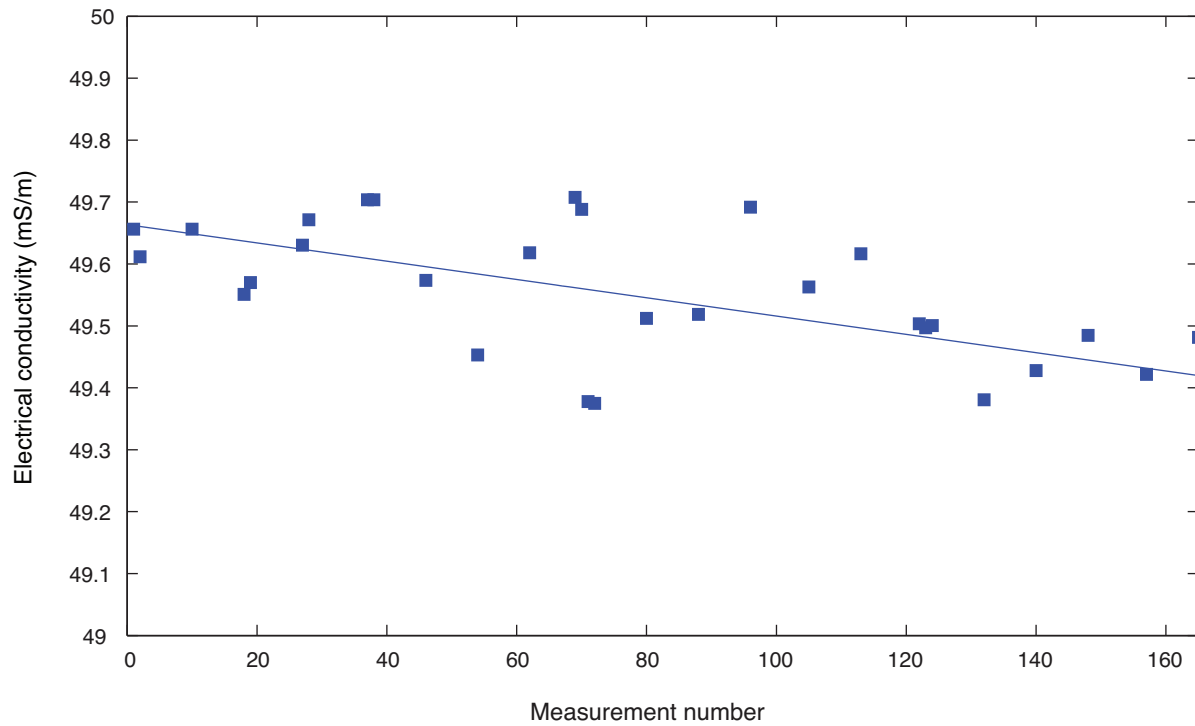
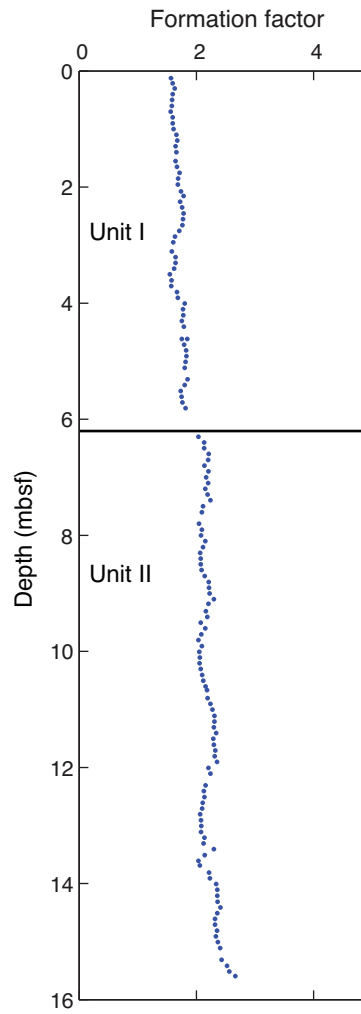


Figure F19. Plot of formation factor as function of depth, Hole U1369B.



**Figure F20.** Plot of thermal conductivity data, Site U1369. Circles = full-space measurements, triangles = values collected during KNOX-02RR site survey cruise (R. Harris, unpubl. data).

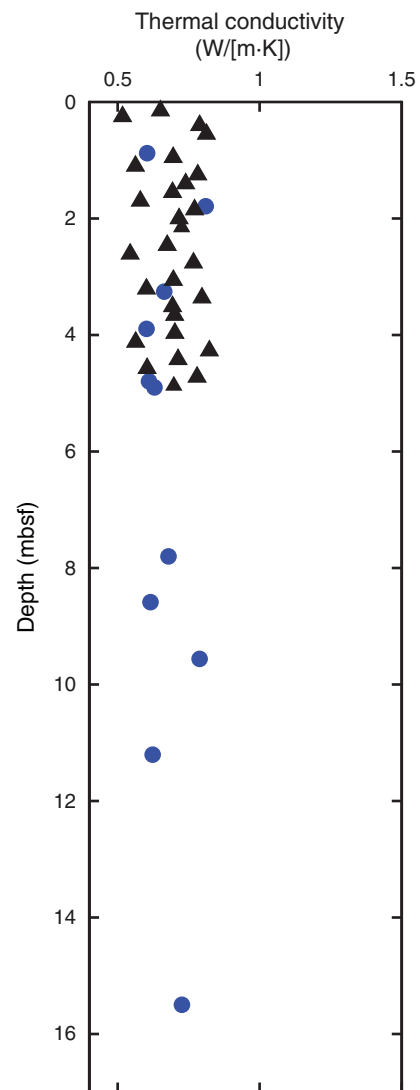
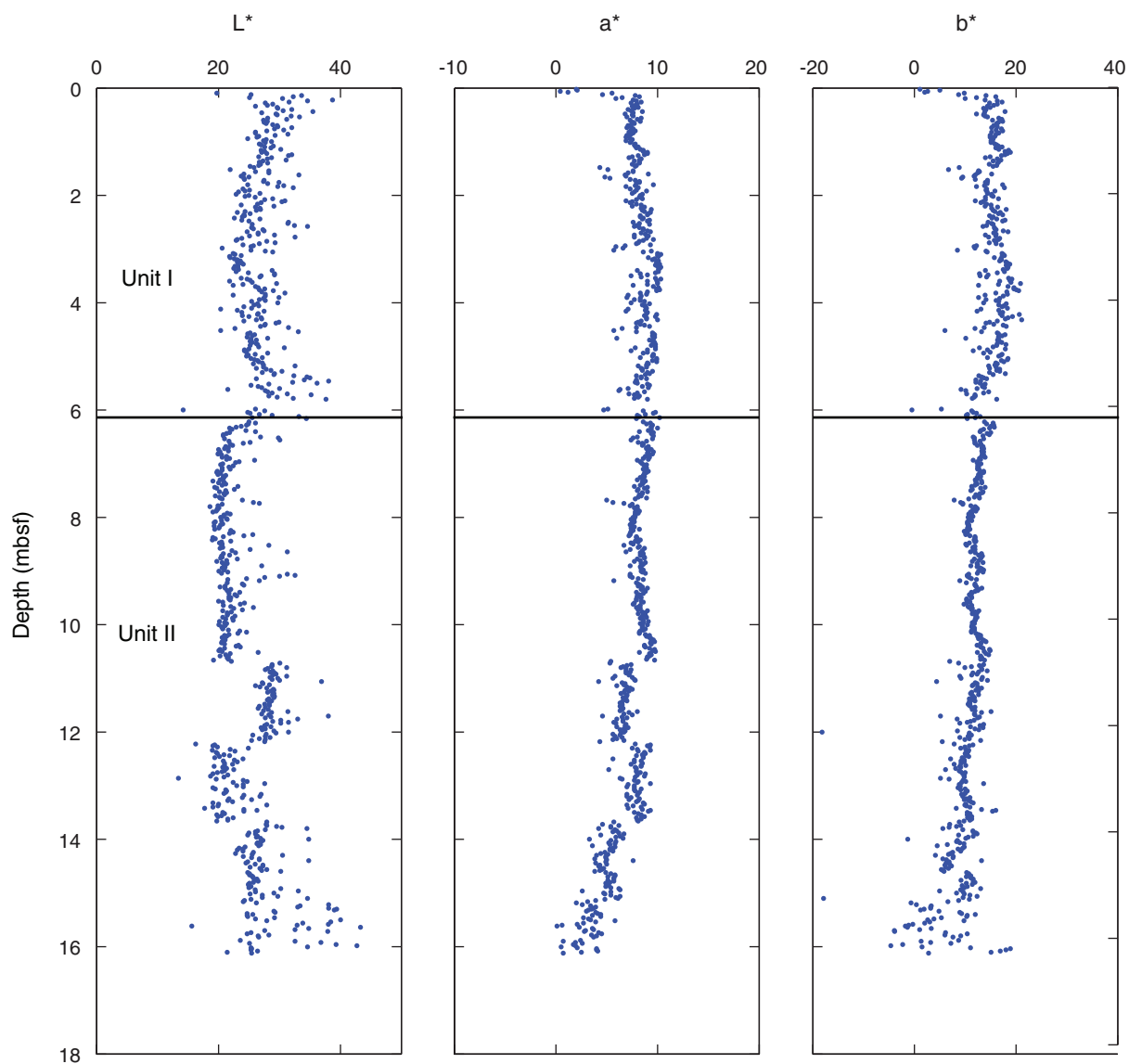
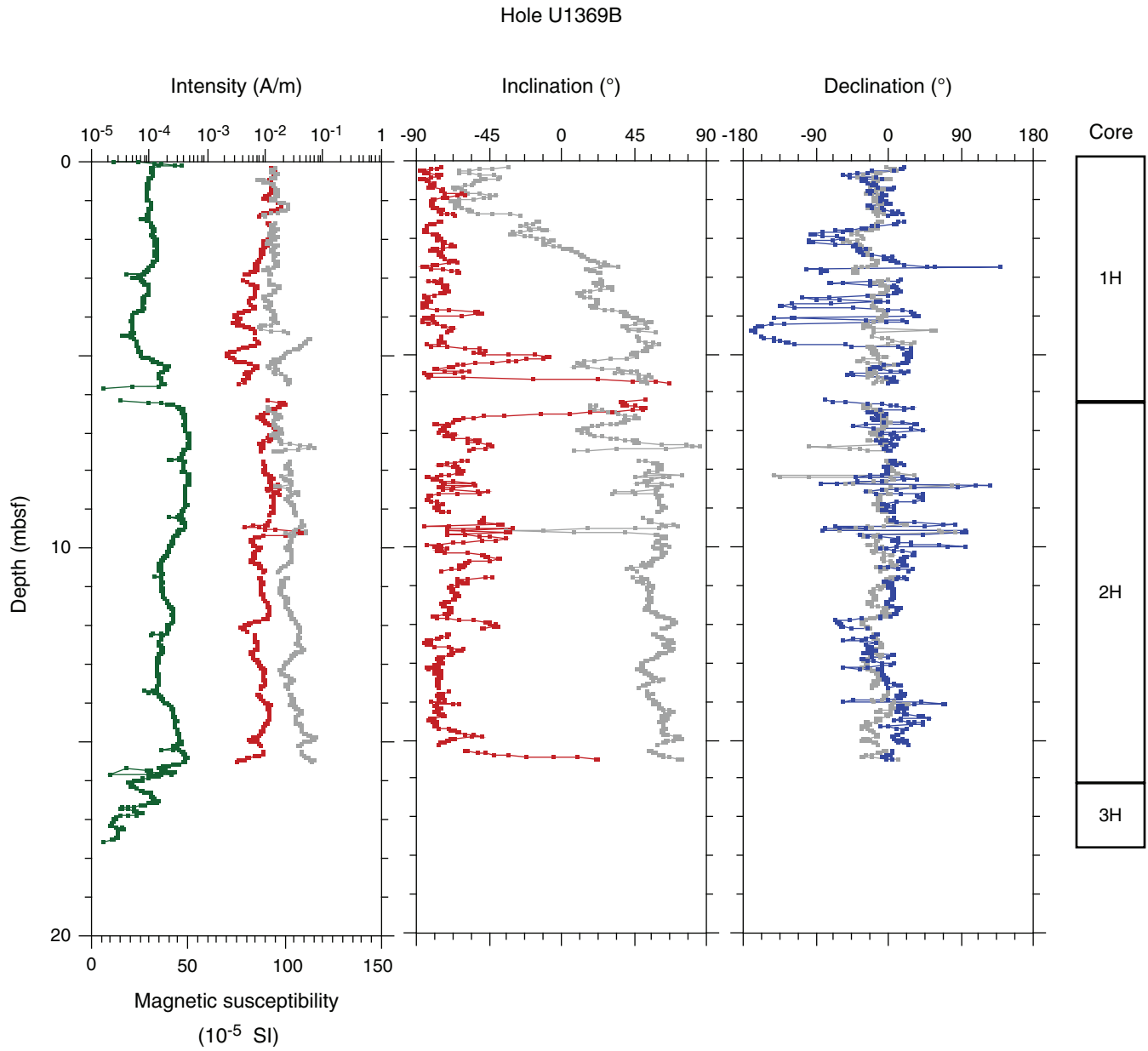


Figure F21. Plots of color spectrometry values, Hole U1369B.



**Figure F22.** Summary of magnetic susceptibility and paleomagnetic intensity, Hole U1369B. Gray = measurement before demagnetization, red = measurement after 20 mT AF demagnetization step (inclination and intensity), blue = declination measurements, green = magnetic susceptibility data.



**Figure F23.** Summary of magnetic susceptibility and paleomagnetic results, Hole U1369C. Gray = measurement before demagnetization, red = measurement after 20 mT AF demagnetization step (inclination and intensity), blue = declination measurements, green = magnetic susceptibility data.

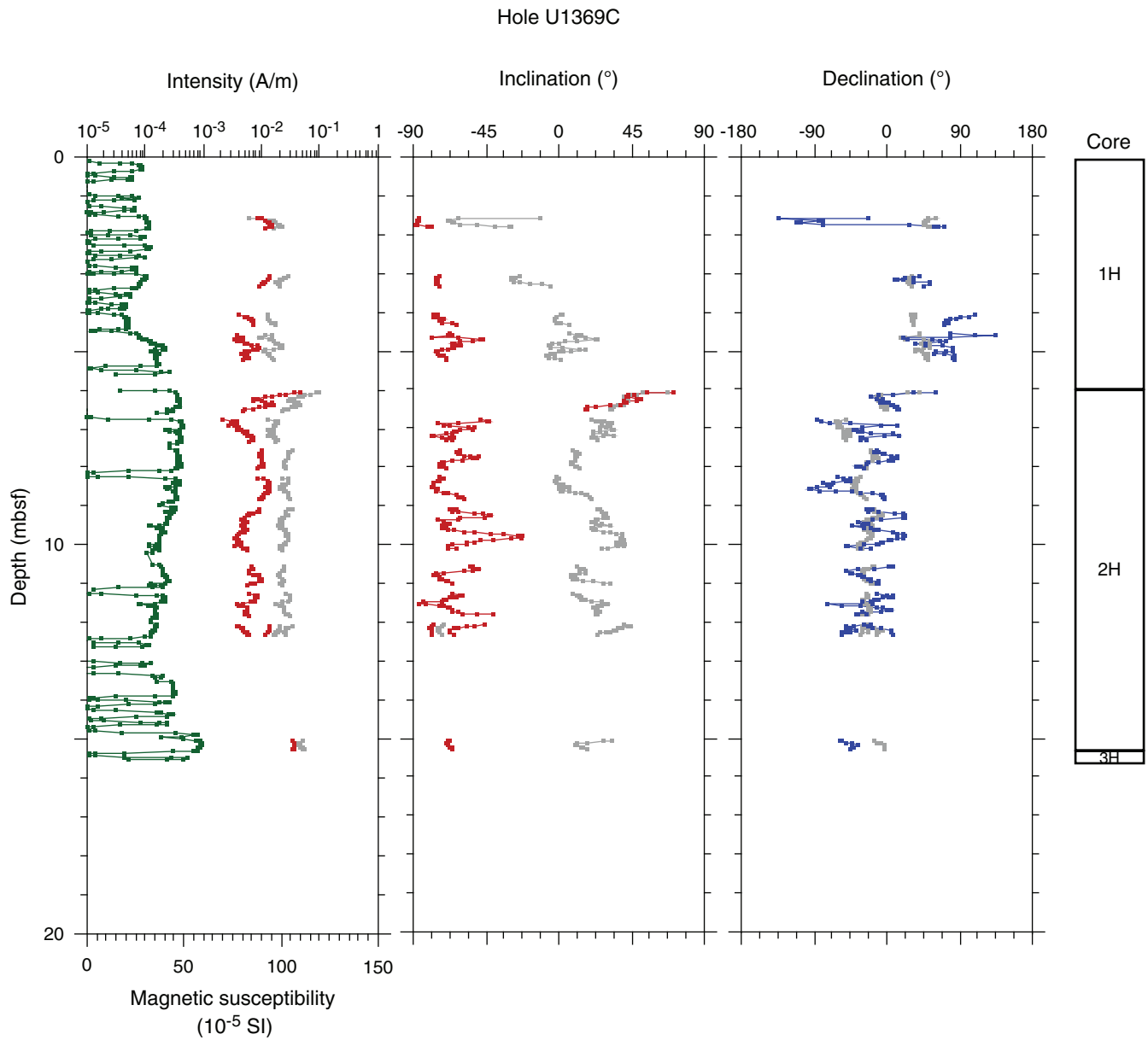


**Figure F24.** Summary of magnetic susceptibility and paleomagnetic results, Hole U1369E. Gray = measurement before demagnetization, red = measurement after 20 mT AF demagnetization step (inclination and intensity), blue = declination measurements, green = magnetic susceptibility data.

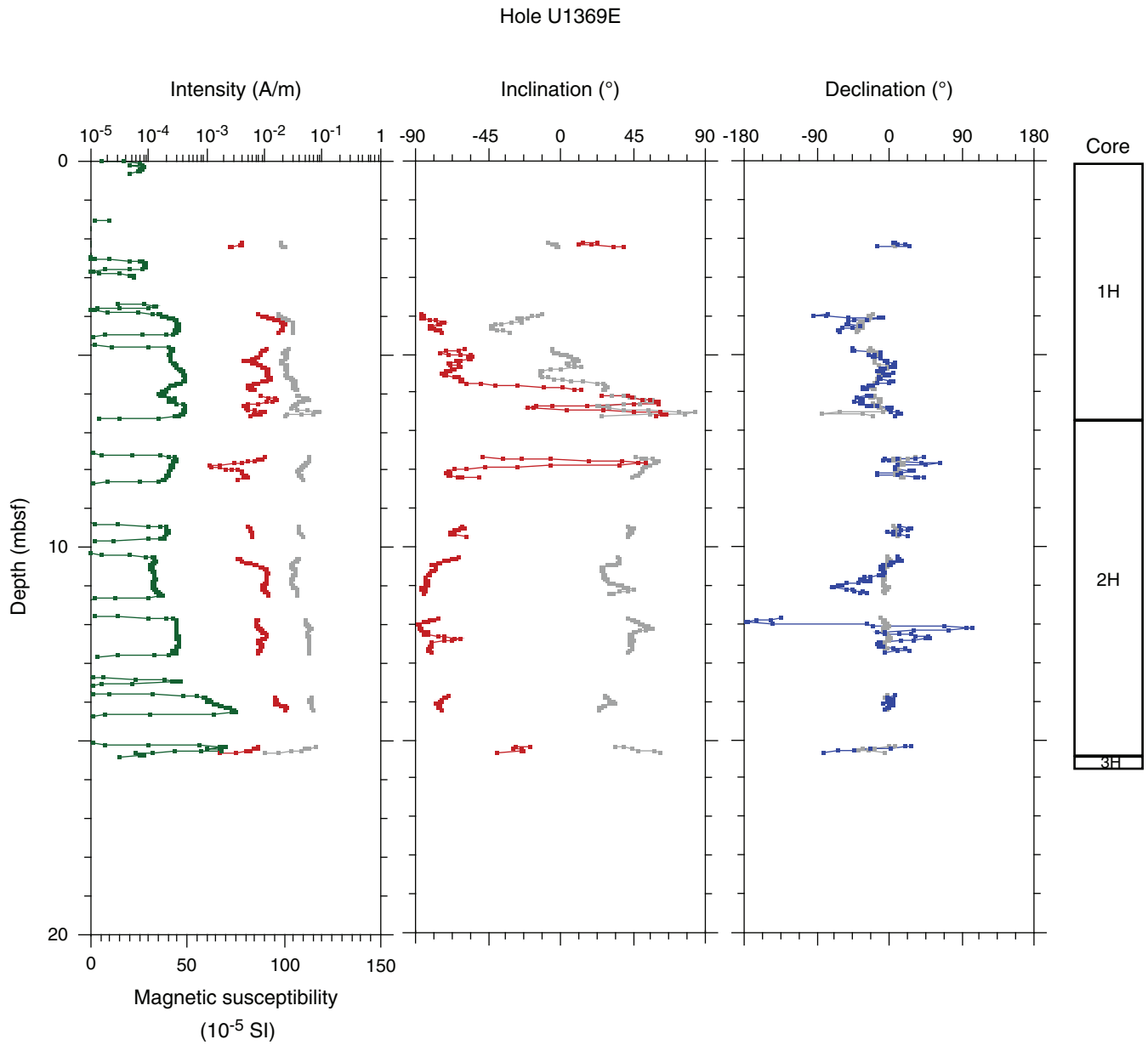


**Figure F25.** Results of hole-to-hole correlation using magnetic susceptibility (green) and magnetic intensity (red) data from Holes U1369B and U1369C. Black lines indicate correlation points between holes. Gray = measurement before demagnetization.

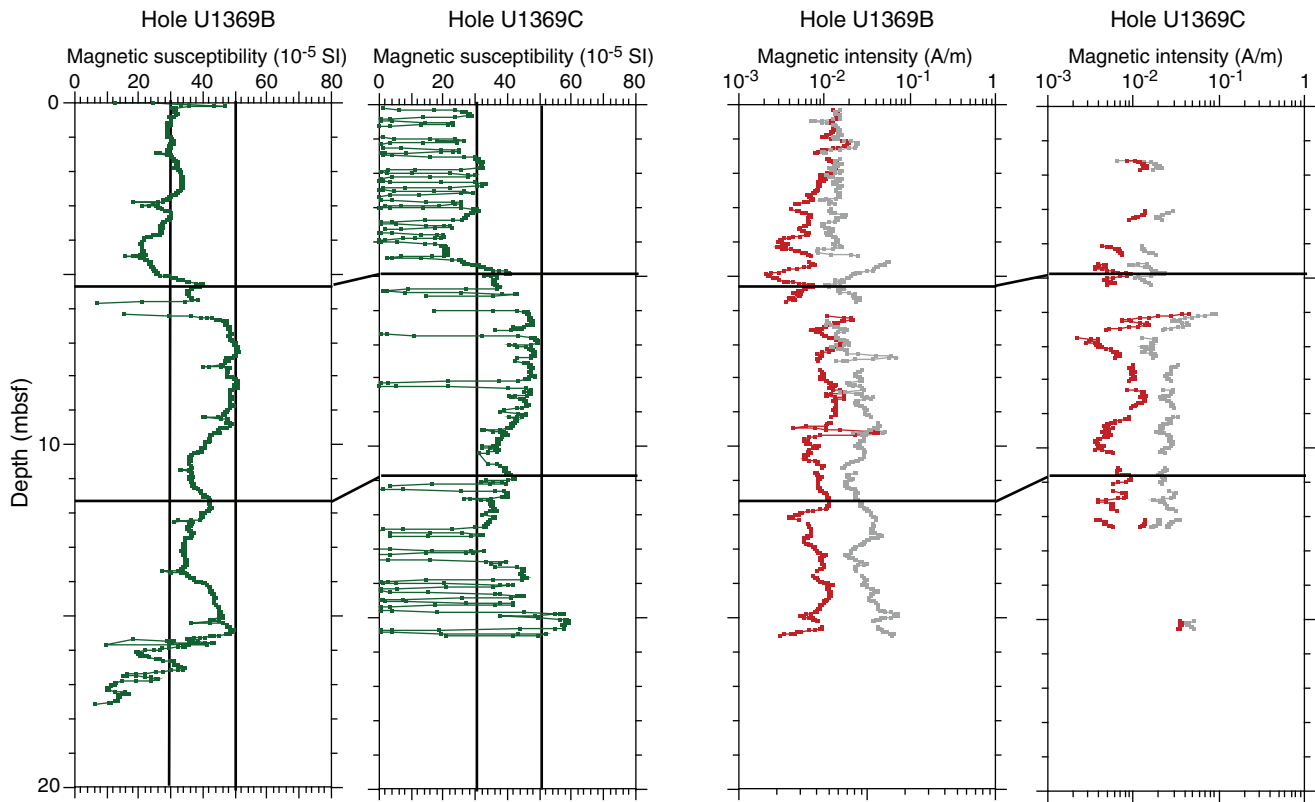


**Figure F26.** Correlation of polarity records between Holes U1369B and U1369C. Inclination (red) and declination (blue) after the 20 mT AF demagnetization step. Black lines indicate correlation points between holes. Gray = measurement before demagnetization.

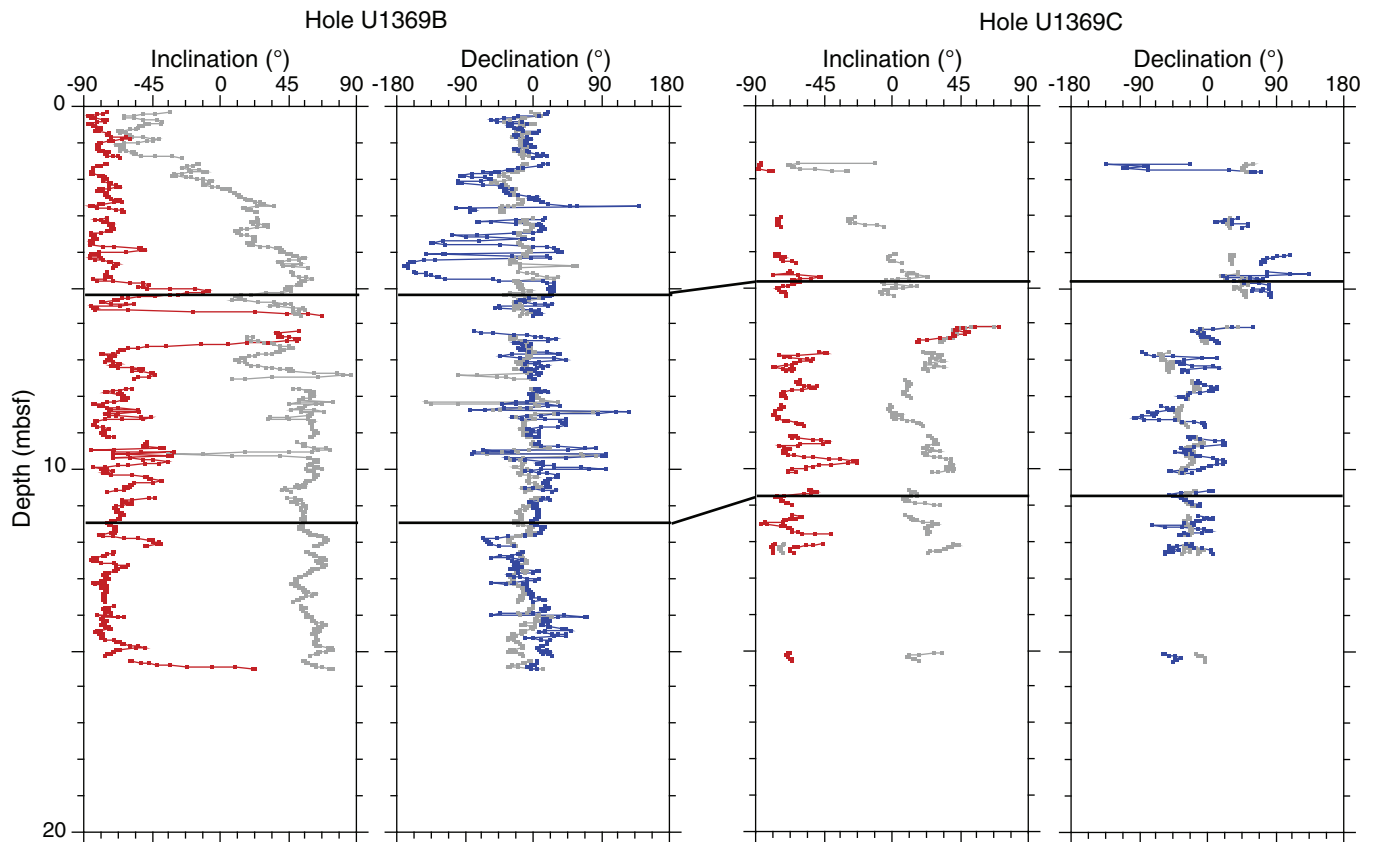


**Figure F27.** A. Plot of combined dissolved oxygen concentrations measured with optodes (Hole U1369B) and electrodes (Holes U1369B, U1369C, and U1369E). B. Combined dissolved oxygen concentrations measured in Hole U1369B in the uppermost 3 m of sediment.

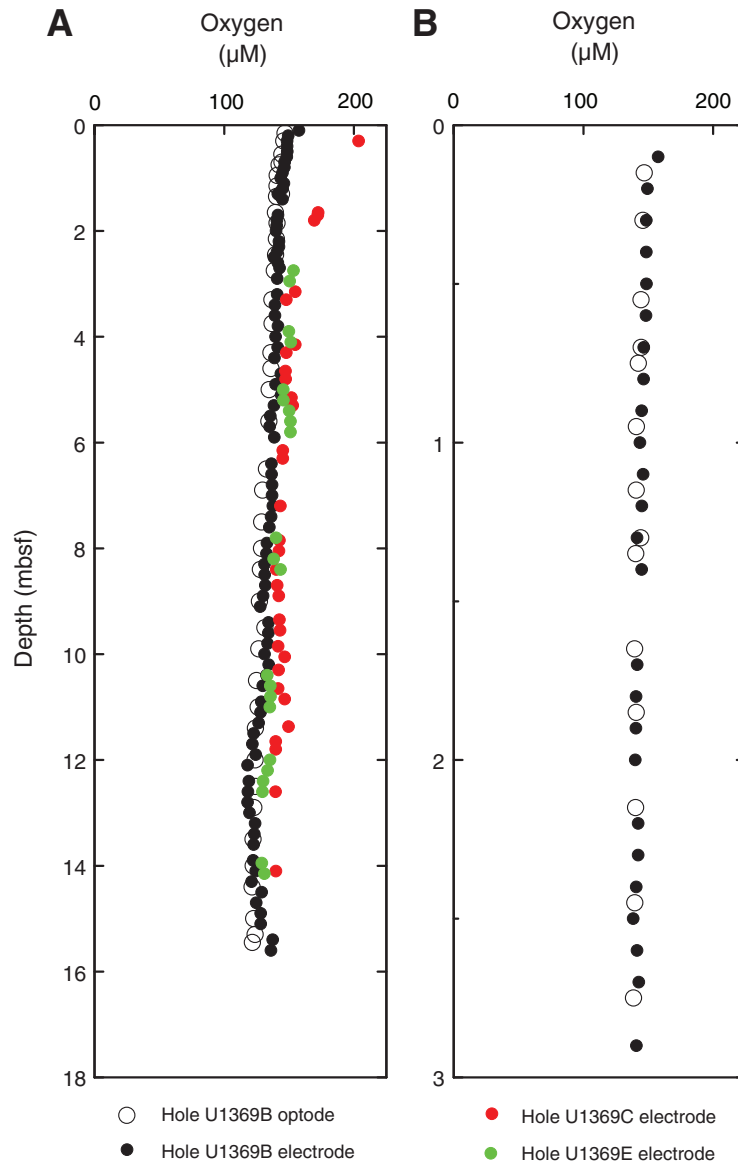
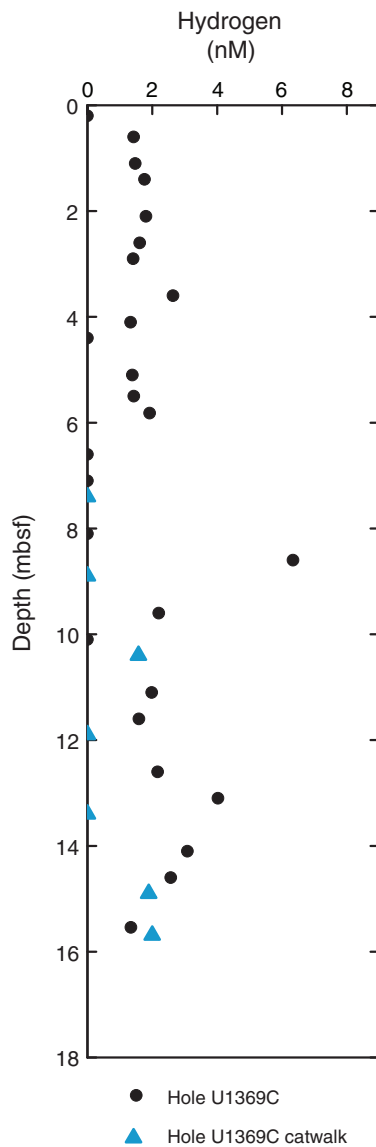


Figure F28. Plot of dissolved hydrogen concentrations, Hole U1369C.





**Figure F29.** Plots of dissolved interstitial water constituents, Hole U1369C. IC = ion chromatography, ICP = inductively coupled plasma–atomic emission spectroscopy. **A.** Nitrate. **B.** Phosphate. **C.** Silicate. **D.** Alkalinity. **E.** Dissolved inorganic carbon (DIC). (Continued on next two pages.)

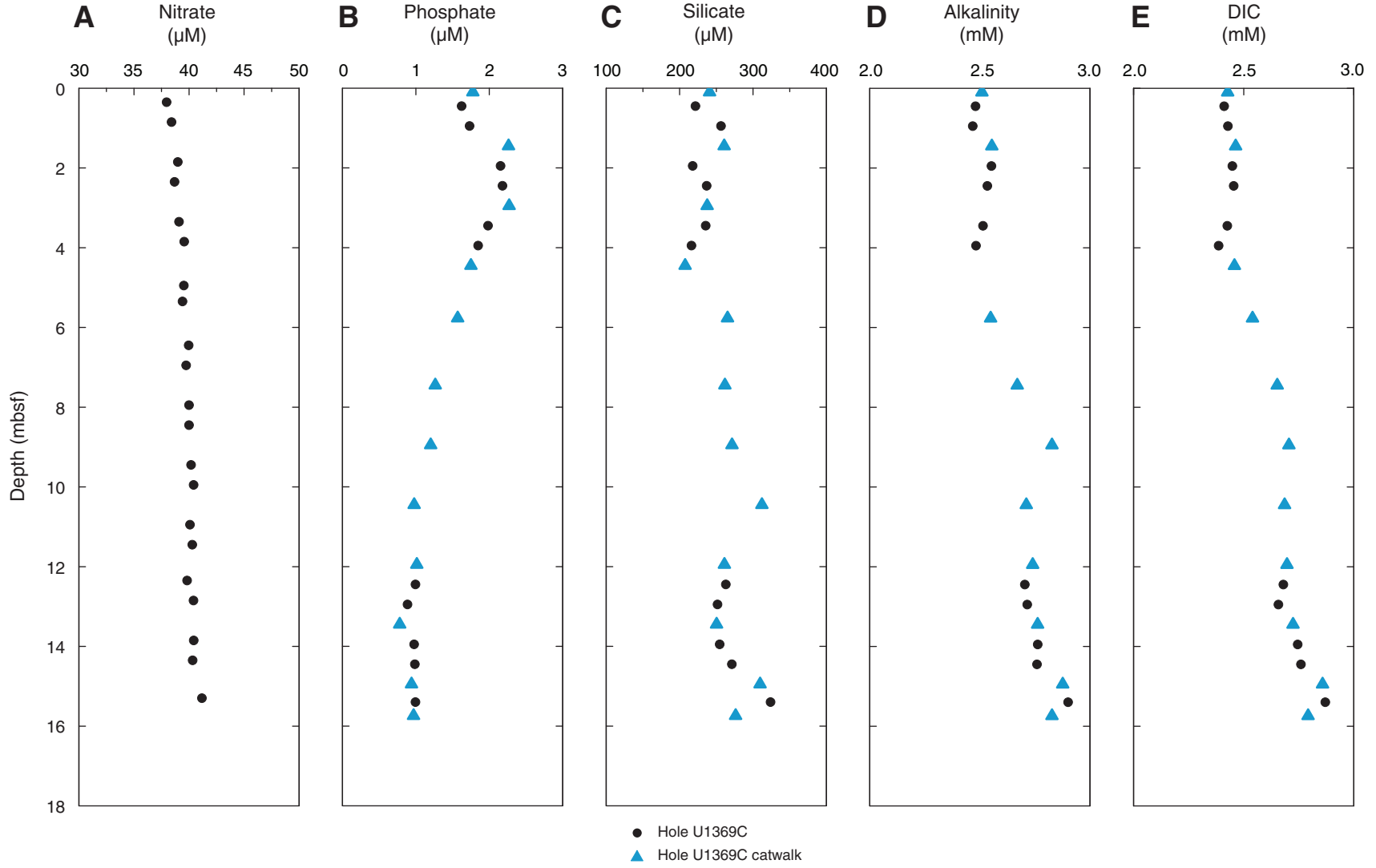




Figure F29 (continued). F. Sulfate. G. Sulfate anomaly. H. Chloride. I. Calcium. J. Magnesium. (Continued on next page.)

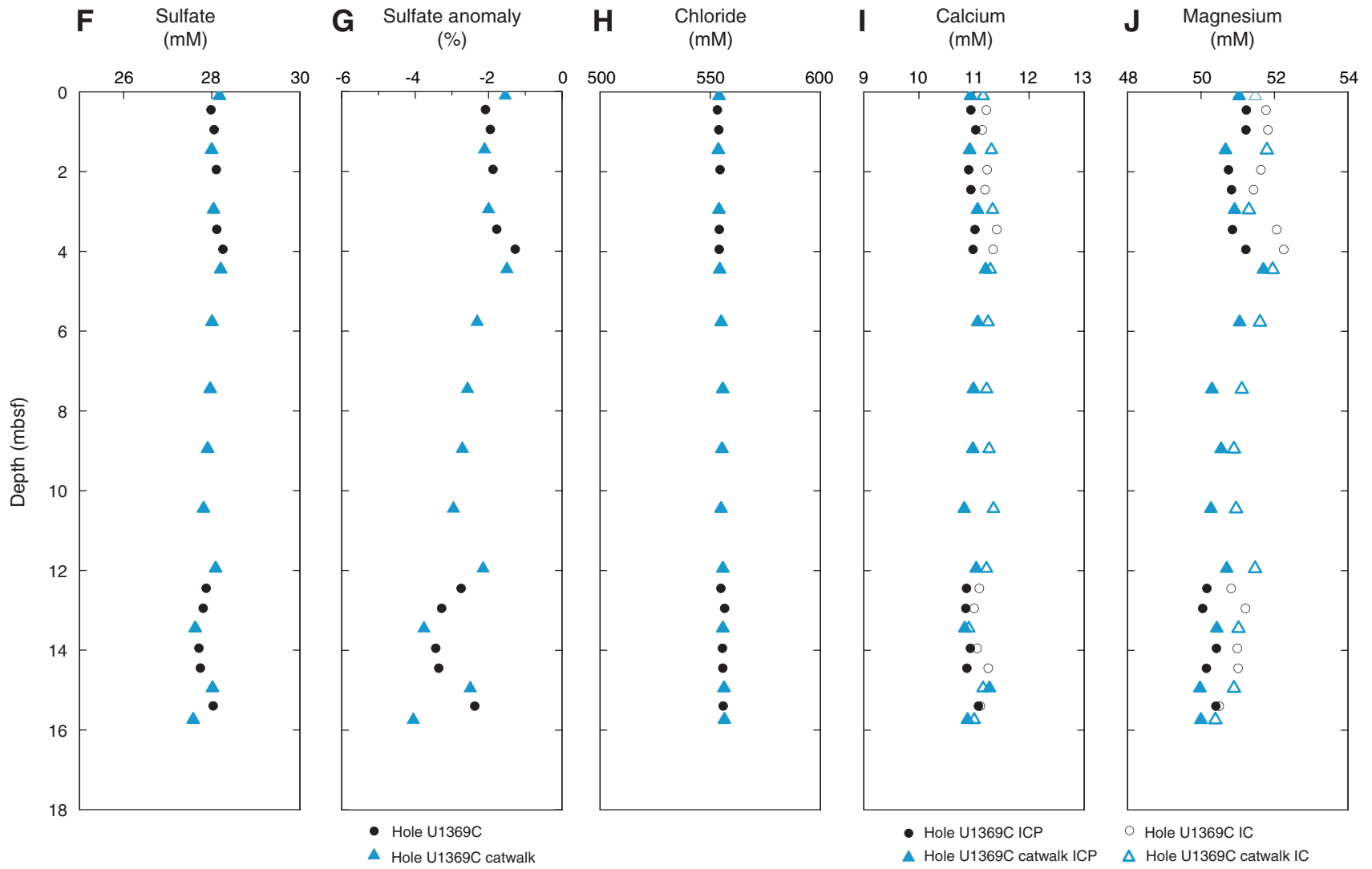




Figure F29 (continued). K. Sodium. L. Potassium. M. Boron. N. Iron. O. Manganese. (Continued on next page.)

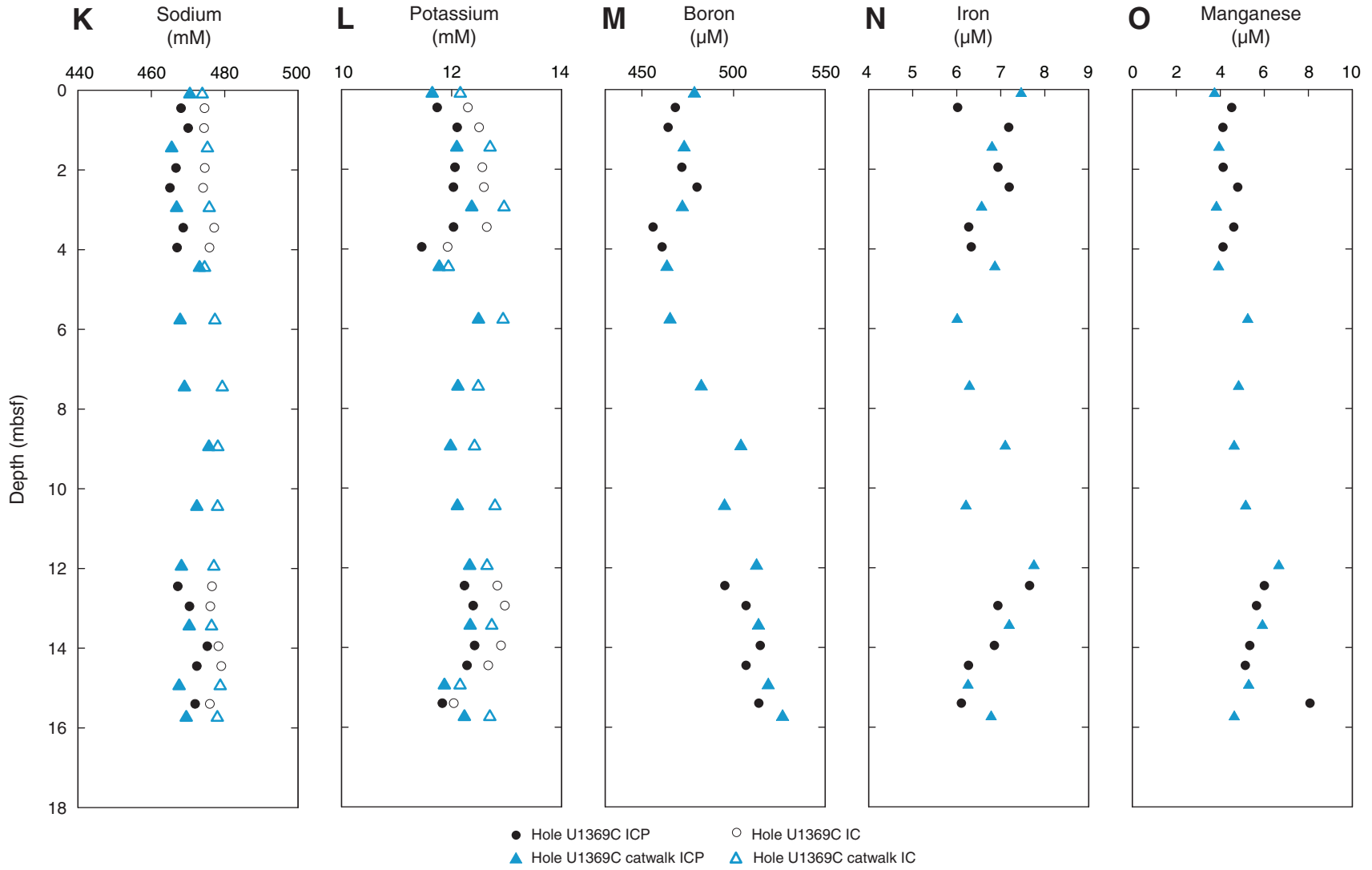
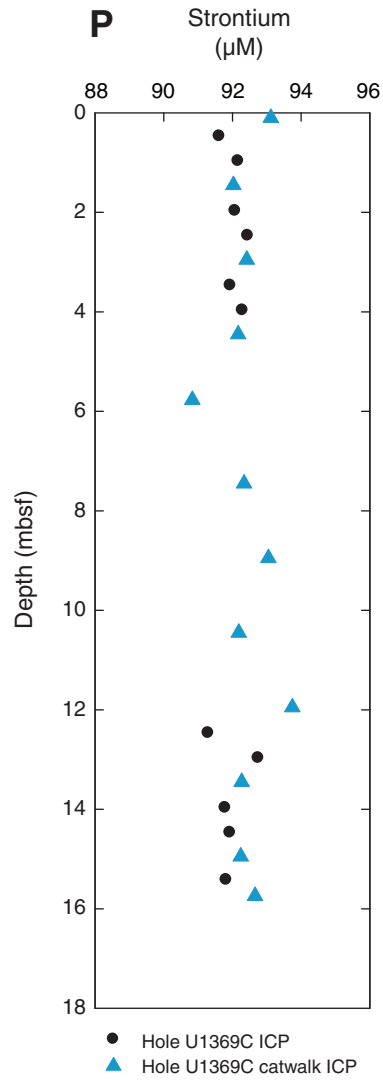
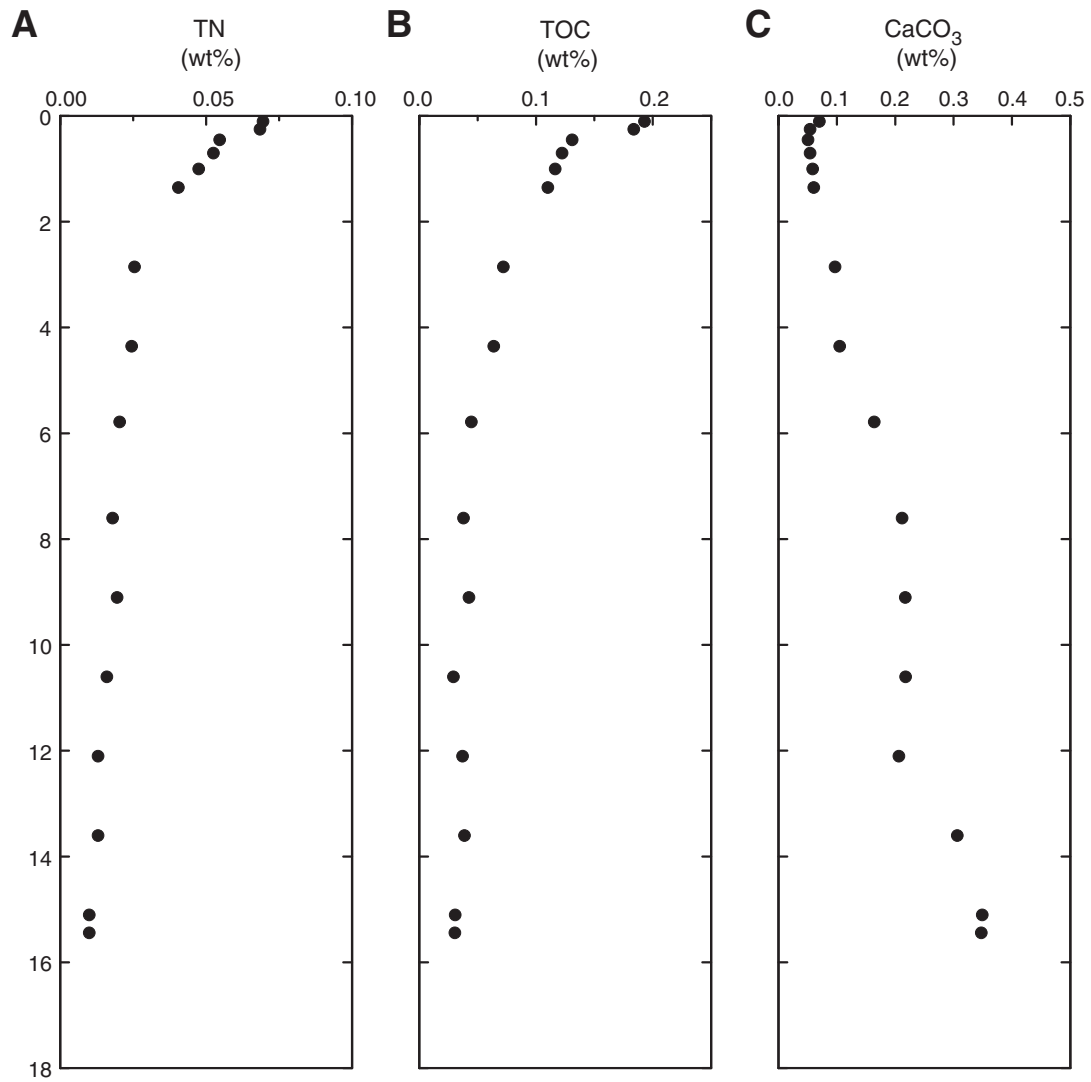


Figure F29 (continued). P. Strontium.



**Figure F30.** Plot of solid-phase nitrogen and oxygen content, Hole U1369B. **A.** Total nitrogen (TN). **B.** Total organic carbon (TOC). **C.** Total carbonate ( $\text{CaCO}_3$ ).



**Figure F31.** Plot of abundance of microbial cells and virus-like particles in Site U1369 sediment as determined by epifluorescence microscopy. Counts below the blank were set to  $10^2$  cells/cm<sup>3</sup> in order to present them in the graph. See “Microbiology” in the “Methods” chapter (Expedition 329 Scientists, 2011a) for a detailed description of the blank and minimum detection limit (MDL) calculation. Red line = MDL for cell counts from extracts, blue line = MDL for nonextracted samples, solid red circles = abundances above MDL, open red circles = direct counts below MDL, solid black squares = VLP counts, solid blue diamonds = nonextracted direct counts above MDL, open blue diamonds = nonextracted direct counts below MDL.

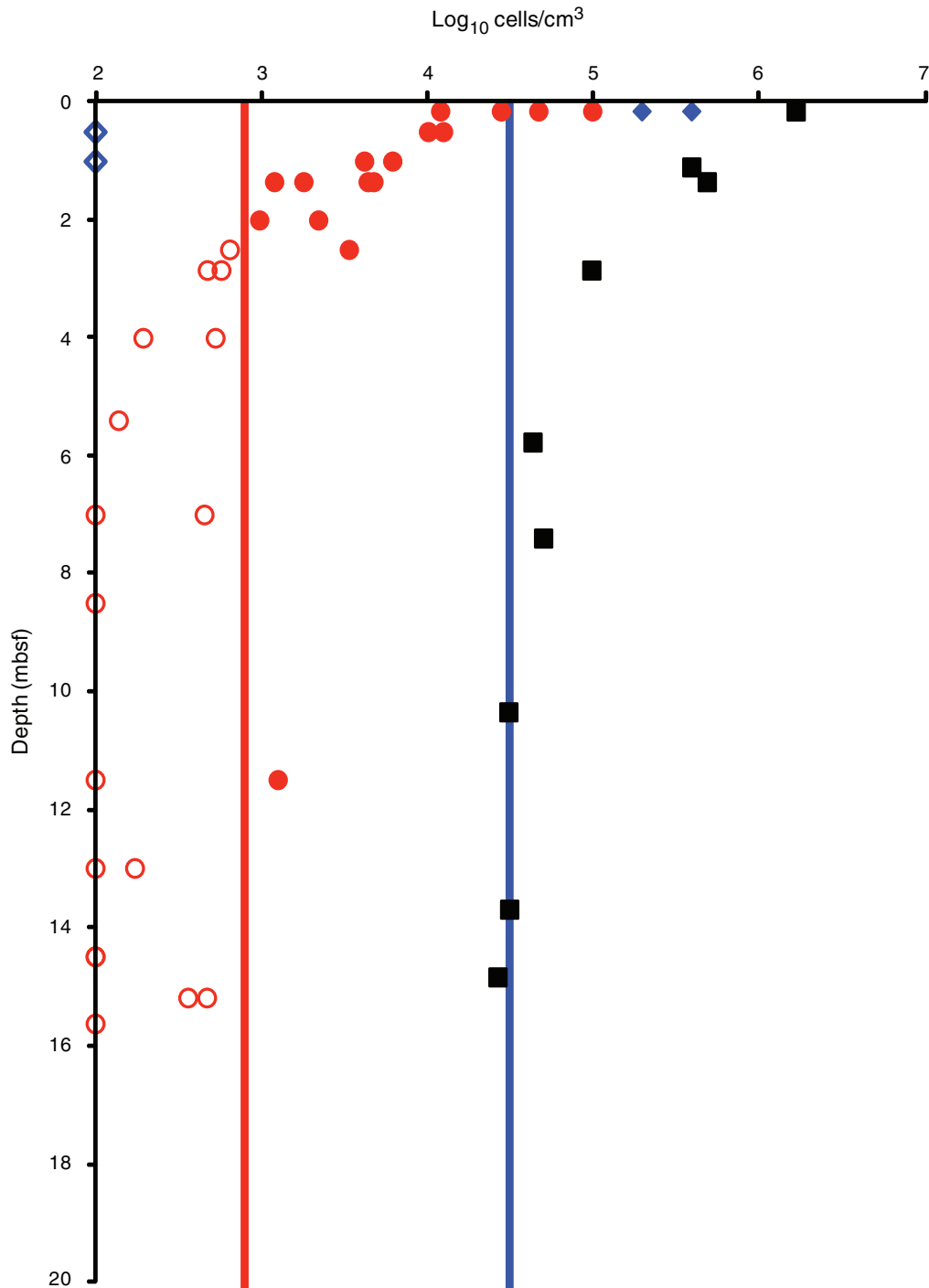


Table T1. Operations summary, Site U1369. (Continued on next page.)

**Hole U1369A**

Latitude: 39°18.6177'S  
 Longitude: 139°48.0383'W  
 Time on hole (h): 10.5  
 Seafloor (drill pipe measurement below rig floor, m DRF): 5290.5  
 Distance between rig floor and sea level (m): 11.2  
 Water depth (drill pipe measurement from sea level, mbsl): 5279.4  
 Total penetration (drilling depth below seafloor, m DSF): 12.2  
 Total length of cored section (m): washdown to basement  
 Total core recovered (m): NA  
 Core recovery (%): NA  
 Total number of cores: NA

**Hole U1369B**

Latitude: 39°18.6178'S  
 Longitude: 139°48.0522'W (20 m west of Hole U1369A)  
 Time on hole (h): 9  
 Seafloor (drill pipe measurement below rig floor, m DRF): 5286.3  
 Distance between rig floor and sea level (m): 11.2  
 Water depth (drill pipe measurement from sea level, mbsl): 5275.2  
 Total penetration (drilling depth below seafloor, m DSF): 15.9  
 Total length of cored section (m): 15.9  
 Total core recovered (m): 18.14  
 Core recovery (%): 114.1  
 Total number of cores: 3

**Hole U1369C**

Latitude: 39°18.6070'S  
 Longitude: 139°48.0519'W (20 m north of Hole U1369B)  
 Time on hole (h): 5  
 Seafloor (drill pipe measurement below rig floor, m DRF): 5288.0  
 Distance between rig floor and sea level (m): 11.2  
 Water depth (drill pipe measurement from sea level, mbsl): 5276.9  
 Total penetration (drilling depth below seafloor, m DSF): 14.6  
 Total length of cored section (m): 14.6  
 Total core recovered (m): 16.1  
 Core recovery (%): 110.3  
 Total number of cores: 3

**Hole U1369D**

Latitude: 39°18.6069'S  
 Longitude: 139°48.0378'W (20 m east of Hole U1369C)  
 Time on hole (h): 0.75  
 Seafloor (drill pipe measurement below rig floor, m DRF): 5288.0  
 Distance between rig floor and sea level (m): 11.2  
 Water depth (drill pipe measurement from sea level, mbsl): 5276.9  
 Total penetration (drilling depth below seafloor, m DSF): unknown  
 Total length of cored section (m): 0.1 (recorded as)  
 Total core recovered (m): 0.08  
 Core recovery (%): 80.0 (recorded as)  
 Total number of cores: 1

**Hole U1369E**

Latitude: 39°18.6070'S  
 Longitude: 139°48.0246'W (20 m east of Hole U1369D)  
 Time on hole (h): 15.25  
 Seafloor (drill pipe measurement below rig floor, m DRF): 5288.8  
 Distance between rig floor and sea level (m): 11.2  
 Water depth (drill pipe measurement from sea level, mbsl): 5277.7  
 Total penetration (drilling depth below seafloor, m DSF): 15.5  
 Total length of cored section (m): 15.5  
 Total core recovered (m): 15.49  
 Core recovery (%): 99.9  
 Total number of cores: 3

Table T1 (continued).

Core	Date (2010)	Time (h)	Depth DSF (m)			Depth CSF (m)			Length of core recovered (m)	Recovery (%)	Sections (N)	Coring shoe type
			Top of cored interval	Bottom of cored interval	Interval advanced (m)	Top of cored interval	Bottom of cored interval	Interval advanced (m)				
329-U1369A-11	23 Nov	1300	*****Drilled from 0.0 to 12.2 m DSF*****									
329-U1369B-1H	23 Nov	1425	0.0	6.2	6.2	0.0	6.18	6.18	100	5	STD	
2H	23 Nov	1600	6.2	15.7	9.5	6.2	16.14	9.94	105	8	STD	
3H	23 Nov	1815	15.7	15.9	0.2	15.7	17.72	2.02	1010	3	STD	
329-U1369C-1H	23 Nov	2210	0.0	6.0	6.0	0.0	6.03	6.03	100	5	STD	
2H	23 Nov	2335	6.0	14.5	8.5	6.0	16.06	10.06	118	8	STD	
3H	24 Nov	0105	14.5	14.6	0.1	14.5	14.55	0.01	10	1	STD	
329-U1369D-1H	24 Nov	0245	0.0	0.1	0.1	0.0	0.09	0.08	80	1	STD	
329-U1369E-1H	24 Nov	0425	0.0	6.8	6.8	0.0	6.84	6.84	101	6	STD	
2H	24 Nov	0600	6.8	15.4	8.6	6.8	15.43	8.63	100	7	STD	
3H	24 Nov	0730	15.4	15.5	0.1	15.4	15.42	0.02	20	1	STD	
Advanced totals:					58.3	49.81			108	45		
Total interval cored:					46.1							

NA = not applicable. DSF = drilling depth below seafloor, CSF = core depth below seafloor. H = APC core, 1 = drilled interval. STD = standard. Time is UTC.

Table T2. Electrical conductivity measurements of surface seawater, Site U1369.

Measurement number	Electrical conductivity (mS/cm)	Temperature (°C)	Correction factor at 20°C (mS/cm)	Seawater electrical conductivity at 20°C (mS/cm)
1	52.10	22.3	50.30	49.70
2	52.20	22.4	50.40	49.60
10	52.10	22.3	50.30	49.70
18	52.30	22.6	50.60	49.60
19	52.30	22.6	50.60	49.60
27	52.20	22.4	50.40	49.60
28	52.30	22.5	50.50	49.70
37	52.20	22.3	50.30	49.70
38	52.20	22.3	50.30	49.70
46	52.10	22.4	50.40	49.60
54	52.10	22.5	50.50	49.50
62	52.10	22.3	50.30	49.60
69	51.90	22.1	50.00	49.70
70	51.90	22.1	50.00	49.70
71	53.00	23.4	51.40	49.40
72	52.90	23.3	51.30	49.40
80	52.90	23.2	51.20	49.50
88	52.80	23.1	51.10	49.50
96	52.80	22.9	50.90	49.70
105	52.80	23.0	51.00	49.60
113	52.70	22.9	50.90	49.60
122	52.60	22.9	50.90	49.50
123	52.70	23.0	51.00	49.50
124	52.20	22.5	50.50	49.50
132	52.10	22.6	50.60	49.40
140	52.20	22.6	50.60	49.40
148	52.20	22.6	50.60	49.50
157	52.30	22.7	50.70	49.40
165	52.10	22.5	50.50	49.50
173	52.20	22.7	50.70	49.30
178	52.10	22.6	50.60	49.30

Table T3. Formation factor measurements, Site U1369. (Continued on next two pages.)

Core, section, interval (cm)	Depth (mbsf)	Measurement number	Temperature-corrected seawater conductivity (mS/cm)	Sediment temperature (°C)	Sediment electrical conductivity (mS/cm)	Correction factor at 20°C (mS/cm)	Sediment electrical conductivity at 20°C (mS/cm)	Drift-corrected sediment electrical conductivity at 20°C (mS/cm)	Formation factor
329-U1369B-									
1H-1, 12	0.12	3	49.66	21.20	32.55	49.12	31.74	31.74	1.56
1H-1, 21	0.21	4	49.66	21.20	31.95	49.12	31.15	31.16	1.59
1H-1, 30	0.30	5	49.66	21.20	31.18	49.12	30.40	30.41	1.63
1H-1, 40	0.40	6	49.65	21.20	31.91	49.12	31.11	31.12	1.60
1H-1, 50	0.50	7	49.65	21.20	32.14	49.12	31.34	31.34	1.58
1H-1, 60	0.60	8	49.65	21.20	32.18	49.12	31.38	31.38	1.58
1H-1, 70	0.70	9	49.65	21.20	32.63	49.12	31.82	31.82	1.56
1H-1, 80	0.80	11	49.65	21.20	31.89	49.12	31.09	31.10	1.60
1H-1, 90	0.90	12	49.65	21.20	31.92	49.12	31.12	31.13	1.59
1H-1, 100	1.00	13	49.64	21.20	31.57	49.12	30.78	30.79	1.61
1H-1, 110	1.10	14	49.64	21.20	30.66	49.12	29.89	29.91	1.66
1H-1, 120	1.20	15	49.64	21.20	30.36	49.12	29.60	29.62	1.68
1H-1, 130	1.30	16	49.64	21.20	30.97	49.12	30.20	30.21	1.64
1H-1, 140	1.40	17	49.64	21.20	30.68	49.12	29.91	29.93	1.66
1H-2, 5	1.55	20	49.63	20.90	30.81	48.81	30.23	30.25	1.64
1H-2, 15	1.65	21	49.63	20.90	30.31	48.81	29.74	29.76	1.67
1H-2, 25	1.75	22	49.63	20.90	29.50	48.81	28.94	28.96	1.71
1H-2, 35	1.85	23	49.63	20.90	29.89	48.81	29.33	29.35	1.69
1H-2, 45	1.95	24	49.63	21.00	30.10	48.91	29.47	29.49	1.68
1H-2, 57	2.07	25	49.63	21.00	29.15	48.91	28.54	28.56	1.74
1H-2, 65	2.15	26	49.63	21.00	28.40	48.91	27.81	27.83	1.78
1H-2, 75	2.25	29	49.62	21.00	29.41	48.91	28.80	28.82	1.72
1H-2, 85	2.35	30	49.62	21.00	28.81	48.91	28.21	28.23	1.76
1H-2, 95	2.45	31	49.62	21.00	28.43	48.91	27.84	27.86	1.78
1H-2, 105	2.55	32	49.62	21.00	28.56	48.91	27.96	27.99	1.77
1H-2, 115	2.65	33	49.61	21.00	28.76	48.91	28.16	28.19	1.76
1H-2, 125	2.75	34	49.61	21.00	29.62	48.91	29.00	29.03	1.71
1H-2, 135	2.85	35	49.61	21.00	30.96	48.91	30.31	30.35	1.63
1H-2, 145	2.95	36	49.61	21.00	31.54	48.91	30.88	30.91	1.60
1H-3, 10	3.11	39	49.61	20.40	31.63	48.30	31.36	31.40	1.58
1H-3, 20	3.21	40	49.60	20.40	30.40	48.30	30.14	30.18	1.64
1H-3, 30	3.31	41	49.60	20.40	30.45	48.30	30.19	30.23	1.64
1H-3, 40	3.41	42	49.60	20.40	30.81	48.30	30.55	30.59	1.62
1H-3, 50	3.51	43	49.60	20.40	32.23	48.30	31.96	32.00	1.55
1H-3, 60	3.61	44	49.60	20.40	31.76	48.30	31.49	31.53	1.57
1H-3, 70	3.71	45	49.60	20.40	31.80	48.30	31.53	31.57	1.57
1H-3, 80	3.81	47	49.59	20.70	30.10	48.61	29.66	29.70	1.67
1H-3, 90	3.91	48	49.59	20.70	29.78	48.61	29.34	29.38	1.69
1H-3, 100	4.01	49	49.59	20.70	27.89	48.61	27.48	27.52	1.80
1H-3, 110	4.11	50	49.59	20.70	28.40	48.61	27.98	28.02	1.77
1H-3, 120	4.21	51	49.59	20.70	28.29	48.61	27.87	27.92	1.78
1H-3, 130	4.31	52	49.59	20.70	28.63	48.61	28.21	28.25	1.76
1H-3, 140	4.41	53	49.59	20.70	28.09	48.61	27.68	27.72	1.79
1H-4, 10	4.61	55	49.58	20.80	28.76	48.71	28.28	28.32	1.75
1H-4, 20	4.71	56	49.58	20.80	28.10	48.71	27.63	27.67	1.79
1H-4, 30	4.81	57	49.58	20.80	27.57	48.71	27.11	27.15	1.83
1H-4, 40	4.91	58	49.58	20.80	27.51	48.71	27.05	27.10	1.83
1H-4, 50	5.01	59	49.58	20.80	27.74	48.71	27.27	27.32	1.81
1H-4, 60	5.11	60	49.57	20.80	28.01	48.71	27.54	27.59	1.80
1H-4, 10	4.61	61	49.57	20.80	27.25	48.71	26.79	26.84	1.85
1H-4, 80	5.31	63	49.57	20.60	27.11	48.51	26.77	26.82	1.85
1H-4, 90	5.41	64	49.57	20.60	27.88	48.51	27.53	27.58	1.80
1H-4, 100	5.51	65	49.57	20.60	28.94	48.51	28.57	28.63	1.73
1H-4, 110	5.61	66	49.57	20.60	28.68	48.51	28.32	28.37	1.75
1H-4, 120	5.71	67	49.56	20.60	28.39	48.51	28.03	28.09	1.76
1H-4, 130	5.81	68	49.56	20.60	27.58	48.51	27.23	27.29	1.82
2H-1, 10	6.30	73	49.56	21.50	25.06	49.43	24.28	24.33	2.04
2H-1, 20	6.40	74	49.55	21.50	23.97	49.43	23.23	23.28	2.13
2H-1, 30	6.50	75	49.55	21.50	23.94	49.43	23.20	23.25	2.13
2H-1, 40	6.60	76	49.55	21.50	23.11	49.43	22.39	22.44	2.21
2H-1, 50	6.70	77	49.55	21.50	23.18	49.43	22.46	22.51	2.20
2H-1, 60	6.80	78	49.55	21.50	23.87	49.43	23.13	23.18	2.14
2H-1, 70	6.90	79	49.55	21.50	23.12	49.43	22.40	22.46	2.21
2H-1, 80	7.00	81	49.54	21.30	23.45	49.22	22.82	22.87	2.17
2H-1, 90	7.10	82	49.54	21.30	23.07	49.22	22.45	22.50	2.20

Table T3 (continued). (Continued on next page.)

Core, section, interval (cm)	Depth (mbsf)	Measurement number	Temperature-corrected seawater conductivity (mS/cm)	Sediment temperature (°C)	Sediment electrical conductivity (mS/cm)	Correction factor at 20°C (mS/cm)	Sediment electrical conductivity at 20°C (mS/cm)	Drift-corrected sediment electrical conductivity at 20°C (mS/cm)	Formation factor
2H-1, 100	7.20	83	49.54	21.30	23.56	49.22	22.92	22.98	2.16
2H-1, 110	7.30	84	49.54	21.30	23.13	49.22	22.51	22.56	2.20
2H-1, 120	7.40	85	49.54	21.30	22.68	49.22	22.07	22.12	2.24
2H-1, 130	7.50	86	49.54	21.30	24.02	49.22	23.37	23.43	2.11
2H-1, 140	7.60	87	49.54	21.30	24.21	49.22	23.56	23.62	2.10
2H-2, 10	7.80	89	49.53	21.20	24.81	49.12	24.19	24.25	2.04
2H-2, 20	7.90	90	49.53	21.20	24.18	49.12	23.58	23.64	2.10
2H-2, 30	8.00	91	49.53	21.20	24.35	49.12	23.74	23.81	2.08
2H-2, 40	8.10	92	49.53	21.20	23.52	49.12	22.93	23.00	2.15
2H-2, 50	8.20	93	49.53	21.20	23.96	49.12	23.36	23.43	2.11
2H-2, 60	8.30	94	49.52	21.20	24.50	49.12	23.89	23.96	2.07
2H-2, 70	8.40	95	49.52	21.20	24.40	49.12	23.79	23.86	2.08
2H-2, 80	8.50	97	49.52	21.20	24.39	49.12	23.78	23.85	2.08
2H-2, 90	8.60	98	49.52	21.30	24.30	49.22	23.64	23.71	2.09
2H-2, 100	8.70	99	49.52	21.30	23.71	49.22	23.07	23.14	2.14
2H-2, 110	8.80	100	49.52	21.30	22.99	49.22	22.37	22.44	2.21
2H-2, 120	8.90	101	49.51	21.30	22.92	49.22	22.30	22.37	2.21
2H-2, 130	9.00	102	49.51	21.30	22.80	49.22	22.18	22.25	2.23
2H-2, 140	9.10	103	49.51	21.30	22.08	49.22	21.48	21.55	2.30
2H-2, 148	9.18	104	49.51	21.30	23.00	49.22	22.38	22.45	2.21
2H-3, 10	9.31	106	49.51	21.30	23.47	49.22	22.84	22.91	2.16
2H-3, 20	9.41	107	49.51	21.30	23.19	49.22	22.56	22.64	2.19
2H-3, 30	9.51	108	49.50	21.30	24.41	49.22	23.75	23.83	2.08
2H-3, 40	9.61	109	49.50	21.40	23.61	49.32	22.92	23.00	2.15
2H-3, 50	9.71	110	49.50	21.40	24.34	49.32	23.63	23.71	2.09
2H-3, 60	9.81	111	49.50	21.40	24.97	49.32	24.25	24.33	2.03
2H-3, 70	9.91	112	49.50	21.40	24.26	49.32	23.56	23.63	2.09
2H-3, 80	10.01	114	49.50	21.40	24.79	49.32	24.07	24.15	2.05
2H-3, 90	10.11	115	49.49	21.40	24.67	49.32	23.95	24.04	2.06
2H-3, 100	10.21	116	49.49	21.40	24.69	49.32	23.97	24.06	2.06
2H-3, 110	10.31	117	49.49	21.40	24.49	49.32	23.78	23.86	2.07
2H-3, 120	10.41	118	49.49	21.40	24.20	49.32	23.50	23.58	2.10
2H-3, 130	10.51	119	49.49	21.40	23.96	49.32	23.26	23.35	2.12
2H-3, 140	10.61	120	49.49	21.40	23.55	49.32	22.87	22.95	2.16
2H-3, 146	10.67	121	49.48	21.40	23.24	49.32	22.57	22.65	2.19
2H-4, 10	10.81	125	49.48	21.30	23.07	49.22	22.45	22.53	2.20
2H-4, 20	10.91	126	49.48	21.30	22.58	49.22	21.97	22.05	2.24
2H-4, 30	11.01	127	49.48	21.30	22.27	49.22	21.67	21.75	2.27
2H-4, 40	11.11	128	49.47	21.30	21.97	49.22	21.38	21.46	2.31
2H-4, 50	11.21	129	49.47	21.30	21.96	49.22	21.37	21.45	2.31
2H-4, 60	11.31	130	49.47	21.30	22.03	49.22	21.44	21.52	2.30
2H-4, 70	11.41	131	49.47	21.30	21.63	49.22	21.05	21.13	2.34
2H-4, 80	11.51	133	49.47	21.30	22.14	49.22	21.54	21.63	2.29
2H-4, 90	11.61	134	49.47	21.30	22.05	49.22	21.45	21.54	2.30
2H-4, 100	11.71	135	49.46	21.20	21.74	49.12	21.20	21.28	2.32
2H-4, 110	11.81	136	49.46	21.20	21.83	49.12	21.29	21.37	2.31
2H-4, 120	11.91	137	49.46	21.20	21.47	49.12	20.93	21.02	2.35
2H-4, 130	12.01	138	49.46	21.20	22.92	49.12	22.35	22.44	2.20
2H-4, 140	12.11	139	49.46	21.20	22.57	49.12	22.01	22.10	2.24
2H-5, 10	12.31	141	49.46	21.20	23.42	49.12	22.84	22.93	2.16
2H-5, 20	12.41	142	49.45	21.20	23.74	49.12	23.15	23.25	2.13
2H-5, 30	12.51	143	49.45	21.20	23.63	49.12	23.04	23.14	2.14
2H-5, 40	12.61	144	49.45	21.20	23.93	49.12	23.33	23.43	2.11
2H-5, 50	12.71	145	49.45	21.20	24.06	49.12	23.46	23.56	2.10
2H-5, 60	12.81	146	49.45	21.20	24.44	49.12	23.83	23.93	2.07
2H-5, 70	12.91	147	49.45	21.20	24.28	49.12	23.67	23.78	2.08
2H-5, 80	13.01	149	49.44	21.20	24.20	49.12	23.60	23.70	2.09
2H-5, 90	13.11	150	49.44	21.20	24.26	49.12	23.65	23.76	2.08
2H-5, 100	13.21	151	49.44	21.20	23.63	49.12	23.04	23.14	2.14
2H-5, 110	13.31	152	49.44	21.20	23.77	49.12	23.18	23.28	2.12
2H-5, 120	13.41	153	49.44	21.20	21.98	49.12	21.43	21.53	2.30
2H-5, 130	13.51	154	49.44	21.20	23.55	49.12	22.96	23.07	2.14
2H-5, 140	13.61	155	49.43	21.20	24.78	49.12	24.16	24.27	2.04
2H-5, 148	13.69	156	49.43	21.20	24.52	49.12	23.91	24.02	2.06
2H-6, 10	13.81	158	49.43	20.90	22.62	48.81	22.19	22.30	2.22
2H-6, 20	13.91	159	49.43	20.90	22.48	48.81	22.06	22.16	2.23
2H-6, 30	14.01	160	49.43	21.00	21.48	48.91	21.03	21.13	2.34

Table T3 (continued).

Core, section, interval (cm)	Depth (mbsf)	Measurement number	Temperature-corrected seawater conductivity (mS/cm)	Sediment temperature (°C)	Sediment electrical conductivity (mS/cm)	Correction factor at 20°C (mS/cm)	Sediment electrical conductivity at 20°C (mS/cm)	Drift-corrected sediment electrical conductivity at 20°C (mS/cm)	Formation factor
2H-6, 40	14.11	161	49.43	21.00	21.29	48.91	20.85	20.95	2.36
2H-6, 50	14.21	162	49.42	21.00	21.31	48.91	20.87	20.97	2.36
2H-6, 60	14.31	163	49.42	21.00	21.24	48.91	20.80	20.90	2.37
2H-6, 70	14.41	164	49.42	21.00	20.84	48.91	20.40	20.50	2.41
2H-6, 80	14.51	166	49.42	20.90	21.26	48.81	20.86	20.96	2.36
2H-6, 90	14.61	167	49.42	20.90	21.63	48.81	21.22	21.33	2.32
2H-6, 100	14.71	168	49.42	20.90	21.61	48.81	21.20	21.31	2.32
2H-6, 110	14.81	169	49.41	20.80	21.24	48.71	20.88	20.99	2.35
2H-6, 120	14.91	170	49.41	20.80	21.42	48.71	21.06	21.17	2.33
2H-6, 130	15.01	171	49.41	20.80	21.12	48.71	20.77	20.87	2.37
2H-6, 140	15.11	172	49.41	20.80	20.76	48.71	20.41	20.52	2.41
2H-7, 10	15.32	174	49.41	20.30	20.34	48.20	20.21	20.32	2.43
2H-7, 20	15.42	175	49.41	20.30	19.61	48.20	19.49	19.59	2.52
2H-7, 30	15.52	176	49.40	20.30	19.28	48.20	19.16	19.26	2.57
2H-7, 38	15.60	177	49.40	20.30	18.54	48.20	18.42	18.52	2.67

Table T4. Dissolved oxygen concentrations determined using electrodes, Holes U1369B, U1369C, and U1369E.

Core, section, interval (cm)	Depth (mbsf)	O <sub>2</sub> (µM)	Core, section, interval (cm)	Depth (mbsf)	O <sub>2</sub> (µM)	Core, section, interval (cm)	Depth (mbsf)	O <sub>2</sub> (µM)	Core, section, interval (cm)	Depth (mbsf)	O <sub>2</sub> (µM)
329-U1369B-			1H-4, 80	5.30	138.4	2H-5, 100	13.20	123.8	2H-3, 65	9.85	141.6
1H-1, 10	0.10	157.6	1H-4, 100	5.50	135.6	2H-5, 120	13.40	123.2	2H-3, 85	10.05	146.7
1H-1, 20	0.20	149.3	1H-4, 120	5.70	135.1	2H-5, 140	13.60	122.7	2H-3, 110	10.30	142.0
1H-1, 30	0.30	148.5	1H-4, 140	5.90	138.7	2H-6, 20	13.90	122.4	2H-4, 15	10.65	141.6
1H-1, 40	0.40	148.6	2H-1, 20	6.40	136.4	2H-6, 40	14.10	124.3	2H-4, 35	10.85	146.7
1H-1, 50	0.50	148.6	2H-1, 40	6.60	136.6	2H-6, 60	14.30	121.1	2H-4, 87	11.37	149.6
1H-1, 60	0.60	148.3	2H-1, 60	6.80	136.9	2H-6, 80	14.50	128.9	2H-4, 115	11.65	139.8
1H-1, 70	0.70	146.5	2H-1, 80	7.00	136.9	2H-6, 100	14.70	124.7	2H-4, 130	11.80	139.7
1H-1, 80	0.80	146.5	2H-1, 100	7.20	137.5	2H-6, 120	14.90	128.2	2H-5, 20	12.60	139.6
1H-1, 90	0.90	145.0	2H-1, 120	7.40	136.2	2H-6, 140	15.10	128.2	2H-6, 20	14.10	139.9
1H-1, 100	1.00	143.5	2H-1, 140	7.60	134.8	2H-7, 20	15.40	137.4			
1H-1, 110	1.10	146.1	2H-2, 20	7.90	133.0	2H-7, 40	15.60	136.1	329-U1369E-		
1H-1, 120	1.20	145.1	2H-2, 40	8.10	132.6				1H-2, 15	2.75	153.4
1H-1, 130	1.30	141.4	2H-2, 60	8.30	131.1	329-U1369C-			1H-2, 35	2.95	150.5
1H-1, 140	1.40	144.9	2H-2, 80	8.50	131.3	1H-1, 30	0.30	203.7	1H-3, 20	3.90	149.8
1H-2, 20	1.70	141.5	2H-2, 100	8.70	131.7	1H-2, 15	1.65	172.4	1H-3, 40	4.10	151.4
1H-2, 30	1.80	140.6	2H-2, 120	8.90	130.0	1H-2, 20	1.70	172.1	1H-4, 20	5.00	145.6
1H-2, 40	1.90	140.5	2H-2, 140	9.10	127.7	1H-2, 30	1.80	169.5	1H-4, 40	5.20	145.7
1H-2, 50	2.00	140.1	2H-3, 20	9.40	134.2	1H-3, 15	3.15	154.8	1H-4, 60	5.40	150.1
1H-2, 70	2.20	142.2	2H-3, 40	9.60	134.1	1H-3, 30	3.30	148.0	1H-4, 80	5.60	151.1
1H-2, 80	2.30	142.2	2H-3, 60	9.80	133.5	1H-3, 115	4.15	154.8	1H-4, 100	5.80	151.1
1H-2, 90	2.40	140.7	2H-3, 80	10.00	131.2	1H-3, 130	4.30	148.0	2H-1, 20	7.80	140.0
1H-2, 100	2.50	138.4	2H-3, 100	10.20	134.4	1H-4, 15	4.65	147.3	2H-1, 60	8.20	138.2
1H-2, 110	2.60	141.4	2H-3, 120	10.40	132.5	1H-4, 30	4.80	147.5	2H-1, 80	8.40	143.5
1H-2, 120	2.70	142.7	2H-3, 140	10.60	129.8	1H-4, 65	5.15	151.9	2H-3, 20	10.40	133.3
1H-2, 140	2.90	140.9	2H-4, 20	10.90	128.6	1H-4, 80	5.30	152.8	2H-3, 40	10.60	135.5
1H-3, 20	3.20	140.9	2H-4, 40	11.10	128.0	2H-1, 15	6.15	145.2	2H-3, 60	10.80	135.6
1H-3, 40	3.40	139.1	2H-4, 60	11.30	126.5	2H-1, 30	6.30	145.2	2H-3, 80	11.00	135.2
1H-3, 60	3.60	139.2	2H-4, 80	11.50	122.7	2H-1, 120	7.20	143.3	2H-4, 20	12.00	135.3
1H-3, 80	3.80	141.5	2H-4, 100	11.70	121.7	2H-2, 20	7.85	142.6	2H-4, 40	12.20	133.5
1H-3, 100	4.00	139.7	2H-4, 120	11.90	124.3	2H-2, 40	8.05	142.3	2H-4, 60	12.40	130.1
1H-3, 120	4.20	141.3	2H-4, 140	12.10	118.0	2H-2, 90	8.40	140.2	2H-4, 80	12.60	129.6
1H-3, 140	4.40	138.7	2H-5, 20	12.40	119.0	2H-2, 120	8.70	140.9	2H-5, 15	13.95	129.0
1H-4, 20	4.70	143.7	2H-5, 40	12.60	118.2	2H-2, 140	8.90	142.1	2H-5, 35	14.15	131.0
1H-4, 40	4.90	139.6	2H-5, 60	12.80	118.0	2H-3, 15	9.35	142.6			
1H-4, 60	5.10	143.9	2H-5, 80	13.00	119.5	2H-3, 35	9.55	143.0			

Table T5. Dissolved oxygen concentrations determined using optodes, Hole U1369B.

Core, section, interval (cm)	Depth (mbsf)	O <sub>2</sub> ( $\mu$ M)
329-U1369B-		
1H-1, 15	0.15	147.0
1H-1, 30	0.30	146.0
1H-1, 55	0.55	144.5
1H-1, 70	0.70	144.5
1H-1, 75	0.75	142.3
1H-1, 97	0.97	140.9
1H-1, 115	1.15	140.7
1H-1, 130	1.30	144.2
1H-1, 135	1.35	140.4
1H-2, 15	1.65	139.5
1H-2, 35	1.85	140.7
1H-2, 65	2.15	140.2
1H-2, 95	2.45	139.6
1H-2, 125	2.75	138.6
1H-3, 30	3.30	136.7
1H-3, 75	3.75	136.9
1H-3, 130	4.30	136.0
1H-4, 10	4.60	136.1
1H-4, 50	5.00	134.7
1H-4, 110	5.60	134.4
2H-1, 30	6.50	132.6
2H-1, 70	6.90	129.7
2H-1, 130	7.50	128.9
2H-2, 30	8.00	128.8
2H-2, 70	8.40	127.9
2H-2, 130	9.00	127.2
2H-3, 30	9.50	131.4
2H-3, 70	9.90	126.7
2H-3, 130	10.50	124.9
2H-4, 30	11.00	126.2
2H-4, 70	11.40	124.1
2H-4, 130	12.00	123.9
2H-5, 30	12.50	124.2
2H-5, 70	12.90	122.9
2H-5, 130	13.50	122.3
2H-6, 30	14.00	122.4
2H-6, 70	14.40	121.5
2H-6, 130	15.00	122.8
2H-7, 10	15.30	123.9
2H-7, 25	15.45	121.7

**Table T6.** Dissolved hydrogen measured by headspace gas method, Site U1369.

Core, section	Depth (mbsf)	H <sub>2</sub> (nM)	Catwalk sampling
329-U1369C-			
1H-1	0.20	BD	No
1H-1	0.60	1.4	No
1H-1	1.10	1.5	No
1H-1	1.40	1.8	No
1H-2	2.10	1.8	No
1H-2	2.60	1.6	No
1H-2	2.90	1.4	No
1H-3	3.60	2.6	No
1H-3	4.10	1.3	No
1H-3	4.40	BD	No
1H-4	5.10	1.4	No
1H-4	5.50	1.4	No
1H-4	5.80	1.9	No
1H-1	6.60	BD	No
1H-1	7.10	BD	No
1H-1	7.40	BD	Yes
1H-2	8.10	BD	No
1H-2	8.60	6.3	No
2H-2	8.90	BD	Yes
2H-3	9.60	2.2	No
2H-3	10.10	BD	No
2H-3	10.40	1.6	Yes
2H-4	11.10	2.0	No
2H-4	11.60	1.6	No
2H-4	11.90	BD	Yes
2H-5	12.60	2.2	No
2H-5	13.10	4.0	No
2H-5	13.40	BD	Yes
2H-6	14.10	3.1	No
2H-6	14.60	2.6	No
2H-6	14.90	1.9	Yes
2H-7	15.50	1.3	No
2H-7	15.70	2.0	Yes

BD = below detection (<1.3 nM).



Table T7. Interstitial fluid chemistry, Site U1369.

Core, section, interval (cm)	Depth (m)	pH TITRAUTO	Alkalinity (mM) TITRAUTO	DIC (mM) OI-IC	Cl (mM) M-IC	SO <sub>4</sub> (mM) M-IC	SO <sub>4</sub> (%) Calc. anom.	PO <sub>4</sub> (μM) Spec.	Si (μM) Spec.	Ca (mM) Dx-IC	Mg (mM) Dx-IC	Na (mM) Dx-IC	K (mM) Dx-IC	Ca (mM) ICPAES	Mg (mM) ICPAES	Na (mM) ICPAES	K (mM) ICPAES	B (μM) ICPAES	Fe (μM) ICPAES	Mn (μM) ICPAES	Sr (μM) ICPAES	Catwalk sampling
329-U1369C-																						
1H-1, 5-15	0.10	7.68	2.51	2.43	554.05	28.18	-1.55	1.78	240.8	10.17	51.48	473.88	12.16	9.94	51.04	471	11.65	478.7	7.47	3.74	93.12	Yes
1H-1, 40-50	0.45	7.73	2.48	2.41	553.28	27.98	-2.08	1.62	221.7	10.23	51.77	474.52	12.30	9.94	51.23	468	11.74	468.3	6.02	4.52	91.59	No
1H-1, 90-100	0.95	7.67	2.47	2.43	553.91	28.05	-1.95	1.73	256.5	10.15	51.82	474.39	12.50	10.03	51.23	470	12.10	464.4	7.18	4.12	92.14	No
1H-1, 140-150	1.45	7.66	2.55	2.46	553.68	28.00	-2.11	2.26	260.8	10.32	51.79	475.29	12.70	9.92	50.67	466	12.10	473.1	6.80	3.94	92.03	Yes
1H-2, 40-50	1.95	7.71	2.55	2.45	554.48	28.10	-1.88	2.15	217.8	10.24	51.63	474.59	12.56	9.91	50.75	467	12.06	471.8	6.94	4.13	92.05	No
1H-2, 90-100	2.45	7.75	2.53	2.45	—	—	—	2.18	237.0	10.20	51.43	474.11	12.59	9.94	50.83	465	12.03	480.1	7.19	4.79	92.42	No
1H-2, 140-150	2.95	—	—	—	553.96	28.04	-2.00	2.27	237.6	10.34	51.30	475.79	12.95	10.06	50.91	467	12.37	472.1	6.57	3.82	92.42	Yes
1H-3, 40-50	3.45	7.73	2.51	2.43	554.14	28.12	-1.77	1.98	235.6	10.41	52.06	477.14	12.64	10.02	50.86	469	12.04	456.1	6.27	4.62	91.91	No
1H-3, 90-100	3.95	7.76	2.48	2.39	554.07	28.26	-1.27	1.85	216.2	10.35	52.25	475.86	11.93	9.98	51.22	467	11.46	461.1	6.33	4.13	92.27	No
1H-3, 140-150	4.45	7.60	3.10	2.46	554.32	28.20	-1.50	1.75	207.6	10.30	51.95	474.51	11.94	10.21	51.70	473	11.78	463.7	6.87	3.92	92.17	Yes
1H-4, 122-132	5.77	7.46	2.55	2.54	554.98	28.00	-2.31	1.57	265.3	10.26	51.61	477.35	12.94	10.07	51.05	468	12.49	465.4	6.01	5.25	90.83	Yes
2H-1, 140-150	7.45	7.71	2.67	2.65	555.69	27.96	-2.57	1.26	261.7	10.23	51.11	479.33	12.48	9.99	50.29	469	12.11	482.4	6.29	4.83	92.34	Yes
2H-2, 140-150	8.95	7.71	2.83	2.71	555.35	27.91	-2.71	1.20	271.4	10.28	50.90	478.14	12.42	9.98	50.55	476	11.98	504.0	7.10	4.63	93.05	Yes
2H-3, 140-150	10.45	7.70	2.71	2.69	554.88	27.81	-2.96	0.98	312.1	10.35	50.95	478.06	12.79	9.82	50.27	472	12.11	495.1	6.21	5.16	92.19	Yes
2H-4, 140-150	11.95	7.76	2.74	2.70	555.72	28.09	-2.15	1.01	261.2	10.23	51.47	477.04	12.64	10.04	50.70	468	12.33	512.6	7.76	6.66	93.74	Yes
2H-5, 40-50	12.45	7.75	2.70	2.68	554.85	27.87	-2.75	1.00	263.0	10.10	50.82	476.57	12.83	9.87	50.16	467	12.24	495.3	7.66	6.01	91.27	No
2H-5, 90-100	12.95	7.72	2.72	2.66	556.56	27.81	-3.28	0.89	251.7	10.00	51.21	476.09	12.97	9.85	50.05	470	12.39	506.9	6.94	5.65	92.73	No
2H-5, 140-150	13.45	7.79	2.76	2.72	555.71	27.62	-3.76	0.78	250.4	9.90	51.02	476.41	12.73	9.83	50.43	470	12.34	513.6	7.19	5.92	92.27	Yes
2H-6, 40-50	13.95	7.74	2.76	2.75	555.55	27.71	-3.44	0.98	254.7	10.06	50.99	478.30	12.90	9.94	50.42	475	12.42	514.6	6.86	5.34	91.76	No
2H-6, 90-100	14.45	7.74	2.76	2.76	555.72	27.74	-3.36	0.99	271.2	10.26	51.01	479.07	12.67	9.87	50.15	472	12.28	506.9	6.27	5.14	91.91	No
2H-6, 140-150	14.95	7.78	2.88	2.86	556.27	28.02	-2.50	0.94	309.7	10.17	50.90	478.77	12.16	10.28	49.97	468	11.87	519.0	6.26	5.29	92.24	Yes
2H-7, 35-45	15.40	7.76	2.90	2.87	555.89	28.03	-2.37	1.00	323.9	10.11	50.50	475.97	12.04	10.08	50.40	472	11.83	513.8	6.11	8.08	91.80	No
2H-7, 69-79	15.74	7.71	2.83	2.79	556.43	27.58	-4.05	0.97	276.4	10.00	50.39	477.99	12.69	9.88	50.00	470	12.23	526.8	6.78	4.63	92.66	Yes

TITRAUTO = automated titration, IC = ion chromatography, OI-IC = OI analytical IC, M-IC = Metrohm IC, Calc. anom. = calculated anomaly, Spec. = spectrophotometry, Dx-IC = Dionex IC, ICPAES = inductively coupled plasma-atomic emission spectroscopy. — = no data.

Table T8. Interstitial fluid chemistry in Rhizon samples, Site U1369.

Core, section, interval (cm)	Depth (mbsf)	NO <sub>3</sub> (μM)	PO <sub>4</sub> (μM)	Cl (mM)	SO <sub>4</sub> (mM)	SO <sub>4</sub> (%)
329-U1369C-						
1H-1, 30–40	0.35	38.0	2.10	554.3	27.9	-2.4
1H-1, 80–90	0.85	38.4	2.39	556.1	28.0	-2.4
1H-2, 30–40	1.85	39.0	2.28	554.6	27.9	-2.7
1H-2, 80–90	2.35	38.7	2.47	555.1	27.9	-2.7
1H-3, 30–40	3.35	39.1	—	555.7	28.1	-2.2
1H-3, 80–90	3.85	39.6	2.54	555.2	28.2	-1.6
1H-4, 40–50	4.95	39.5	1.79	—	—	-2.2
1H-4, 80–90	5.35	39.4	2.15	555.7	28.1	-2.2
2H-1, 40–50	6.45	40.0	2.10	555.9	27.7	-3.6
2H-1, 90–100	6.95	39.7	1.80	556.7	27.7	-3.7
2H-2, 40–50	7.95	40.0	2.01	—	—	-3.9
2H-2, 90–100	8.45	40.0	2.18	557.0	27.6	-4.1
2H-3, 40–50	9.45	40.2	2.16	555.5	27.6	-3.8
2H-3, 90–100	9.95	40.4	1.06	557.1	27.6	-4.2
2H-4, 40–50	10.95	40.1	1.14	557.8	27.6	-4.2
2H-4, 90–100	11.45	40.3	1.17	556.9	27.7	-3.6
2H-5, 30–40	12.35	39.8	1.29	563.8	28.0	-3.7
2H-5, 80–90	12.85	40.4	1.58	559.5	27.8	-3.8
2H-6, 30–40	13.85	40.4	1.77	556.8	27.4	-4.7
2H-6, 80–90	14.35	40.3	1.28	557.5	27.4	-5.0
2H-7, 25–35	15.30	41.2	1.16	556.4	27.1	-5.7

— = no data.

Table T9. Solid-phase carbon and nitrogen, Site U1369.

Core, section, interval (cm)	Depth (mbsf)	TC (wt%)	TN (wt%)	TOC (wt%)	TIC (wt%)	CaCO <sub>3</sub> (wt%)
329-U1369B-						
1H-1, 10–11	0.11	0.24	0.070	0.193	0.01	0.07
1H-1, 25–26	0.26	0.20	0.069	0.184	0.01	0.05
1H-1, 45–46	0.46	0.17	0.055	0.131	0.01	0.05
1H-1, 70–71	0.71	0.14	0.053	0.122	0.01	0.05
1H-1, 100–101	1.01	0.13	0.048	0.116	0.01	0.06
1H-1, 135–136	1.36	0.12	0.041	0.110	0.01	0.06
1H-2, 135–136	2.86	0.08	0.026	0.072	0.01	0.10
1H-3, 135–136	4.36	0.08	0.025	0.064	0.01	0.10
1H-4, 128–129	5.79	0.06	0.020	0.045	0.02	0.16
2H-1, 140–141	7.61	0.06	0.018	0.038	0.03	0.21
2H-2, 140–141	9.11	0.06	0.020	0.043	0.03	0.22
2H-3, 140–141	10.61	0.04	0.016	0.029	0.03	0.22
2H-4, 140–141	12.11	0.05	0.013	0.037	0.02	0.21
2H-5, 140–141	13.61	0.06	0.013	0.039	0.04	0.31
2H-6, 140–141	15.11	0.05	0.010	0.031	0.04	0.35
2H-7, 24–25	15.45	0.06	0.010	0.031	0.04	0.35

TC = total carbon, TN = total nitrogen, TOC = total organic carbon, TIC = total inorganic carbon.

Table T10. Epifluorescence microscopy cell counts in sediment samples, Site U1369.

Core, section, interval (cm)	Depth (mbsf)	Cell count ( $\log_{10}$ cells/cm <sup>3</sup> )					
		Extracted				Nonextracted	
		Count 1	Count 2	Count 3	Count 4	Count 1	Count 2
329-U1368C-							
1H-1, 15–20	0.15	4.7	5.0	4.5	4.1	5.6	5.3
1H-1, 50–60	0.50	4.1	4.0			BD	BD
1H-1, 100–110	1.00	3.8	3.6			BD	BD
1H-1, 135–140	1.35	3.3	3.1	3.6	3.7		
1H-2, 50–60	2.00	3.0	3.3				
1H-2, 100–110	2.50	3.5	2.8				
1H-2, 135–140	2.85	2.7	2.8				
1H-3, 50–60	3.50						
1H-3, 100–110	4.00	2.3	2.7				
1H-3, 135–140	4.35						
1H-4, 50–60	5.00						
1H-4, 90–100	5.40	1.4	2.1				
1H-4, 127–132	5.77						
2H-1, 50–60	6.50						
2H-1, 100–110	7.00	2.7	2.0				
2H-1, 135–140	7.35						
2H-2, 50–60	8.00						
2H-2, 100–110	8.50	2.0					
2H-2, 135–140	8.85						
2H-3, 50–60	9.50						
2H-3, 100–110	10.00	2.0					
2H-3, 135–140	10.35						
2H-4, 50–60	11.00						
2H-4, 100–110	11.50	3.1	1.7				
2H-4, 135–140	11.85						
2H-5, 50–60	12.50						
2H-5, 100–110	13.00	2.2	2.0				
2H-5, 135–140	13.35						
2H-6, 50–60	14.00						
2H-6, 100–110	14.50	2.0	2.0				
2H-6, 135–140	14.85						
2H-7, 45–54	15.45						
2H-7, 64–69	15.64	2.7	2.7				
329-U1368E-							
2H-6, 90–100	15.20	2.6	2.7				
2H-6, 90–100*	15.20						
329-U1368C-							
2H-7, 64–69	15.64	2.0	2.5				

\* = sample mainly composed of sands (see “[Lithostratigraphy](#)”). Extracted Count 3 and 4 data counted by another shipboard microbiologist. BD = below detection. Blank cells = no count (will be counted postexpedition).

**Table T11.** Abundance of virus-like particles in sediment samples determined by epifluorescence microscopy, Site U1369.

Core, section	Depth (mbsf)	VLP/cm <sup>3</sup>	STD
329-U1369C-			
1H-1	0.15	1.70E+06	1.04E+05
1H-1	0.50		
1H-1	1.00		
1H-1	1.35	4.94E+05	3.22E+04
1H-2	2.00		
1H-2	2.50		
1H-2	2.85	9.92E+04	7.46E+03
1H-3	3.50		
1H-3	4.00		
1H-3	4.35		
1H-4	5.40		
1H-4	5.77	4.38E+04	3.72E+03
2H-1	7.00		
2H-1	7.35		
2H-2	8.50		
2H-2	8.85		
2H-3	10.00		
2H-3	10.35	3.13E+04	2.81E+03
2H-4	11.50		
2H-4	11.85		
2H-5	13.00		
2H-5	13.35		
2H-6	14.85	2.69E+04	2.13E+03
2H-7	15.64		
329-U1369E-			
1H-1	1.10	3.98E+05	3.17E+04
2H-1	7.40	5.08E+04	4.00E+03
2H-5	13.70	3.17E+04	2.98E+03
2H-6	15.20		

VLP = virus-like particle, STD = standard deviation. Blank cells = no count (samples will be analyzed postexpedition).

**Table T12.** List of samples and culture media used for onboard cultivation experiments, Site U1369.

Core, section	Media used for cultivation
329-U1369E-	
1H-1	Mmm1, Mmm2, SPG-ASW, MA, MB, MR2A, SPG-JL, SLURRY
1H-2	Mmm1, Mmm2, SPG-ASW, MA, MB, MR2A, SPG-JL, SLURRY
1H-3	MA, MB, MR2A, SLURRY
1H-4	MA, MB, MR2A, SLURRY
2H-1	MA, MB, MR2A, SPG-JL, SLURRY
2H-3	SPG-JL, SLURRY
2H-4	MA, MB, MR2A, SLURRY
2H-5	Mmm1, Mmm2, SPG-ASW
2H-6	Mmm1, SPG-ASW, MA, MB, MR2A, SPG-JL, SLURRY

SLURRY = sediment stored anoxically in flushed serum bottles or in syringes kept in sterile foil bags. For more detailed information on the media, see ["Microbiology"](#) in the "Methods" chapter (Expedition 329 Scientists, 2011a).